

# Lifetime predictions of miniature fuses and semiconductor protection fuses

**Citation for published version (APA):**

Meng, X. Z. (1995). *Lifetime predictions of miniature fuses and semiconductor protection fuses*. [Phd Thesis 1 (Research TU/e / Graduation TU/e), Electrical Engineering]. Technische Universiteit Eindhoven.  
<https://doi.org/10.6100/IR449473>

**DOI:**

[10.6100/IR449473](https://doi.org/10.6100/IR449473)

**Document status and date:**

Published: 01/01/1995

**Document Version:**

Publisher's PDF, also known as Version of Record (includes final page, issue and volume numbers)

**Please check the document version of this publication:**

- A submitted manuscript is the version of the article upon submission and before peer-review. There can be important differences between the submitted version and the official published version of record. People interested in the research are advised to contact the author for the final version of the publication, or visit the DOI to the publisher's website.
- The final author version and the galley proof are versions of the publication after peer review.
- The final published version features the final layout of the paper including the volume, issue and page numbers.

[Link to publication](#)

**General rights**

Copyright and moral rights for the publications made accessible in the public portal are retained by the authors and/or other copyright owners and it is a condition of accessing publications that users recognise and abide by the legal requirements associated with these rights.

- Users may download and print one copy of any publication from the public portal for the purpose of private study or research.
- You may not further distribute the material or use it for any profit-making activity or commercial gain
- You may freely distribute the URL identifying the publication in the public portal.

If the publication is distributed under the terms of Article 25fa of the Dutch Copyright Act, indicated by the "Taverne" license above, please follow below link for the End User Agreement:

[www.tue.nl/taverne](http://www.tue.nl/taverne)

**Take down policy**

If you believe that this document breaches copyright please contact us at:

[openaccess@tue.nl](mailto:openaccess@tue.nl)

providing details and we will investigate your claim.

# **Lifetime Predictions of Miniature Fuses and Semiconductor Protection Fuses**

PROEFSCHRIFT

ter verkrijging van de graad van doctor aan de  
Technische Universiteit Eindhoven, op gezag van  
de Rector Magnificus, prof.dr. J.H. van Lint, voor  
een commissie aangewezen door het College van  
Dekanen in het openbaar te verdedigen op  
vrijdag 8 december 1995 om 14.00 uur

door

**Xian Zhong Meng**

geboren te Ningxia, China

Dit proefschrift is goedgekeurd door de promotoren:

prof.dr.-ing. H. Rijanto  
en  
prof.ir. G.C. Damstra

Copromotor:

ir. J.G.J. Sloot

**CIP-DATA KONINKLIJKE BIBLIOTHEEK, DEN HAAG**

Meng, Xian Zhong

Lifetime predictions of miniature fuses and semiconductor  
protection fuses / Xian Zhong Meng. - Eindhoven :

Eindhoven University of Technology

Thesis Technische Universiteit Eindhoven.

ISBN 90-386-0476-9

Subject headings: Electric fuses / electric transients /  
thermal buckling

## **Lifetime Predictions of Miniature Fuses and Semiconductor Protection Fuses**

*To Ying  
and  
our parents*

# Table of Contents

|   |    |
|---|----|
| Nomenclature  | vi |
| Part I Introduction                                       |    |
| Chapter 1 Overview  | 2  |
| 1.1 Electric fuses  | 2  |
| 1.2 Literature review                                     | 3  |
| 1.3 Topics related with this thesis                       | 4  |
| 1.4 Content of this thesis                                | 10 |
| Part II Experiments                                       |    |
| Chapter 2 Lifetime Experiments with Short Current Pulses  | 14 |
| 2.1 Studies of a time lag fuse                            | 14 |
| 2.2 Statistical distribution                              | 18 |
| 2.3 Results and discussion                                | 18 |
| 2.4 Influence of internal constructions on lifetimes      | 24 |
| 2.5 Conclusions   | 27 |
| Chapter 3 Lifetime Experiments with Long Current Pulses   | 28 |
| 3.1 Experiments   | 28 |
| 3.2 Results   | 29 |
| 3.3 Resistance changes                                    | 32 |
| 3.4 Lifetime relationships                                | 32 |
| 3.5 Conclusions   | 36 |
| Chapter 4 Experiments for Notched Strip Fuses             | 37 |
| 4.1 Experimental set-up                                   | 37 |
| 4.2 Lifetime experiments with short current pulses        | 41 |
| 4.3 Motion of notched elements                            | 44 |
| 4.4 Minimum melting $I^2t$ value                          | 47 |
| 4.5 Microscopic study of deformation                      | 48 |
| 4.6 Conclusions   | 51 |
| Part III Thermal Modelling                                |    |
| Chapter 5 Nonlinear Thermal Modelling for Miniature Fuses | 53 |
| 5.1 Thermal models  | 53 |
| 5.2 Analogies and circuits                                | 55 |
| 5.3 Applications  | 57 |

|  |     |
|--|-----|
| 5.4 Conclusions.....   | 64  |
| Chapter 6 Thermal Modelling for Semiconductor Fuses                      | 65  |
| 6.1 Considerations for thermal modelling .....                           | 65  |
| 6.2 Network representation.....  | 68  |
| 6.3 Data input and output files.....                                     | 72  |
| 6.4 Results and discussion .....   | 72  |
| 6.5 Conclusions.....   | 74  |
| Part IV Thermal Buckling and Lifetime Predictions                        |     |
| Chapter 7 Thermal Buckling of Wire Elements                              | 76  |
| 7.1 Buckling concept.....  | 76  |
| 7.2 Analytical study.....  | 77  |
| 7.3 Finite element formulation.....                                      | 79  |
| 7.4 Displacement measurements.....                                       | 82  |
| 7.5 Results and discussion .....   | 83  |
| 7.6 Conclusions and future work .....                                    | 90  |
| Chapter 8 Lifetime Predictions   | 91  |
| 8.1 Introduction.....  | 91  |
| 8.2 Lifetime prediction for short current pulses .....                   | 92  |
| 8.3 Lifetime prediction of miniature fuses for long current pulses ..... | 96  |
| 8.4 Lifetime prediction for a continuous loading .....                   | 100 |
| 8.5 Change of current - time characteristics .....                       | 101 |
| 8.6 Lifetime prediction for notched strip fuses.....                     | 102 |
| 8.7 Application of the method to results from literature.....            | 105 |
| 8.8 Recommendations.....   | 106 |
| 8.9 Conclusions.....   | 107 |
| Part V General Conclusions   |     |
| Chapter 9 Conclusions  | 109 |
| 9.1 Main results.....  | 109 |
| 9.2 Suggestions for future work.....                                     | 110 |
| Appendix Photos of Fuses and Experiment Setup                            | 112 |
| Reference  | 113 |
| Summary  | 120 |
| Samenvatting   | 122 |
| Acknowledgements   | 124 |
| Curriculum Vitae   | 125 |

## Nomenclature

|                |  |
|----------------|--|
| $A$            | cross sectional area ( $m^2$ ).                          |
| $C$            | capacitance (F).   |
| $C_{th}$       | thermal capacitor (F or J/K).                            |
| $D_{max}$      | maximum displacement (m).                                |
| $E$            | modulus of elasticity (Pa)                               |
| $Gr$           | Grashof number.  |
| $I$            | current (A).   |
| $I_m$          | area moment of inertia about neutral axis ( $m^4$ ).     |
| $I_n$          | rated current (A).                                       |
| $I_{peak}$     | peak current (A).  |
| $I^2t$         | integration of current square over time ( $A^2s$ ).      |
| $I^2t_{pulse}$ | $I^2t$ of a current pulse ( $A^2s$ ).                    |
| $I^2t_{min}$   | minimum melting $I^2t$ value of fuses ( $A^2s$ ).        |
| $I_p$          | prospective current (A).                                 |
| $I_c$          | injected current for coupled network (A or $A^2$ . ohm). |
| $K_n$          | constant.  |
| $M$            | moment (N.m).  |
| $M_0$          | initial moment (N.m).                                    |
| $N$            | in-plane force (N).                                      |
| $N$            | number of current pulses to blowing.                     |
| $N_D$          | initial in-plane force (N).                              |
| $N_0$          | number of current pulses for the reference parameter.    |
| $N_{seg}$      | number of segment.                                       |
| $Nu$           | Nusselt number.  |
| $P$            | input energy to a segment (W).                           |
| $Pr$           | Prandtl number.  |
| $Q$            | activation energy (J).                                   |
| $R$            | resistance ( $\Omega$ ).                                 |
| $Ra$           | Rayleigh number.   |
| $R_{el}$       | electrical resistance (ohm).                             |
| $R_{th}$       | thermal resistance (ohm or K/W).                         |
| $S$            | radial surface ( $m^2$ ).                                |
| $T$            | temperature rise (K, $^{\circ}C$ ).                      |
| $T_w$          | temperature of the wire (K).                             |
| $T_{int}$      | temperature inside the glass tube (K).                   |
| $T_w$          | air temperature outside the glass tube (K).              |
| $T_{cr}$       | critical temperature rise (K, $^{\circ}C$ ).             |
| $U_T$          | total potential energy (J).                              |
| $V$            | voltage (V).   |
| $W_b$          | energy for real elongation (J).                          |
| $W_d$          | deformation energy (J).                                  |



## Nomenclature

---

|           |   |
|-----------|---|
| $W_m$     | bending energy for buckling shape (J).  |
| $c$       | specific heat ( $J \cdot kg^{-1} \cdot K^{-1}$ ).                                 |
| $d_s$     | actual elongation related with spring (m).  |
| $e$       | axial strain.   |
| $e_m$     | strain.   |
| $e_b$     | strain.   |
| $g$       | gravity constant ( $g = 9.81 \text{ m} \cdot \text{s}^{-2}$ ).                    |
| $h$       | heat transition coefficient for the convection ( $W \cdot m^{-2} \cdot K^{-1}$ ). |
| $i$       | current (A).  |
| $j$       | current density ( $A \cdot m^{-2}$ ).   |
| $k$       | curvature ( $m^{-1}$ ).   |
| $k_s$     | spring constant ( $N \cdot m^{-1}$ ).   |
| $l$       | length of a segment (m).  |
| $l_0$     | length of the fuse element (m).   |
| $n$       | number of segments.   |
| $q_s$     | heat dissipation in a segment (W).  |
| $q_k$     | heat conduction in a segment(W).  |
| $q_c$     | heat convection from a segment(W).  |
| $q_r$     | heat radiation from a segment(W).   |
| $r_e$     | outer radius of the end cap (m).  |
| $r_d$     | radius of the wire (m).   |
| $r_g$     | inner radius of the glass tube (m).   |
| $r_o$     | outer radius of the glass tube (m).   |
| $t$       | time (s).   |
| $t_m$     | melting time (s).   |
| $t_{on}$  | on time (s).  |
| $t_{off}$ | off time (s).   |
| $u$       | displacement in $z$ direction (m).  |
| $u_z$     | displacement derivative.  |
| $w$       | displacement in $y$ direction (m).  |
| $w_0$     | initial displacement (m).   |
| $w_z$     | derivative of vertical displacement.  |
| $w_{zz}$  | second order derivative of vertical displacement ( $m^{-1}$ ).                    |
| $x_r$     | relevant dimension (for a cylinder, $x_r$ is the diameter) (m).                   |
| $x, y, z$ | co-ordinates.   |

---

|                           |   |
|---------------------------|---|
| $\alpha$                  | thermal diffusion coefficient ( $\text{m}^2 \cdot \text{s}$ ).                                  |
| $\alpha$                  | temperature coefficient of resistivity ( $\text{K}^{-1}$ ).                                     |
| $\beta$                   | thermal expansion coefficient (for a gas $\beta = 1/T$ , $\text{K}^{-1}$ ).                     |
| $\gamma$                  | deflection factor.  |
| $\gamma$                  | mass density ( $\text{kg} \cdot \text{m}^{-3}$ ).   |
| $\Delta L$                | length increase (m).  |
| $\Delta x$                | length of a subvolume along the $x$ axis (m).   |
| $\Delta y$                | length of a subvolume along the $y$ axis (m).   |
| $\Delta z$                | length of a subvolume along the $z$ axis (m).   |
| $\Delta V$                | volume of a segment ( $\Delta V = lA$ , $\text{m}^3$ ).   |
| $\Delta \varepsilon_a$    | apparent strain range.  |
| $\Delta \varepsilon_m$    | mechanical strain range.  |
| $\Delta \varepsilon_{th}$ | thermal strain range.   |
| $\delta W_{int}$          | virtual work done by internal forces.   |
| $\delta W_{ext}$          | virtual work done by external forces.   |
| $\delta$                  | thermal diffusion depth (m).  |
| $\varepsilon$             | emissivity.   |
| $\varepsilon$             | strain.   |
| $\varepsilon_c$           | creep strain.   |
| $\dot{\varepsilon}_s$     | steady state creep rate ( $\text{s}^{-1}$ ).  |
| $\lambda$                 | thermal conductivity ( $\text{W} \cdot \text{m}^{-1} \text{K}^{-1}$ ).                          |
| $\mu$                     | dynamic viscosity ( $\text{kg} \cdot \text{m}^{-1} \text{s}^{-1}$ ).                            |
| $\nu$                     | kinematic viscosity ( $\text{m}^2 \cdot \text{s}^{-1}$ ).                                       |
| $\rho$                    | resistivity ( $\text{ohm} \cdot \text{m}$ ).  |
| $\sigma$                  | Stefan Boltzmann constant ( $5.67 \cdot 10^{-8} \text{ W} \cdot \text{m}^{-2} \text{K}^{-4}$ ). |
| $\phi$                    | electric potential (V).   |

## **Part I Introduction**

## Chapter 1 Overview

### 1.1 Electric fuses

Fuses are designed for the protection of electric circuits and equipment. Fuses were invented around 1864 [1]. Nowadays, they are produced in a wide variety of physical dimensions, shapes and internal constructions and mainly used in conjunction with fuse clips, mountings and holders. Among many electrical devices, fuses are well known for their popularity in house apparatus and installations.

In the instrument technology, fuses with 2 mA rated current can be found. Because of the explosive development of computer industries, an enormous amount of miniature fuses is required. On the other hand, the rapid increased demand for large semiconductor devices leads to the need of very high ratings of semiconductor protection fuses (ratings higher than 2 kA and 1000 V). For high voltage applications, products with ratings of 100 A and 72.5 kV are applied.

Fuses may be grouped under four headings: miniature fuses, high voltage fuses, low voltage power fuses and semiconductor protection fuses. The heart of a fuse always consists of a conductive strip or wire element, which carries an electric current. This piece of material is made of metals or their alloys and it is defined as a fuse element. Figure 1.1 shows a typical fuse for semiconductor protection. The construction consists of a fuse element, ceramic body, contacts and sand.

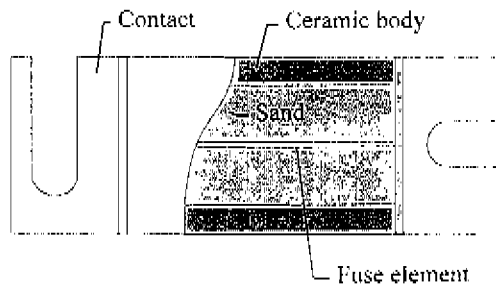


*Figure 1.1 Typical semiconductor protection fuse*

Fuses must be able to open circuits at currents which exceed a given value within a certain time. Application normally requires that the fuse operating time should be shorter for higher current values. This behaviour of the fuse is described by its current - time ( $I - t$ ) characteristic.

The  $I - t$  characteristic is defined as a curve where the value of the melting time is expressed as a function of the prospective symmetric current, under stated conditions of

operation. In the short time range, the Joule integral  $I^2t$  is defined as the integral of the square of the current over a given time interval, if the time interval is short enough. A typical  $I - t$  characteristic of semiconductor fuses is shown in Fig. 1.2, where the melting time  $t$  is expressed as a function of the effective current  $I$  (*r.m.s.*). For short melting times,  $I^2t$  values are provided together with melting times.

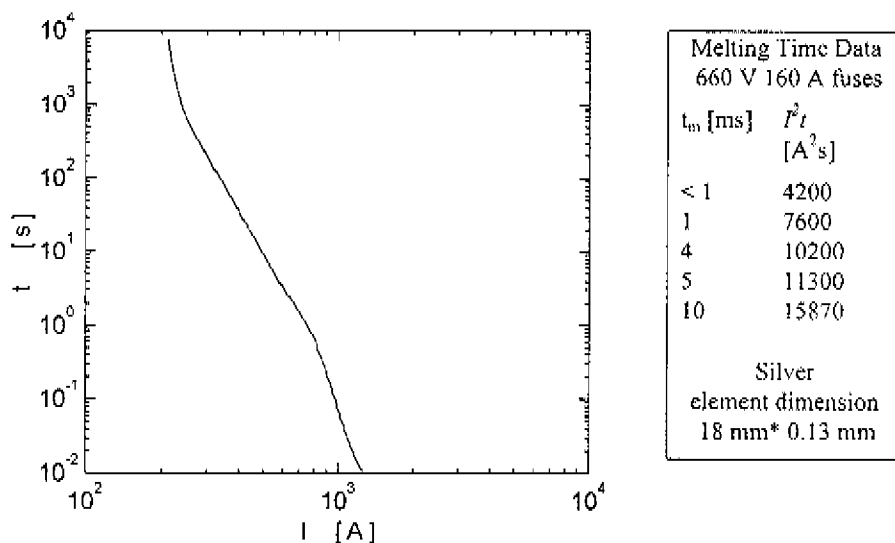


**Figure 1.2** Typical current - time characteristic of a semiconductor protection fuses

In general, because of ageing effects,  $I - t$  characteristics of fuses tend to shift. As a result fuses can blow after a number of current pulses at values faster than expected from the original  $I - t$  curve. It is obvious that the deterioration of  $I - t$  characteristics can lead to unreliable functioning of electrical systems. In order to improve the reliability of electrical systems, lifetime estimation of fuses are required by users and manufacturers.

## 1.2 Literature review

Basic knowledge of fuses has been provided by Wright [1], Johann [2] and Wang [3] in their textbooks. Two literature studies [4, 5] are available for further studies in fuse designs and their applications. In this section, only a brief review will be given and particular attention will be paid to the state of art in the fuse developments.

### 1.2.1 Prearcing characteristics

Extensive contributions have been made since 70's to simulate prearcing characteristics and applications of various types of fuses. Among them, the finite difference method [6, 7], finite element method [8, 9, 10] electrical analogue method [11] and TLM [12]

(Transmission line matrix method) are widely used to conduct the performance simulation. A good guidance for element designs may be provided from the simulation.

Fuses should operate at short circuit or overload current. However, they should not operate at nominal load conditions which are related with continuous or pulsed (cyclic) currents. In practice, the undesired change of fuse behaviour, for instance unexpected blowing, can occur after some time in use as a result of deterioration processes. This is usually called ageing. To describe ageing, lifetime for various applications can be defined as the time for reaching the acceptable change of current - time characteristics of fuses, the time for fuse blowing or the time for a certain percent of resistance increase. For ageing studies, literature review will be presented in Section 1.3.

Many general purpose fuse links are provided with low melting point materials which are attached to fuse elements. As a result of diffusion, a reduction of the melting point of fuse elements is realised. The phenomena related with this effect is referred to as the M - effect named after Metcalf. To achieve desired current - time characteristics of fuses, M-effect was often used. However, for certain current shapes, the M-effect can bring about undesired diffusion and result in ageing. Daalder [13] and Hofmann [14] conducted studies of M-effects, they concluded that if the fuse element is properly designed, interdiffusion has no detrimental effect on fuse performance. Recently, Beaujean [15] proposed a simulation method for current - time characteristics where interactions between silver strip and low melting point materials were considered.

### 1.2.2 Arcing phenomena

Although many studies have been conducted experimentally and theoretically to predict arcing behaviour, the use of various models is limited to specific types and load conditions [16, 17, 18, 19]. The arcing process is still not fully understood, therefore, the description of the arcing process is largely dependent on empirical parameters.

### 1.2.3 Fuse designs

Among many developments, the following new types of fuses can be mentioned: surface mount fuses [20, 21], substrate fuses [22], vacuum fuses [23, 24],  $SiF_6$  fuses [25], electronic fuses [26] and smart fuses [27]. These new developments are focused on high reliability [21, 23, 24, 26, 27], extreme compactness [20, 21, 22] and easy availability [26, 27].

## 1.3 Topics related with this thesis

As it has been mentioned in Section 1.2, two main unsolved problems remain in the description of fuse behaviour, viz. arcing and ageing. The subject of this thesis will be focused on ageing mechanisms, as far as these are caused by thermal mechanical reasons. The studied fuse configurations are limited to those normally chosen for miniature and semiconductor protection fuses. Section 1.3.1 presents state of art of lifetime studies in general. Section 1.3.2 gives a brief descriptions of basic mechanisms of metal deformation. Section 1.3.3 addresses reliability items in existing standards for miniature

fuses, low voltage fuses and high voltage fuses. Section 1.3.4 introduces the minimum  $I^2t$  value and describes the phenomena of thermal buckling related with fuse elements.

### 1.3.1 Lifetime studies in literature

Ageing can take place at continuous loads and cyclic loads. The latter may be distinguished in pulsed current with

high amplitude and short conducting time

low amplitude and long conducting time

Such ageing can happen in circuits with power electronics. Also, motor starting, transformer and capacitor inrush are related with such pulsed currents.

Various attempts have been made to provide solutions for the problem of fuse ageing. For cyclic duties, compressive stresses are induced due to temperature rise during current flow. During the period without current, the compression is released due to cooling. This thermal effect becomes cyclic in nature. More than continuous heating, this cyclic heating results in ageing of the fuse element. In the former investigations, resistance changes, movement and cracks of fuse elements have been noticed. Some specific properties are stated below.

Because of current surges, fuses may be subjected to fatigue problems. Several methods for lifetime estimation for specified currents have been presented in the past. Possibly the first paper [28] correlating cycles to failures with current parameters appeared to be in 1969. In resistance welding applications, fuses should be derated to protect thyristors. Cycles to failure for fuses were presented in a graph as a linear function of the ratio of rated melting  $I^2t$  to the actual  $I^2t$  passed through the fuse during the current conducting time. Taking the fuse element temperature excursion as a parameter was also addressed as an alternative.

In 1974, W.J. Huber experimentally investigated effects of the minimum  $I^2t$  change for fuses to have proper inrush capability for the protection of power transformers [29]. Two successive half cycle current pulses spaced four seconds apart were suggested to test the fuse's rated minimum melt  $I^2t$  value of fuses. It was indicated that the minimum melt  $I^2t$  value of fuses can be taken as a criteria for fuse to withstand the transformer inrush and lightning protection.

For fuses, exposed to a cyclic current, the number of pulses which fuses can withstand, was considered as a linear function of the percentage of the rated current [30]. The on time and off time from five seconds to 10 minutes were used during tests. For fuse selection in the protection of semiconductors, it was recommended that the equivalent *r.m.s.* value of an occasional overload current should not exceed 85% of the current value from  $I - t$  characteristics for the same duration. For frequent overload currents, the limit was reduced to 70%. For cyclic duties, the current for the on time was suggested not to exceed 50% of the value of current corresponding to  $I - t$  characteristics. For this duty and in case of overload duration above 1 hour, the *r.m.s.* current was limited to the rated current. It was suggested that the lifetime of fuses is consumed by electric currents. No motivation of these recommendations was presented by experimental or theoretical analysis.

The microstructure changes of subminiature fuses have been examined [31] by using scanning electron microscope (*SEM*) and energy dispersive X-ray microscope (*EDX*). The fuse elements were made of silver copper alloy wires. After the wire experienced the pulsed current of an on time up to 225 microseconds, partial melting and recrystallization were found in localised areas within the grain structure. Segregation was found at the surface of a wire. Taking the energy dissipation during the pulse current as criteria [32], lifetime limits were determined for fuses of copper silver alloy wires. The thresholds of lifetimes at different temperature rises were expected to be: maximum lifetime condition at 100 °C; more than 20000 cycles at 300 °C; more than 1000 cycles at 500 °C; potential single pulse at 800 °C.

Klepp [33] conducted comparative studies of nickel or tin plated contacts with silver plated contacts. Contact resistance of nickel or tin plated contacts is found to increase in high temperature and aggressive atmosphere. Kueck [34] analysed failures of fuses used in the circuits of nuclear generating stations, suggestions were made for improving reliability of control circuit fuses.

For high voltage fuses, Arai [35] conducted experimental motion studies of elements for model fuselinks in cyclic lifetime tests. The notched fuse element was made of silver. For a straight fuse element, movement of the element was observed during pulsed current by X-ray photography. When fuses experienced cyclic currents, originally bent fuse elements were changed into ripples; cracks were found in the element notches. Ageing in fuse elements was explained by thermal fatigue, lifetimes were presented as a function of current related with current - time characteristics.

High voltage expulsion fuses are widely used in the power system protection. As a circuit fault occurs, the arc in these fuses is extinguished by the expulsion effect of gases produced by the arc. After 15 kV high voltage expulsion fuses were exposed to cyclic currents, deterioration of  $I - t$  characteristics and resistance changes have been observed [36]. Fuse wires made of copper, tin silver copper alloy, and tin lead alloy were used in the experiments. The amplitude of pulsed current was 120% the amplitude of the fuse rated current. The on time was 1 hour. A long off time was adopted to cool down the tested fuse.

For cyclic duties, lifetime was suggested to be presented [37] as a function of current related with  $I^2t$  values during the on time.

As the thermal effect was directly taken into account [38], the lifetime observations were fitted and presented as a function of a combined variable of temperature rise and mean temperature. A coefficient which reflects deflections has been introduced to relate the mechanical strain with lifetime. Its value was determined from the lifetime regression analysis.

Nuisance operation of high voltage fuses during storms has been reported [39, 40, 41, 42] in USA, Canada and Australia. As the fuse operation was considered to be caused by lightning, the estimated operating rate [40] can be up to 0.43% from the field observation. According to Westrom's work, after tin fuse links were used in the system for years of



service, 2% of the fuses showed a time reduction above 10% with the melting current [38]. They recommended large ratings of fuses for the protection to avoid nuisance operation.

Limitation of fuse lifetime, caused by oxidation of silver coated copper wires, has been investigated [43] for continuous currents. Cracks induced in the fuse wires were reported. Because of chemical reactions in the element to occur at an elevated temperature, resistance of a fuse goes up. As regards the resistance changes, measurements have been performed on different element materials. The on time of pulsed current was 1 hour during the cyclic tests. Fuse elements of silver, copper, silver coated copper, nickel coated copper, tin silver copper alloy were studied. For a given current, energy dissipation increases, this results in the final interruption of fuses in services.

These preliminary studies provided qualitative indication of fuse ageing mechanisms. However, because motion of the fuse elements was not defined or even was not taken into account, various parameters in the proposed models have to be determined by using the curve fitting method. Use of this method is limited for certain types, and normally a large number of tests are required.

### 1.3.2 Basic mechanism of metal deformation

Metal deformation [44] can be distinguished in: elastic, plastic and creep types. Elastic and plastic deformations are considered as instantaneous deformation caused by applied stresses, while creep deformation is modelled as time dependent.

Elastic deformation is reversible, plastic deformation is non-linear and irreversible. They are considered as the instantaneous deformation response to the application of a load. Plastic deformation may have two forms: slip and twinning. Slip is the most common form, it is considered as the shearing of crystal blocks over one another e.g. in multiples of the unit displacement. The displacement of crystal blocks occurs consecutively in the small region of slip plane and spread outwards. The boundary between the regions where slip has taken place and where slip has not occurred is called a dislocation. The dislocation is commonly represented as a line in the slip plane. By contrast, twinning is used to describe the fractional displacement of crystal blocks. Plastic deformation causes permanent changes in the material.

Creep [45] stands for the time dependent deformation and rupture, it is also irreversible. Because the failures due to creep are similar to those induced by plastic deformation, the creep deformation is normally treated as a plastic deformation. Creep deformation is divided into intragranular and intergranular deformation. As the name implies, intragranular creep stands for the creep inside a grain and intergranular creep for the creep among grains. Intragranular creep deformation includes crystallographic slip and subgrain formation. The plastic deformation takes place due to slip of dislocations by gliding on certain preferred slip planes. As regards with subgrain formation, because of the inhomogeneity of creep deformation, many opportunities of local bending are provided within a single crystal or individual grains of polycrystals. Local bending further causes dislocations of one sign line up. The dislocations arrange themselves by cross-slip into low angle subgrain boundaries due to interaction between dislocations. Subgrain boundaries are formed in the primary stage of creep. Intergranular creep deformation

includes grain boundary sliding, creep cavity nucleation, fold formation and grain boundary migration.

Based on the diffusion concept, several models have been developed to predict the creep behaviour. From an atomic or molecular perspective, diffusion in solids is the migration of atoms or molecules from one lattice site to another lattice site. The atoms must have sufficient energy to break bonds and then reform them at another lattice site. This energy is known as the activation energy. When two bulk materials are in contact, interdiffusion takes place. At the surface molecules from one material can migrate into another by diffusion and vice-versa with different diffusion rates.

In addition to the stress, elevated temperature and temperature changes can lead to failures, namely thermal fatigue. According to the range for stress  $\sigma$  and temperature  $T$ , different models related with the shear modulus  $G$  and the melting temperature  $T_m$  were proposed in the past [44, 45, 46]. If  $\sigma < 10^5 G$  and  $T > 0.5 T_m$ , lattice diffusion creep (Nabarro-Herring creep) model is used. The creep process is controlled by diffusion of atoms and vacancies under low applied stress, temperature is above  $0.5 T_m$ . Materials deform in the tensile direction. Creep also exists under low stress and low temperature. If  $\sigma < 10^4 G$  and  $T < 0.5 T_m$ , the process can be described by grain boundary diffusion (Coble creep). If  $10^5 G < \sigma < 10^3 G$  and  $T > 0.5 T_m$ , dislocation motion controlled creep deformation occurs by both dislocation gliding and dislocation climbing. If  $\sigma < 10^3 G$  and  $T > 0.5 T_m$ , grain boundary sliding and superplasticity may occur. Grain boundary sliding mainly contributes to the creep in the primary stage. Because the agreement of activation energy of creep and lattice self diffusion, the sliding is considered as a diffusion controlled process. If several mechanisms are mutually independent, the fastest mechanism governs the creep behaviour, while if the mechanisms are dependent, the slowest mechanism governs the creep behaviour.

The creep curve is a strain time relationship where strain is defined as a function of time under a constant load or stress. The slope of the curve is defined as the creep rate. The creep is distinguished into three stages: primary creep, secondary creep and tertiary creep. The creep rate in the secondary creep stage is termed as the steady state creep rate. Because most deformation involves this stage, it is of primary importance.

Considering the effects of cyclic thermal stresses on metals, the number of cycles to failure can be directly related with elastic strain and plastic strain.

Application of metal deformation mechanisms can be found for both large mechanical components and small electronic devices, such as power plant components and printed circuit boards. Overall component dimensions may vary from meters to micrometers. When fuse elements made from metals experience electric currents, thermal and electromagnetic effects can lead to deformations of fuse elements. For current pulses, cyclic thermal stress in the fuse element is involved.

### 1.3.3 Lifetime considerations in standards

In the modern world, there is no doubt that commercial industrial products have to meet their standards. IEC Publication 127 : miniature fuses [47] is the most important standard for miniature fuses. This standard specifies two types of tests related with lifetime

expectancy. The first one is the *endurance test* stated in IEC Publication 127-1 Sub-clause 9.4 and the second is the *pulse test* specified in IEC Publication 127-1 Sub-clause 9.6.

Endurance tests require fuses to withstand 100 cycles. Each cycle consists of an on time of 1 hour with a current and an off time of 15 minutes without current. The current magnitude is normally 1.2 times the rated current of tested fuses. Direct current is used in the test. The voltage drop after tests is measured by applying the rated current to the tested fuse. The increase of the voltage drop is required to be not more than 10% of the value measured before tests.

In contrast to endurance tests, pulse tests are performed to gain information of ability to withstand current surges normally experienced in service. These tests require 1000 times specified current pulses. The voltage drop after tests is measured by exerting the rated current on the tested fuse. The increase of the voltage drop is required to be not more than 10% of the value measured before tests. The main feature of the test is that current pulse has a larger magnitude and a shorter on time compared with that in endurance tests.

In IEC Publication 269-4 (1986) [48], concerning fuse-links for the protection of semiconductor devices, overload curves are required (see IEC 269-4, Sub-Clause 5.6.4 and 8.4.3.4). Fuses are subjected to 100 load cycles, each cycle has a total duration of 0.2 times the conventional time which is defined by fuse ratings. The "on" period with a current value and a duration corresponding to the co-ordinates of the overload capability to be verified, the "off" period forms the rest of the cycle. The time co-ordinates are suggested to be within the range of 0.01 to 60 seconds.

In IEC Publication 644 (1979) [49], concerning high voltage fuses for motor circuit applications, two test sequences are recommended for fuses to withstand repetitive starting conditions. The first test consists of 100 cycles and the second consists of 2000 cycles (see Clause 8).

For most applications, however fuses have to withstand more than  $10^6$  current pulses, 2000 current pulses are often far too less to meet users requirements. Lacking of guidance from existing standards, manufacturers have to accumulate experience to deal with these practical problems, a good service is normally realised by a trial and error method. Therefore to understand ageing mechanisms of fuses and to perform reliability studies are of a practical value for industries.

#### 1.3.4 Minimum $I^2t$ value and thermal buckling

Before main contents of this thesis are outlined, the minimum  $I^2t$  value of fuses and the concept of thermal buckling related with lifetime predictions will be explained and described first.

##### (1) Minimum $I^2t$ value

Current - time characteristics of fuses show a spread for the melting time at a given current. The minimum  $I^2t$  value is the current square times the minimum melting time for a given current. Below this value, fuses do not operate. In many cases, the minimum  $I^2t$

value at 10 ms can be directly related to the selection of fuses for the protection of electrical components.

For miniature fuses, as stated by manufacturers, this value is approximately a constant because the adiabatic heating may be assumed for most wire elements (with 20 mm overall length). For transformer protections, 25 times the transformer rated current for 10 ms is sometimes required in order to have fuses withstand transformer inrush currents. Data sheets for semiconductor devices, for example thyristors, quote a figure for the maximum surge current that devices can survive. A half sine pulse with a width of 10 ms (50 Hz) is usually taken to indicate the  $I^2t$  for fusing. This  $I^2t$  value represents the energy that can be passed by semiconductor devices without damaging them. Therefore in this thesis, the minimum melting  $I^2t$  value is chosen as one of the parameters. In some applications, fuses are required to blow below a certain  $I^2t$  value. Therefore, in principle, the maximum melting  $I^2t$  value and the average melting  $I^2t$  value can also be used.

## (2) Thermal buckling

Thermal buckling is a concept to describe the movement of components due to thermal origins. In 1989, Moulin [50] conducted a review of thermal buckling analysis methods. For electric fuses under discussion, their elements can be considered either as columns with two fixed ends or plates with two fixed edges. For a column with two fixed ends or a plate with two fixed edges, because of the boundary constraints the compressive force increases as the temperature of the column or the plate rises. At the beginning, the column or the plate reserves its original shape. This state is called as *pre buckling*. As the temperature increases further, the column or the plate may start to move. The process is called as thermal *buckling* because of its thermal origin. The temperature rise limit for thermal buckling to take place is defined as the critical temperature rise. After motion of the element is initiated, the displacement of the column or the plate increases significantly with temperature. This is called as thermal post buckling.

## 1.4 Content of this thesis

Previous studies and current standards do not provide general valid methods to describe fuse reliability. This study attempts to describe methods to predict the fuse lifetime expectancy in the case where thermal mechanical processes are dominant. The first task of this work is to answer questions related with the ageing mechanism of miniature fuses during short time pulse currents.

When fuses experience long time cyclic currents, ageing of fuses may differ from that in short time cyclic currents. Accordingly in IEC Publication 127: miniature fuses, endurance tests are specified. To predict fuse lifetimes for long time currents, the second goal is to investigate relevant behaviour during long time currents.

Because of the various dimensions and shapes of fuse elements, it may be asked whether it is possible to find a model for lifetime estimation compatible with all situations. Consequently, to resolve this difficulty becomes the third objective of this work.

For semiconductor protection fuses, notched fuse elements may have different shapes, they can be surrounded by sand or bound sand. There are many parameters which influence lifetime of commercial products, and hence to study these causes and predict lifetime becomes our fourth objective.

*As it has been stated, the prime objective of this thesis is to provide a general theoretical method for lifetime predictions and to evaluate the change of current - time characteristics after fuses are submitted to current pulses. Because lifetime is dependent on the stress - strain relationship, displacements of the fuse element have to be determined. However, displacements are developed due to electric heating which depends on heat transfer processes. Therefore, in accomplishing these tasks, first experimental relationships of lifetime and important parameters are investigated. Secondly, thermal response of fuse elements is analysed for different currents. Thirdly, metal deformation due to thermal effects is studied together with the resulting stress. Finally on the basis of thermal fatigue due to cyclic stress/strain, the lifetime can be predicted theoretically.* Following this scheme, the work is divided into five parts: introduction (Chapter 1), experiments (Chapters 2, 3 and 4), heat transfer modelling (Chapters 5 and 6), thermal buckling (Chapter 7) and lifetime predictions (Chapter 8), and general conclusions (Chapter 9).

Chapter 2 presents experimental results of pulse tests. It describes experimental equipment and test procedures. Fuses are submitted to short current pulses in the order of 10 milliseconds to obtain lifetimes. This chapter also discusses possibilities to present lifetimes as function of several parameters related with current.

Chapter 3 covers lifetime studies related with endurance tests and long time ageing behaviour. Tests are relevant to endurance tests specified in IEC Publication 127: miniature fuses. The chapter discusses the possible relationship between lifetimes and current parameters: magnitude and on time.

Chapter 4 describes experiments for studying the ageing mechanism of semiconductor protection fuses [51]. Experimental observations of lifetimes and deformation are presented.

Chapter 5 presents thermal modelling methods [52] for miniature fuses. Here, heat radiation and convection of fuse elements are considered to be non-linear functions of the element temperature. The purpose is to calculate the temperature response and distribution for fuse elements excited by any currents. Application of this model may also result in current - time characteristics ( $I - t$ ) of miniature fuses which are of importance to manufacturers.

Chapter 6 presents three dimensional thermal transient simulations [53] due to electric current for semiconductor fuses by using EMTP (Electro-Magnetic Transient Program [54]). In the simulation, the current density distribution in the fuse element is considered in two dimensions.

Chapter 7 presents analysis of element motions for thermally stressed fuses due to electric currents. The present study describes two buckling models. The first one is based on the work [55] where the maximum displacement of a straight fuse wire is obtained to

be a function of the element temperature. The second buckling model uses the finite element method, it describes displacements in the axial direction and the perpendicular direction of the wire. Both models attempt to analyse the stress and strain of fuse wires due to thermal origin. The purpose is to predict the breaking location and to gain an insight of mechanical responses due to electric currents.

Chapter 8 presents models for lifetime predictions for miniature fuses [56, 57, 58] and for semiconductor protection fuses for cyclic currents. It discusses ageing origins of both types of fuses and possibilities for improving fuse lifetimes. General applications of the methods to various types of fuses are addressed.

Chapter 9 summarises main conclusions from the previous chapters.

## **Part II Experiments**

## Chapter 2 Lifetime Experiments with Short Current Pulses

This chapter presents and analyses experimental results of lifetime reduction of commercial miniature fuses by the short current pulse. For current pulses,  $I^2t$ ,  $I_{peak}$ ,  $t_{on}$  and  $t_{off}$  may be defined as follows:

|            |   |
|------------|---|
| $I^2t$     | is the current square integral over a period $t$ for a single current pulse (unit in $A^2s$ ) |
| $I_{peak}$ | is the peak current of a current pulse (unit in A)  |
| $t_{on}$   | is the current pulse time (unit in ms)  |
| $t_{off}$  | is the time period between two successive current pulses (unit in second).                    |

As far as the current pulse time is concerned in this thesis, current pulses may be classified into two categories: short current pulses and long current pulses. A short current pulse means that the current pulse time is in order of several milliseconds.

As stated in the first chapter, miniature fuses have different element shapes as regards to their applications. On the basis of current - time characteristics, miniature fuses are distinguished as: very fast acting fuses (FF), fast acting fuses (F), medium time lag fuses (M), time lag fuses (T) and very time lag fuses (TT). Essential difference among them exists in their prearcing  $I^2t$  values. For example, prearcing  $I^2t$  values show big differences at 10 times the rated current. Fast acting fuses open earlier than time lag fuses for a short circuit current. So in practice, to withstand inrush currents during the switching of equipment, time lag fuses are suggested in favour. Materials of fuse elements often differ for various current ratings. As a consequence, the question of lifetime variations rises due to properties of element materials. Before any large scale studies on lifetimes are started, a case study is carried out. So to get an impression of effects of current pulses on fuse lifetimes, experiments start with a typical time lag fuse.

Because of construction differences of fuses, it is reasonable to ask whether conclusions drawn from the case study represent generalities or not. In other words, a general method should be pursued for all practical fuses. To find the solution for these problems, several typical configurations are studied. Because experimental procedures for all fuses are more or less the same, experimental descriptions will take the time lag fuse as an example for the illustration.

This chapter mainly covers two parts. The first part describes the efforts to study lifetimes of a typical time lag fuse and the second part describes the influence of other parameters of fuses on lifetimes. Main objectives are:

- to determine experimentally the lifetime of miniature fuses exposed to cyclic current with rectangular and sinusoidal pulse shapes for long off times.
- to study the influence of the internal construction of fuses on their lifetimes.

### 2.1 Studies of a time lag fuse

#### 2.1.1 Test object

Figure 2.1 shows a typical construction of the chosen test object (Littelfuse type 218.800). The fuse element of these time lag fuses is a straight wire element and is positioned inside a glass



tube. Two ends of the wire element are soldered onto end caps. The element of tested fuses is made from a clad wire of 50% silver and 50% tin-zinc alloy by weight. The wire diameter is 0.103 mm. Fuses are rated at 800 mA and the minimum melting  $I^2t$  value is 1.3 A<sup>2</sup>s, as indicated by the fuse manufacturer (see Appendix).

### 2.1.2 Measurements of voltage drops

To study fuse ageing, technical information of new fuses should be collected. As resistance change was considered as one of the main points related with fatigue, measurements of voltage drops were performed.

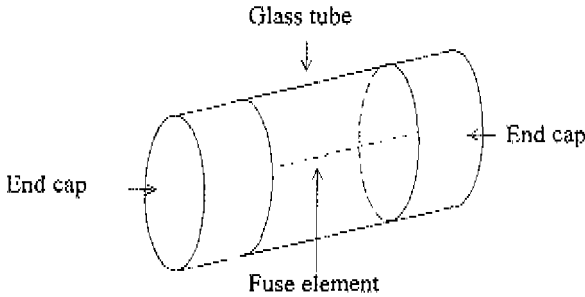


**Figure 2.1** Typical time lag miniature fuse

According to IEC Publication 127 : miniature fuses [47], the rated current should be used for determining the voltage drop and then the power loss. In normal practice, the heat produced by 10% of the rated current is considered to be negligible. For these reasons, to measure the cold resistance of fuses 10% of rated current can be chosen. To guarantee the measuring accuracy, the four terminal method [59, 60] was adopted. Figure 2.2 shows the principle scheme, where  $I$  is the applied current,  $U$  is the measured voltage between two terminals.

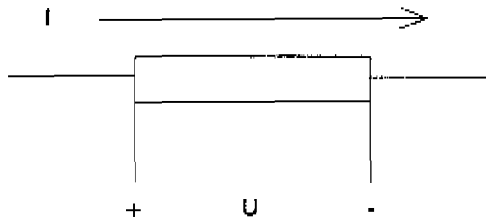


**Figure 2.2** Four terminal method for measuring the fuse resistance

For 800 mA time lag fuses, voltage drops across 74 fuse samples were obtained by using the fuse rated current (800 mA). Accordingly, 80 mA was taken in the measurement to determine the cold resistance.

### 2.1.3 Test circuits for current pulses with half sinusoidal wave forms

To study the influence of current wave forms on fuse lifetimes, two typical current wave forms were used: pulsed currents with half sinusoidal and rectangular wave forms. The peak current ranged up to 20 amperes. The relative  $I^2t$  value varied from 0.16 to 0.85 which was defined as the ratio of the  $I^2t$  value of the pulsed current to the minimum melting  $I^2t$  value of fuses as stated by the manufacturer.

In the following, experiments for current pulses with a half sinusoidal wave form will be discussed. Pulse tests in this work are aimed at collecting lifetime data of fuses, when fuses are subjected to current pulses. To continue the pulse test, test facilities are required to be properly coordinated so that a series of current pulses are exposed to fuses. Secondly, the time interval between two pulses are adjustable. Resistance or voltage drops in this period should also be measured. To accomplish these duties, an experimental set-up was constructed as shown in Fig. 2.3.

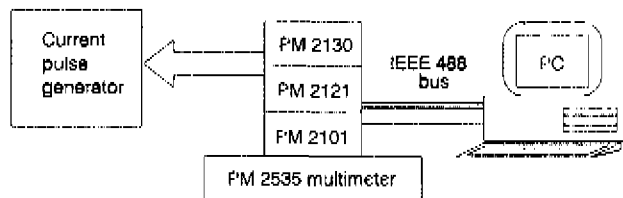


**Figure 2.3** Experimental setup for performing pulse tests [61]

The set-up mainly consisted of a computer, a digital input/output unit (PM 2130), a digital low level switch (PM 2121), an IEEE interface (IEEE 488 PM 2101), a digital multimeter (PM 2535) and a current pulse generator. The digital I/O unit and the low level switch were used to produce switching signals and control operation for tests. With the digital multimeter, voltage drops across tested fuses can be measured by using a current source of 80 mA (or 800 mA). The generator was actually an LC circuit with a thyristor which can be controlled by the computer interface to obtain current pulses with an approximately half sinusoidal wave form. Several fuses were tested in one series at the same time. Figure 2.4 shows the test circuit of one unit in the current pulse generator which was designed by P. van Rietschoten (see Appendix).

To evaluate the lifetime distribution, in the first stage this process was repeated until all fuses operated, afterwards until three of five fuses interrupted. Resistance values and the number of pulses which fuses withstood were stored in disk files. Additionally, the fuse voltage, the current and the  $I^2t$  value of pulsed currents were saved.

### 2.1.4 Test circuits for current pulses with rectangular wave forms

To study fuse ageing due to applying a rectangular current pulse, similar duties mentioned in Section 2.1.3 were carried out to gather lifetimes.

The experimental set-up [62] designed by P. van Rietschoten is shown in Fig. 2.5. The system mainly consisted of a d.c. supply, a digital control unit, counters, an electronic switch, a current

detect switch, a digital potential meter (DPM) and a shunt. The d.c. supply can deliver a current between 800 mA to 20 A. Within  $100 \mu\text{s}$ , the current reaches its top value and keeps constant. In one series 12 fuses can be tested, during the test the resistance of fuses was measured. After fuse breaking the numbers of cycles to failure were recorded by counters and put into the computer for further analysis.

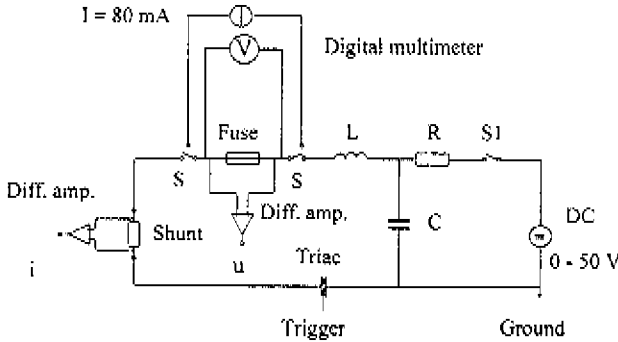


**Figure 2.4** Test circuit diagram for sinusoidal pulsed currents  
*S, S1* : Relays (V23100 - V71); Triac : Tic - 263 M  
 $L = 2.2 \text{ mH}$ ,  $C = 1.3 \text{ mF}$ ,  $R = 220 \text{ ohm}$

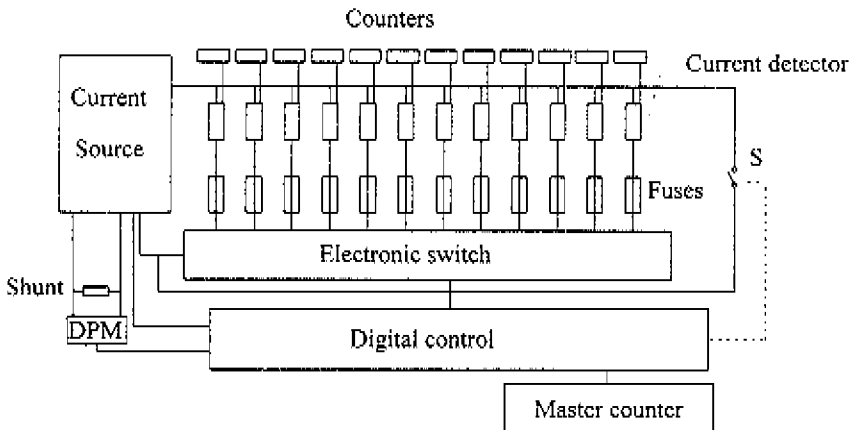


**Figure 2.5** Test circuit diagram for current pulses with rectangular wave forms [62]

## 2.2 Statistical distribution

Two types of distributions, namely the *normal distribution* and the *Weibull distribution*, are used in this thesis to estimate the distribution of observed parameters, such as voltage drops, resistance and the number of current pulses to failures. The model of the *normal distribution* is a summation of independent identically distributed random variables. It is widely used to evaluate parameters of products to describe their new situation. For example, dimensions, weight and etc.

The *Weibull distribution* has been widely used in reliability studies as a model for the lifetime of products including the description of a wide range of fatigue phenomena. For this reason, this distribution is chosen as a starting point in this research. The most popular method of lifetime analysis is to fit the distribution to lifetime data by the maximum likelihood method (ML). As an alternative, the distribution is often fitted to lifetime data by using a graphic procedure, one advantage of this method is to visually check whether the observed lifetimes belong to this distribution.

For the Weibull distribution, its *cumulative density function* is

$$F(t) = 1 - \exp(-(\lambda t)^\beta) \quad \text{for } t \geq 0 \quad (2.1)$$

where  $t$  is the random variable,  $\lambda > 0$  and  $\beta > 0$  are the scale and shape parameters, respectively. In this situation  $t$  is the time related with the number of current pulses which fuses can withstand.

The *density function* for the Weibull distribution is

$$f(t) = \lambda^\beta \beta t^{\beta-1} \exp(-(\lambda t)^\beta) \quad t > 0$$

The *mean value* of the Weibull distribution is

$$E[\tau] = \lambda^{-1} \Gamma(1 + \beta^{-1})$$

Reorganisation of Eq. 2.1 leads to

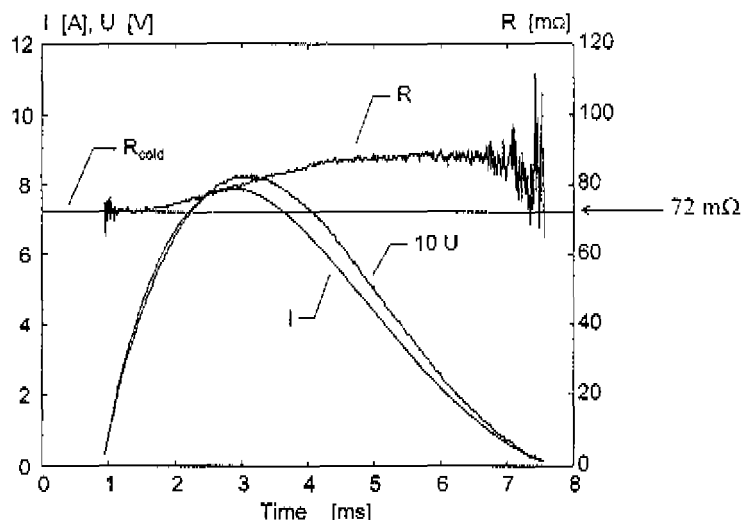
$$\log_{10} [ -\log_e(1 - F(t)) ] = \beta \log_{10} \lambda + \beta \log_{10} t$$

To obtain a linear relationship between lifetime  $\log_{10} t$  and the corresponding value of the cumulative density function,  $\log_{10} t$  must be plotted against  $\log_{10} [-\log_e(1-F(t))]$ . The common practice [63] is to plot  $\log_{10} t_k$  against  $P_k = (k-0.5)/n$ , where  $t_1, t_2, \dots, t_k, \dots, t_n$  are the ordered observations from the population,  $n$  is the number of total samples ( $1 \leq k \leq n$ ). If the experimental results can be fitted to a straight line in this graph, the validity of the Weibull distribution is assumed. The slope of the line is a measure of parameter  $\beta$ .

## 2.3 Results and discussion

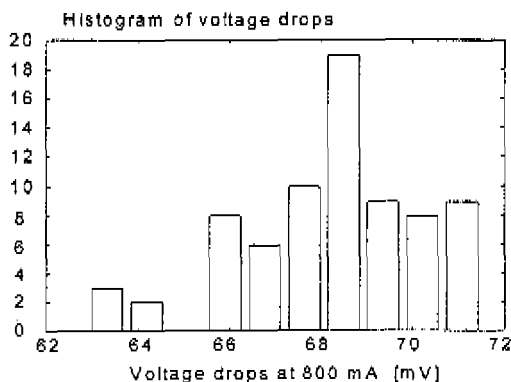
During pulse tests, both sinusoidal and rectangular wave forms of current pulses were used, the purpose is to examine the influence of wave forms on the fuse lifetime. The current through the tested fuse and the corresponding voltage across the fuse were measured by a digital oscilloscope. Figure 2.6 shows typical traces for a current pulse with the sinusoidal wave form. A time lag for the voltage trace exists as compared with its corresponding current. This physically means that during the period of a current pulse, the fuse wire element is heated up (resistance increases).

Before the test with current pulse started, conditions of new products were evaluated first, the initial cold resistance was measured for 74 samples. Voltage drops of fuses were measured at a d.c. current of 800 mA (rated current).



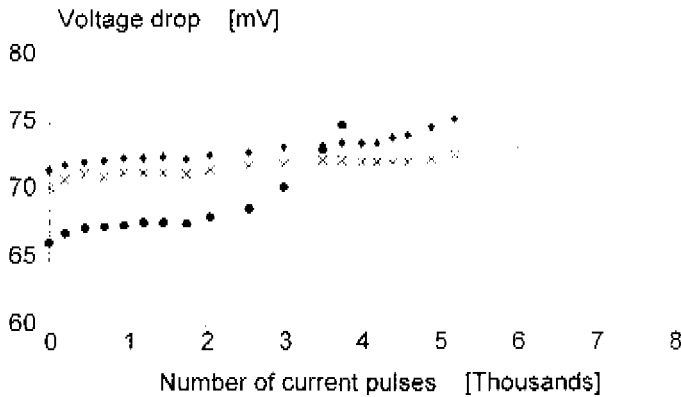
**Figure 2.6** Measured pulsed current and corresponding voltage  
*I* : measured current; *U* : measured voltage;  
*R* : resistance;  $R_{\text{cold}}$  : initial resistance

Figure 2.7 presents the histogram of voltage drops. If the voltage drop is assumed to follow the normal distribution, then the mean value  $\mu = 68.3$  mV and the standard deviation  $\sigma = 1.9$  can be obtained. The 90% confidence interval of this voltage distribution is [65, 71.4] mV, which is corresponding to resistance values from 81.3 to 89.3 m $\Omega$ .



**Figure 2.7** Histogram of the voltage drops before current pulses  
 if the normal distribution for voltage drops is assumed,  
 then mean value  $\mu = 68.3$  mV and standard deviation  $\sigma = 1.9$

For both types of pulses, parameters of current pulses  $I^2t$ ,  $I_{peak}$  and  $t_{on}$  are measured by using a digital oscilloscope. Also during the lifetime test, the voltage drops were measured until the end of life. For three time lag fuses, Fig. 2.8 displays typical measuring results of voltage drops as a function of time. Measurements were performed between current pulses. Approximately sinusoidal current pulses were applied (see Fig. 2.6) with  $I^2t = 0.61 \text{ A}^2\text{s}$ ,  $I_{peak} = 14.6 \text{ A}$ ,  $t_{on} = 6.2 \text{ ms}$ ,  $t_{off} = 3 \text{ s}$ .



**Figure 2.8** Measured voltage drops at 800 mA against number of sinusoidal current pulses  
 $I^2t = 0.61 \text{ A}^2\text{s}$ ,  $I_{peak} = 14.6 \text{ A}$ ,  $t_{on} = 6.2 \text{ ms}$ ,  $t_{off} = 3 \text{ s}$  for 3 fuses

Figure 2.9 shows measured voltage drops for three fuses exposed to rectangular current pulses with the same  $I^2t$ . The parameters of current pulses are  $I^2t = 0.61 \text{ A}^2\text{s}$ ,  $I_{peak} = 8 \text{ A}$ ,  $t_{on} = 10 \text{ ms}$ ,  $t_{off} = 3 \text{ s}$ .

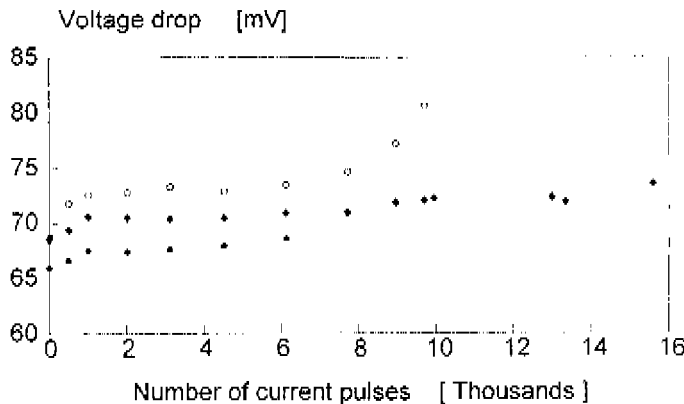


**Figure 2.9** Measured voltage drops against number of rectangular current pulses  
 $I^2t = 0.61 \text{ A}^2\text{s}$ ,  $I_{peak} = 8 \text{ A}$ ,  $t_{on} = 10 \text{ ms}$ ,  $t_{off} = 3 \text{ s}$  for 3 fuses

The common point of Figs. 2.8 and 2.9 is that in general the resistance increases as the number of current pulses increases. Initially, the resistance increases rapidly until the number of applied pulses reaches a value of about 1000 pulses. Afterwards, resistance increases slowly and sometimes it also decreases. At the final stage, near the end of fuse life, resistance increases sharply again. From a number of experiments, it is noticed that fuses show the final resistance increases later when submitted with rectangular current pulses as compared with half sinusoidal current pulses. Examples are shown in Figs. 2.8 and 2.9. This is possibly due to the fact that the input energy rate during the rectangular current pulse (lower  $I_{peak}$ , longer  $t_{on}$ ) is lower than that during sinusoidal current pulses.

Observations of the fuse behaviour just before breaking provide a possible approach to study lifetime criteria. From a large amount of tests, lifetime median and corresponding median of the percentage resistance increases before fuse breaking are obtained. Statistic medians (50% value) of fuse lifetimes and percentages of resistance increases are calculated from five tested samples. The average increase of resistance is found to be 9.8 %.

To estimate fuse lifetimes according to a statistical model, the first goal is to examine whether lifetimes follow a specific pattern of distribution. Figure 2.10 shows the accumulated frequency as a function of lifetime on probability paper of the Weibull distribution. In Fig. 2.10, curve "a" shows the results for  $I^2t = 0.61 \text{ A}^2\text{s}$ ,  $I_{peak} = 14.6 \text{ A}$ ,  $t_{on} = 6.2 \text{ ms}$ ,  $t_{off} = 3 \text{ s}$ ; curve "b" for  $I^2t = 0.61 \text{ A}^2\text{s}$ ,  $I_{peak} = 10.4 \text{ A}$ ,  $t_{on} = 5.6 \text{ ms}$ ,  $t_{off} = 5 \text{ s}$  and curve "c" for  $I^2t = 0.61 \text{ A}^2\text{s}$ ,  $I_{peak} = 8 \text{ A}$ ,  $t_{on} = 10 \text{ ms}$ ,  $t_{off} = 3 \text{ s}$ .

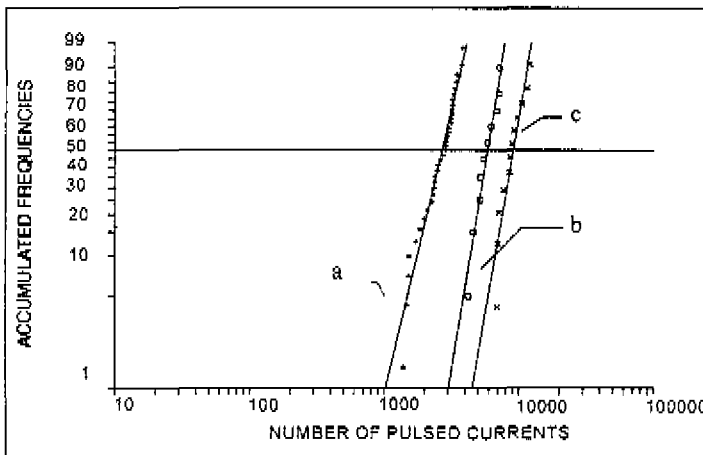


**Figure 2.10** Probability paper for the Weibull distribution of fuse lifetime for current pulses with different parameters

- a :  $I^2t = 0.61 \text{ A}^2\text{s}$ ,  $I_{peak} = 14.6 \text{ A}$ ,  $t_{on} = 6.2 \text{ ms}$ ,  $t_{off} = 3 \text{ s}$ , sinusoidal  
 b :  $I^2t = 0.61 \text{ A}^2\text{s}$ ,  $I_{peak} = 10.4 \text{ A}$ ,  $t_{on} = 5.6 \text{ ms}$ ,  $t_{off} = 5 \text{ s}$ , rectangular  
 c :  $I^2t = 0.61 \text{ A}^2\text{s}$ ,  $I_{peak} = 8 \text{ A}$ ,  $t_{on} = 10 \text{ ms}$ ,  $t_{off} = 3 \text{ s}$ , rectangular

In Fig. 2.10, because observations are fitted into a line, the Weibull distribution can be used to estimate lifetimes. In addition, this graph shows that for the same  $I^2t$  value of current pulses, fuse lifetime will be short as the current pulse time for current decreases. In other words, the peak current increase leads to a decrease of lifetime.

From a large amount of pulse tests, mean lifetimes can be estimated based on the Weibull distribution. Lifetimes expressed in number of current pulses are presented in Table 2.1 as fuses were exposed to half sinusoidal current pulses and rectangular current pulses.

**Table 2.1** Experimental results from the pulse tests

| $I^2t_{pulse}$ | Wave form | $t_{on}$ [ms] | $t_{off}$ [s] | Mean lifetime |
|----------------|-----------|---------------|---------------|---------------|
| 0.89           | s         | 6.2           | 7             | 2.2           |
| 0.65           | s         | 6.2           | 7             | 18            |
| 0.55           | s         | 6.2           | 7             | 372           |
| 0.52           | s         | 6.2           | 7             | 2666          |
| 0.47           | s         | 6.2           | 7             | 5973          |
| 0.47           | s         | 6.2           | 3             | 2656          |
| 0.42           | s         | 6.2           | 7             | 13099         |
| 0.37           | s         | 6.2           | 7             | 55563         |
| 0.57           | r         | 12            | 4             | 1605          |
| 0.57           | r         | 12            | 2             | 1272          |
| 0.52           | r         | 5.6           | 5             | 2261          |
| 0.47           | r         | 5.6           | 5             | 5259          |
| 0.47           | r         | 10            | 3             | 8978          |
| 0.37           | r         | 8             | 3             | 265400        |

In Table 2.1, “s” and “r” represent the sinusoidal and rectangular wave forms respectively. Corresponding parameters are defined as follows:  $I^2t_{pulse}$  is the  $I^2t$  value of each current pulse;  $I^2t_{min}$  is the minimum  $I^2t$  value corresponding to the  $I-t$  characteristic of fuses for the same time as  $t_{on}$ . To simplify the estimation, in this case, the minimum *adiabatic*  $I^2t$  value is used however.

During pulse tests, the gradually changing voltage drops or resistances were measured and results are shown in Fig. 2.8 and Fig. 2.9. On the basis of these observations, three basic patterns can be recognised. Resistance increases during pulse tests in general. At the beginning resistance increases very fast; after about 1000 current pulses, resistances become more or less stable. At the final stage, resistance increases sharply again.

Figure 2.11 shows normalised resistance change patterns for different  $I^2t$  values during pulse tests. Each type of marks represents a trace of voltage drop corresponding to lifetime median for a series of pulse test. This graph indicates that during the fuse lifetime, the resistance of fuses will increase with similar normalised patterns for a broad range of pulse shapes. From this graph, it can be concluded that as the average voltage drops increase up to about 75 mV, the lifetime of fuses is consumed. This offers indeed a useful guideline in practice, to check whether a fuse is nearly at the end of life.



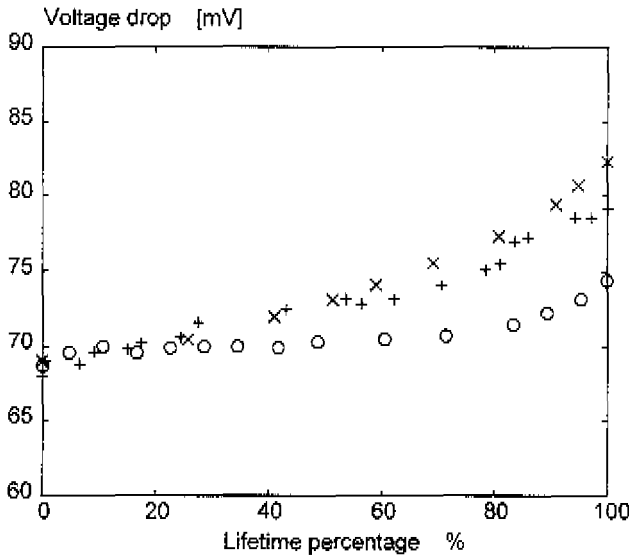


**Figure 2.11** Voltage drop at 800 mA as a function of percentage lifetime for current pulses

+ :  $I^2t = 0.48 \text{ A}^2\text{s}$ ,  $I_{\text{peak}} = 8 \text{ A}$ ,  $t_{\text{on}} = 8 \text{ ms}$ ,  $t_{\text{off}} = 3 \text{ s}$ , rectangular wave shape

x :  $I^2t = 0.74 \text{ A}^2\text{s}$ ,  $I_{\text{peak}} = 8 \text{ A}$ ,  $t_{\text{on}} = 12 \text{ ms}$ ,  $t_{\text{off}} = 4 \text{ s}$ , rectangular wave shape

o :  $I^2t = 0.61 \text{ A}^2\text{s}$ ,  $I_{\text{peak}} = 14.6 \text{ A}$ ,  $t_{\text{on}} = 6.2 \text{ ms}$ ,  $t_{\text{off}} = 3 \text{ s}$ , half sinusoidal wave shape

One should remind that parameters of current pulses in Figs. 2.8-2.11 are measured values, a certain accuracy may be assumed. For instance (see Fig. 2.9),  $I_{\text{peak}} = 8 \text{ A}$  and  $t_{\text{on}} = 10 \text{ ms}$  lead to  $I^2t = 0.64$  instead of 0.61.

Using Table 2.1, Fig. 2.12 presents fusc lifetimes against the relative  $I^2t$  value of current pulses, where  $I^2t_{\text{pulse}}$  is the  $I^2t$  value of a single current pulse;  $I^2t_{\text{min}}$  is the minimum  $I^2t$  value of the melting ( $I^2t_{\text{min}} = 1.3 \text{ A}^2\text{s}$ ). By using the curve fitting method [64], lifetimes are found to be a simple function of the relative  $I^2t$  value of the pulsed current. It is expressed to be

$$\log_{10} N = C_1 \log_{10} \frac{I^2t_{\text{pulse}}}{I^2t_{\text{min}}} + C_0 \quad (2.1)$$

where  $C_1$  and  $C_0$  are constants determined from experimental observations. In this case  $C_1 = -12.6$  and  $C_0 = -0.38$ .  $C_0$  indicates whether ageing of fuses is faster ( $C_0 < 0$ ) than that expected from current-time characteristics.  $C_1$  is a measure for ageing sensitivity to current pulses.

In Fig. 2.12, mark  $\Delta$  indicates lifetimes of fuse where current pulses with a half sinusoidal wave form was applied; mark  $\blacksquare$  indicates lifetimes of fuse where current pulses with a rectangular wave form. It can be seen that as the relative  $I^2t$  value reaches 1, the number of current pulses is also near 1; as the  $I^2t$  value increases, lifetimes decrease. From this graph, it can also be seen that lifetimes for current pulses with a half sinusoidal wave forms slightly differ from those for current pulses with a rectangular wave forms. This encourage us further to investigate the lifetime

behaviour of other types of fuses, on the basis that the  $I^2t$  value of current pulses is the determining factor for the lifetime reduction. Because the test circuits for sinusoidal current wave forms are much easier to build than the test circuits for the current pulses with rectangular wave forms, thus test circuits for producing current pulses with sinusoidal wave forms were constructed to test other types of fuses.

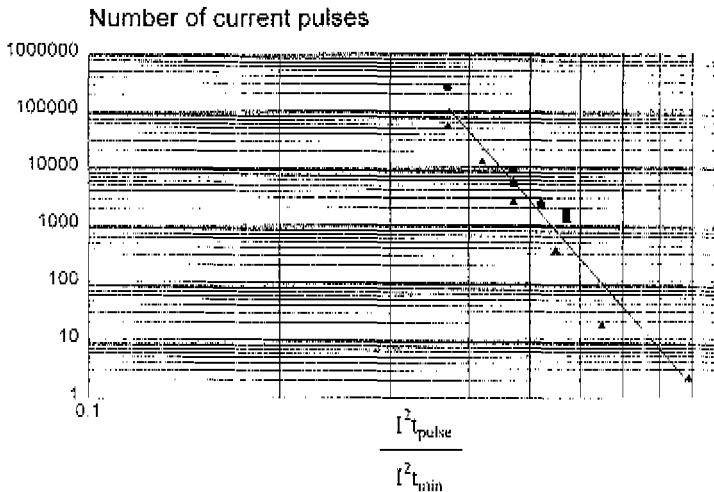


**Figure 2.12** Fuse lifetime as a function of the relative  $I^2t$  value of current pulses  
 $\Delta$  : current pulse with a half sinusoidal wave form  
 $\blacksquare$  : current pulse with a rectangular wave form

## 2.4 Influence of internal constructions on lifetimes

In Section 2.3, lifetime determinations have been presented for a time lag fuse, where the number of cycles to failure showed to be a function of the relative  $I^2t$  value of current pulses.

The question here is whether it is possible to generalise this dependency for other fuse types. In this section, with the same circuits in Fig. 2.4 efforts will be made therefore to determine the lifetimes of other types of fuses. Because test circuits have the same principle scheme, the descriptions of test procedures will not be addressed again.

### 2.4.1 Element materials

For low voltage fuses and high voltage fuses, silver and copper are the best known element materials. For miniature fuses, alloys are also widely used because of practical requirements in manufacturing and applications. To get a general impression, different element materials were chosen. They may be used to make fast acting fuses and time lag fuses.

### 2.4.2 Element shapes

As the element shapes are concerned, there are a number of choices. The most commonly used types are shown in Fig. 2.13: straight wire elements, corrugated elements, wound wire elements

and S-shaped plates. However, in this thesis, results of straight wire elements and corrugated elements are presented only.

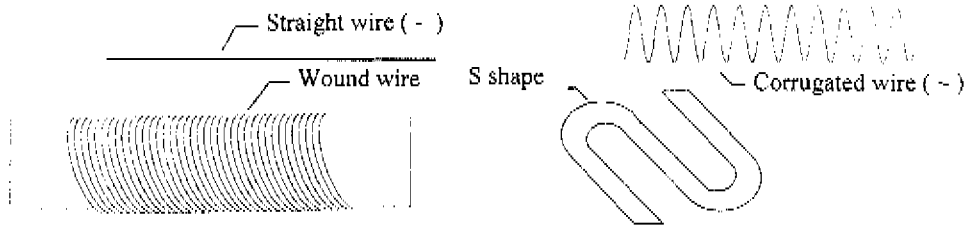


Figure 2.13 Typical element shapes

### 2.4.3 Results and discussion

According to the analysis for fuses (Littelfuse type 218.800) in Section 2.3, the fuse lifetime in number of current pulses can be presented as a linear function of the  $I^2t$  value of the pulsed current, on a double logarithmic scale. To check the general validity of the relationship concerning different element materials and shapes, following types of fuses were used as examples: Nickel wire elements, silver alloy wire elements (Ag,Cu,Zn,Cd: 50%Ag, 15.5%Cu, 16.5%Zn and 18%Cd), silver plated (3%) copper wire elements; silver plated (20%) copper wires, and silver clad wire elements (Ag/SnZn: 50% Ag and 50% tin-zinc alloy 85% Sn and 15% Zn). Experiments were conducted in Littelfuse. Figure 2.14 shows lifetimes of miniature fuses (Littelfuse type 217001, 217002) for current pulses with sinusoidal wave forms, where lines are obtained according to Eq. 2.1 with different coefficients.

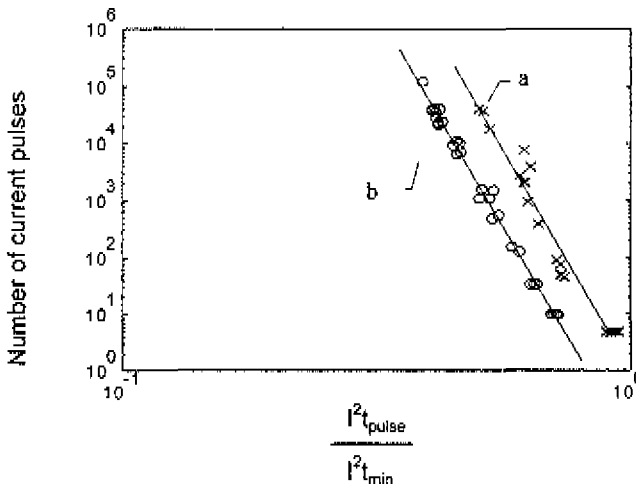


Figure 2.14 Lifetimes for fuse made from silver plated (3%) copper wires for sinusoidal current pulses (Eq. 2.1)

a : Littelfuse type 217002; b : Littelfuse type 217001

For various different types of fuses, the curve slope from the regression analysis Eq. 2.1 is outlined in Table 2.2, where corrugated and straight elements are indicated by “-” and “~” respectively.

**Table 2.2** Slope of lifetime relationship

| Fuse type | $d$ $\mu\text{m}$ | Element material  | Element shape | $C_1$  | $C_0$  |
|-----------|-------------------|-------------------|---------------|--------|--------|
| 217.315   | 50                | Ni                | -             | - 20.3 | - 0.99 |
| 217.500   | 68                | AgCuZnCd          | ~             | - 17.1 | 1.3    |
| 217001    | 60                | Cu, Ag plated 3%  | ~             | - 15.2 | - 1.26 |
| 217002    |                   | Cu, Ag plated 3%  |               | - 15.3 | 0.046  |
| 235001    | 52                | Cu, Ag plated 20% | ~             | - 19.2 | - 3.64 |
| 2351.25   | 62                | Cu, Ag plated 20% | ~             | - 18.8 | + 3.0  |
| 23501.6   | 73                | Cu, Ag plated 20% | ~             | - 19.5 | - 3.1  |
| 235002    | 98                | Cu, Ag plated 20% | ~             | - 16.9 | - 1.54 |
| 218800    | 103               | Ag/Sn,Zn          | -             | - 12.6 | - 0.38 |
| 218001    | 117               | Ag/Sn,Zn          | -             | - 8.6  | + 6.64 |
| 2181.25   | 134               | Ag/Sn,Zn          | -             | - 9.0  | - 1.14 |
| 21801.6   | 156               | Ag/Sn,Zn          | -             | - 9.4  | - 0.90 |
| 235.500   |                   | AgCuZnCd          |               | - 8.8  | 0.27   |
| 235.700   | 63                | AgCuZnCd          | -             | - 7.7  | - 0.17 |
| 237001    | 96                | Ag/Sn,Zn          | ~             | -8.99  | - 0.33 |

From Table 2.2, it is clear that the regression lines from the curve fitting are not always through the unit relative  $I^2t$  value. For the most cases, the points are located to the left of the unit relative  $I^2t$  value. To examine the influence of materials on the relationship, the coefficients  $C_1$  are presented in Fig. 2.15.

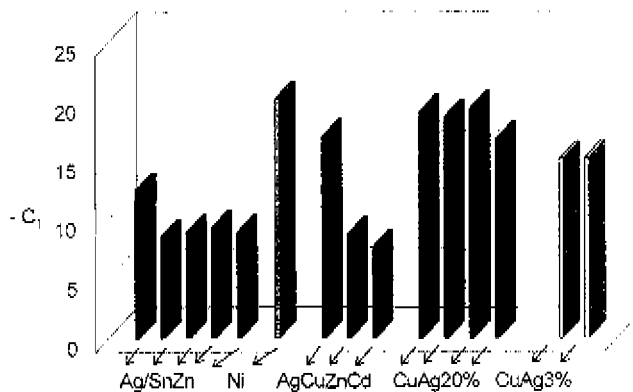


**Figure 2.15** Influence of element materials on slope  $C_1$  in Eq. 2.1

For the same series, as indicated by manufacturers, current - time characteristics are usually presented as a curve with the spread in one graph, where the ratio of prospective current to the rated current is taken as a variable. However, as indicated in Table 2.2 and Fig. 2.15, because of different element materials (see 235 series), the slope for lifetime relationships may differ largely. Consequently, the lifetime relations can no longer be presented as one simple curve for all types of fuses in one series.

A higher slope means that as the  $I^2t$  value decreases, the lifetime increases faster. Figure 2.15 shows that the element made of nickel gives rise to the highest slope for the lifetime relationship, while the element made of alloys produces a low slope. Silver plated copper elements offer also a relatively high slope (217.001, 217002; 235001, 2351.25, 23501.6, 235002), while silver clad wire elements provide a low slope. It is then clear that silver plated copper wire elements give the best lifetime results for corrugated elements. Fuse elements made from nickel and silver plated copper have high melting points and a relatively high slope. In practice, fast acting fuses are normally made from the materials with high melting points, it is therefore suggested that fast acting fuses are better than time lag fuses, as the number of current pulses for fuses to withstand is concerned.

## 2.5 Conclusions

In this chapter, lifetime experiments of miniature fuses for short current pulses were performed. According to statistical analysis for the time lag fuses (Littelfuse type 218.800), lifetimes of fuses can be described by the Weibull distribution, using  $I^2t$  as a characteristic. During the lifetime of fuses, resistance increases as fuses are subjected to short current pulses with the pulse time in order of 10 ms. The value of resistance increase before breaking is about 10% for the time lag fuses studied (Littelfuse type 218.800).

Lifetime is mainly determined by the  $I^2t$  value of current pulses, the wave shape of current pulses has a secondary influence on the lifetime of fuses. From the regression analysis, the lifetime of fuses is found to decrease exponentially with the  $I^2t$ . The slope of the line (the fuse lifetime as a function of the  $I^2t$  of the pulsed current) is from 7 to 20 for most miniature fuses. To improve the lifetime of fuses, the high steepness or slope is desired.

From comparisons of lifetime relationships for different fuses in Table 2.2, silver plated copper is considered to be a good material for fuse elements. Withstand abilities for time lag fuses are generally not so good as fast acting fuses on the basis of the relative  $I^2t$  value, which is contradictory to common practice.

## Chapter 3 Lifetime Experiments with Long Current Pulses

In Chapter 2, lifetime studies have been performed on the basis of experimental observations when miniature fuses are subjected to short current pulses. In normal service, fuses may also carry low currents with a long conducting time either cyclic or continuous. Fuses are expected not to operate also under these circumstances.

In situations of frequent switching, fuses experience cyclic loading. In IEC publication: 127 miniature fuses, endurance tests are specified to evaluate the quality of fuses to withstand long time cyclic currents. The pulse time is required to be one hour, followed by a period of 15 minutes without current. This duty should be repeated 100 times.

The question here is whether fuses still fulfil their tasks after these tests. Therefore, the objective of this chapter is to evaluate fuse lifetimes for more extended current cycles and amplitudes. This chapter covers endurance studies for miniature fuses during long pulse time current pulses and continuous loading. On the basis of experimental observations, the number of current pulses is related with the pulse current and the on time, using statistical analytic methods based on the Weibull distribution.

### 3.1 Experiments

#### 3.1.1 Test objects

Commercial miniature fuses (Littelfuse Series 218.800) were chosen as test objects. The technical data have been discussed already in Chapter 2.

#### 3.1.2 Test method

To investigate the deformation of fuses and monitor the long term fatigue process, experiments were performed for current pulses with different magnitudes and pulse times. Resistance increase has been noticed as an indicator of fatigue [65] for electrical interconnections. Therefore, during the experiments, resistance was measured between current pulses by using the four terminal method. Numbers of current pulses which fuses withstood were collected. The experimental set-up for this study is the same as shown in Fig. 2.5.

To get comparable results with endurance tests specified in IEC 127 miniature fuses, the first experiment was performed for different currents with the same on and off times as stated in IEC 127 (one hour on and 15 minutes off).

Before the test started, initial voltages across the fuse-link were measured. A testing current  $I$  specified from  $1.2 \cdot I_n$  up to  $1.8 \cdot I_n$  flowed through the fuse-link for a period  $t_{on}$  of one hour, where  $I_n$  was the rated current of the fuse. One minute before the end of the on time  $t_{on}$ , the voltage across the fuse-link was measured and stored in the computer. The current was then switched off for a period  $t_{off}$  of 15 minutes.

To investigate the influence of the current pulse time  $t_{on}$ , the second experiment was carried out with a changeable pulse times  $t_{on}$  in range from 10 seconds to 10 minutes.

The third experiment was performed to examine whether the resistance would change due to a continuous d.c. current ( $I = 1.5 * I_n$ ). The test lasted about 250 hours.

## 3.2 Results

### 3.2.1 Endurance

From the first experiment, resistance changes were obtained and found to increase with the number of current pulses. Figure 3.1 shows typical results of resistance increase percentages for eight fuses until all fuses interrupted, where  $R_0$  is the cold resistance. The test current was 1.5 time the rated current with  $t_{on} = 1$  hour and  $t_{off} = 15$  minutes. This graph indicates that resistances may increase up to 50% before fuse blowing.

For current pulses with 1.4 to 1.7 times the rated current, the final resistance increase before fuse blowing is presented in Fig. 3.2, where  $R_0$  is the cold resistance. Above 1.5 times the rated current, the resistance change decreases. Extrapolation of the results indicates that above 1.9 times the rated current, resistance increases do not occur before final fuse operation. This value is in agreement with the minimum fusing current according to characteristics from the fuse manufacturer. For currents smaller than 1.5 times the rated current, it seems that the resistance increases slowly and tends to approach a constant value.

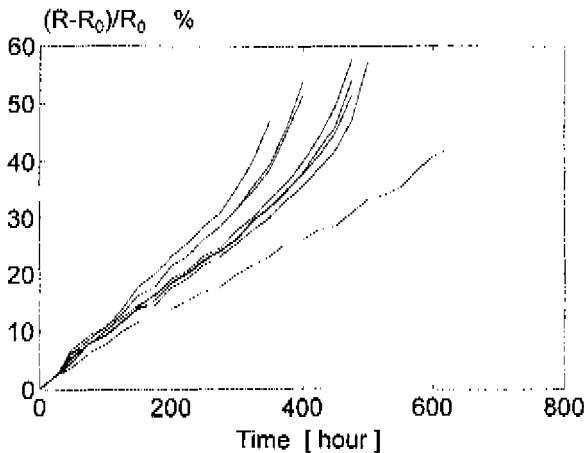


**Figure 3.1** Resistance increase as a function of time during current pulses for 8 fuses with  $I = 1.5 I_n$ ,  $t_{on} = 1$  hour,  $t_{off} = 15$  minutes

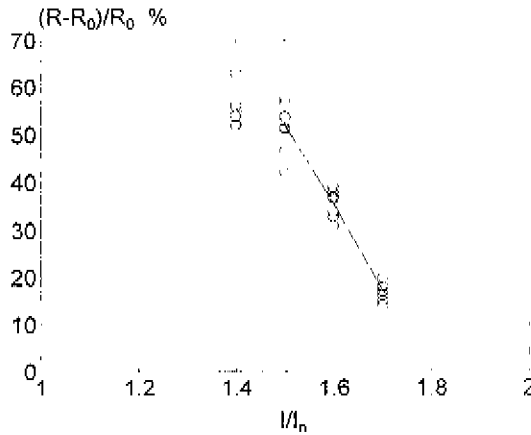


**Figure 3.2** Final resistance increase in endurance tests

From the endurance experiments, for currents with one hour on time and 15 minutes off time, results are summarised in Table 3.1.

**Table 3.1** Results from extended endurance tests

| $I/I_n$<br>( $I_n = 800 \text{ mA}$ ) | the minimum number<br>of current pulses<br>from 20 fuses (5% value) |
|---------------------------------------|---|
| 1.5                                   | 91  |
| 1.6                                   | 19  |
| 1.7                                   | 2   |
| 1.8                                   | 1   |

### 3.2.2 Influence of the on time on lifetimes

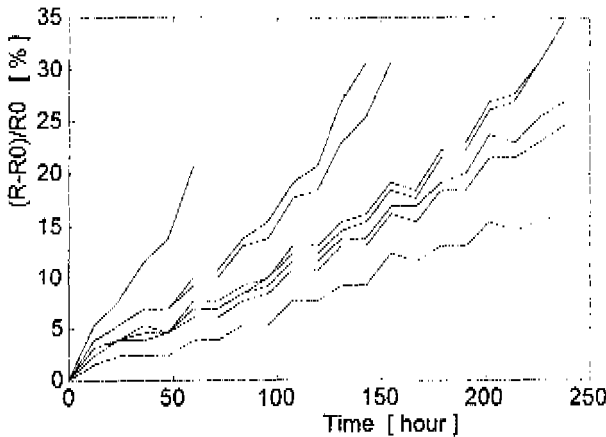
From the second experiment, numbers of current pulses which fuses withstood were obtained in Table 3.2. The testing current  $I$  varied from 1.4 A to 1.7 A with the on time  $t_{on}$  from 1/6 to 10 minutes,  $t_{off}$  from 1 to 5 minutes.

After fuses were subjected to long current pulses, resistance was found to increase. For practical applications, it is also of importance to know whether this is true for continuous loading. Figure 3.3 gives an impression of the gradual resistance increase for a typical current of 1.5 times the rated current.



**Table 3.2** Number of current pulses fuses withstood

| $I$<br>[A] | $t_{on}$<br>[min] | $t_{off}$<br>[min] | Number of Current Pulses |     |     |     |     |     |     |     |      |      |
|------------|-------------------|--------------------|--------------------------|-----|-----|-----|-----|-----|-----|-----|------|------|
|            |                   |                    | 416                      | 435 | 816 | 868 | 102 | 107 | 110 | 114 | 1298 | 1455 |
| 1.41       | 1                 | 1                  | 416                      | 435 | 816 | 868 | 102 | 107 | 110 | 114 | 1298 | 1455 |
| 1.52       | 1                 | 1                  | 148                      | 113 | 20  | 75  | 26  | 74  | 94  | 117 | 24   | 110  |
| 1.58       | 1                 | 1                  | 3                        | 4   | 7   | 10  | 13  | 14  | 15  | 19  | 30   | 59   |
| 1.62       | 1                 | 1                  | 2                        | 2   | 3   | 4   | 5   | 5   | 6   | 6   | 8    | 9    |
| 1.47       | 5                 | 5                  | 18                       | 38  | 49  | 54  | 63  | 66  | 80  | 109 | 109  | 127  |
| 1.52       | 5                 | 5                  | 5                        | 8   | 8   | 15  | 16  | 20  | 20  | 26  | 30   | 49   |
| 1.58       | 5                 | 5                  | 1                        | 1   | 2   | 3   | 4   | 4   | 6   | 7   | 9    | 1    |
| 1.50       | 5                 | 1                  | 1                        | 4   | 5   | 7   | 10  | 11  | 15  | 18  | 25   | 33   |
| 1.47       | 10                | 1                  | 11                       | 13  | 20  | 22  | 26  | 29  | 34  | 34  | 36   | 67   |
| 1.42       | 10                | 1                  | 69                       | 88  | 95  | 112 | 119 | 120 | 137 | 155 | 183  | 232  |
| 1.52       | 10                | 1                  | 10                       | 13  | 11  | 2   | 8   | 9   | 9   | 2   | 9    | 15   |
| 1.37       | 10                | 1                  | 334                      | 152 | 295 | 393 | 385 | 427 | 368 | 410 | 174  | 261  |
| 1.52       | 10                | 1                  | 1                        | 2   | 9   | 7   | 10  | 8   | 12  | 8   | 14   | 8    |
| 1.53       | 1/6               | 1                  | 683                      | 156 | 663 | 632 | 342 | 131 | 739 | 910 | 2013 | 1002 |
| 1.58       | 1/6               | 1                  | 41                       | 91  | 115 | 117 | 161 | 163 | 174 | 181 | 230  | 241  |
| 1.61       | 1/6               | 1                  | 98                       | 170 | 62  | 36  | 56  | 37  | 45  | 23  | 61   | 24   |
| 1.72       | 1/6               | 1                  | 9                        | 6   | 10  | 5   | 7   | 2   | 8   | 4   | 3    | 4    |
| 1.47       | 1/6               | 1                  | 650                      | 313 | 272 | 155 | 190 | 325 | 221 | 328 | 1769 | 6107 |

**Figure 3.3** Resistance increase at a continuous current  $1.5 I_n$  for eight fuses

### 3.3 Resistance changes

From experiments it can be concluded that for continuous loading as well as current pulses, resistance increases. For a typical current of 1.5 times the rated current, cyclic loadings result in a higher value of the final resistance increase about 50% in average. For continuous loadings with the same current, the final resistance increase is about 25%. On the other hand, fuses may allow a shorter service time (about 200 hours) for continuous loadings, in contrast to the time for cyclic loadings (about 500 hours).

In the IEC recommendations, it was suggested that endurance tests provided a qualification for fuses in the normal service, where both continuous loading and cyclic loading are involved. However, comparisons of both situations show a discrepancy in resistance increase between our experimental results and IEC recommendations. At this moment, no physical explanation has been found and further studies are needed. It is therefore suggested that more concerns should be added in the IEC recommendations for these aspects.

### 3.4 Lifetime relationships

Figure 3.4 and Fig. 3.5 show lifetime distributions on the Weibull paper for different experimental conditions from Table 3.2.

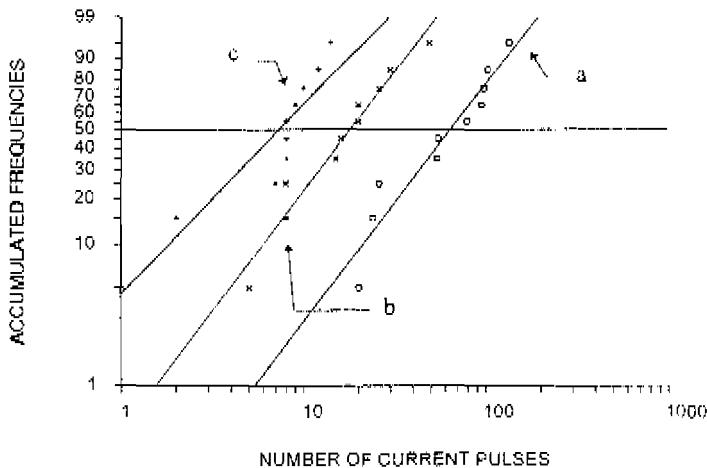


**Figure 3.4** Distribution of number of current pulses fuses withstood

a :  $I = 1.52$ ,  $t_{on} = 1$  minute,  $t_{off} = 1$  minute

b :  $I = 1.52$ ,  $t_{on} = 5$  minutes,  $t_{off} = 5$  minutes

c :  $I = 1.52$ ,  $t_{on} = 10$  minutes,  $t_{off} = 1$  minute

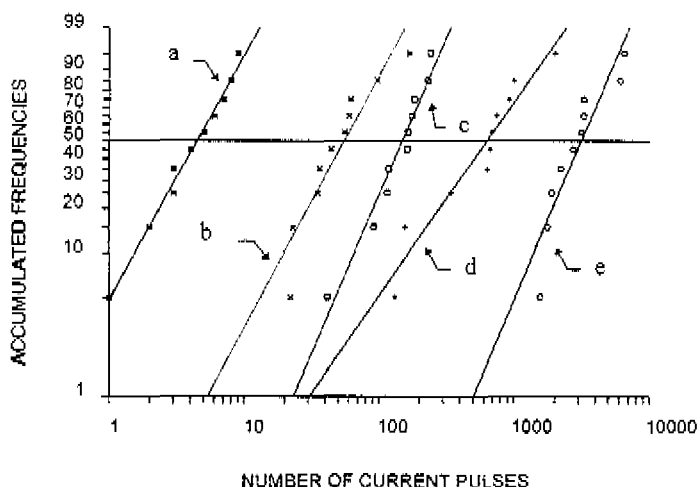


**Figure 3.5** Distribution of number of current pulses fuses withstood  
 $t_{on} = 10$  seconds,  $t_{off} = 1$  minute  
 a :  $I = 1.72$ , b :  $1.61$ , c :  $1.58$ , d :  $1.53$ , e :  $1.47$  A

It may be seen that in general the data agree reasonably well with a straight line on Weibull paper. It is therefore concluded that the lifetime distribution obeys Weibull distribution. Another feature is that for different current parameters the slopes of regression lines ( $\beta$ ) are approximately the same.

In Chapter 2, it has been demonstrated that for short current pulses the  $I^2t$  value of a current pulse can be used as a parameter in the prediction of fuse lifetimes. However, for a long pulse time current, because much energy is transferred to end caps and surroundings, induced deformation can not be expected to be simple expressions of the  $I^2t$  value. Therefore alternatives should be found.

Attempts in this chapter are to resolve the problem based on statistical approaches. To comply this task, experimental data for lifetimes (numbers of current pulses which fuses withstood) will be used to estimate the 5%, 95% values and the mean of fuse lifetimes for a specific current pulse. Once these estimations are available, the effort is to define an expression in general.

The visual examination (see Figs. 3.4 and 3.5) has shown that lifetimes obey the Weibull distribution. Using lifetime data in Table 3.2, the maximum likelihood method is adopted to find the scale and shape parameters of the distribution. Results of the scale and shape parameters ( $\lambda$ ,  $\beta$ ) from estimations are summarised in Table 3.3.

Table 3.3 shows a number of experimental lifetimes and derived parameters for the Weibull distribution. To enable a comparison of the different results, it is suggested to use regression analysis on the basis of statistical results.

**Table 3.3** Parameter estimations according to Table 3.2

| $I$<br>[A] | $t_{on}$<br>[min] | $t_{off}$<br>[min] | 5%   | mean<br>$N$ | 95%  | $\lambda$ | $\beta$ |
|------------|-------------------|--------------------|------|-------------|------|-----------|---------|
| 1.41       | 1                 | 1                  | 460  | 963         | 1466 | 0.0009    | 3.5     |
| 1.52       | 1                 | 1                  | 20   | 80          | 158  | 0.011     | 2.0     |
| 1.58       | 1                 | 1                  | 1.7  | 17.4        | 45.8 | 0.0053    | 1.2     |
| 1.62       | 1                 | 1                  | 1.7  | 5           | 8.9  | 0.17      | 2.4     |
| 1.47       | 5                 | 5                  | 22.4 | 71          | 129  | 0.012     | 2.3     |
| 1.52       | 5                 | 5                  | 3.8  | 19.7        | 42.4 | 0.045     | 1.7     |
| 1.58       | 5                 | 5                  | 0.6  | 3.8         | 8.9  | 0.23      | 1.5     |
| 1.50       | 5                 | 1                  | 1.5  | 13          | 32   | 0.071     | 1.3     |
| 1.47       | 10                | 1                  | 7.9  | 29          | 56   | 0.03      | 2.1     |
| 1.42       | 10                | 1                  | 54.7 | 131         | 211  | 0.0068    | 3.0     |
| 1.52       | 10                | 1                  | 2.8  | 8.8         | 15.7 | 0.1       | 2.3     |
| 1.37       | 10                | 1                  | 177  | 319         | 455  | 0.0028    | 4.3     |
| 1.52       | 10                | 1                  | 2.1  | 7.9         | 15   | 0.11      | 2.1     |
| 1.53       | 1/6               | 1                  | 108  | 726         | 1688 | 0.0012    | 1.5     |
| 1.58       | 1/6               | 1                  | 60   | 151         | 248  | 0.0059    | 2.9     |
| 1.61       | 1/6               | 1                  | 11   | 60          | 135  | 0.015     | 1.6     |
| 1.72       | 1/6               | 1                  | 1.2  | 4.8         | 9.4  | 0.18      | 2.0     |
| 1.47       | 1/6               | 1                  | 914  | 3244        | 6174 | 0.0002    | 2.1     |

For different current parameters, a comparable constant slope ( $\beta$ ) has been found in the Weibull distribution plot (see Figs. 3.4 and 3.5). Therefore, the slope  $\beta$  may be assumed to be independent of the on time  $t_{on}$  and the off time  $t_{off}$  at a reference current or vice versa. On the other hand, the scale parameter  $\lambda$  increases as the  $I^2 t$  value of pulsed current increases for the same on time  $t_{on}$ . This suggests that the scale parameter  $\lambda$  depends on the current  $I$  and the on time  $t_{on}$ . Because for  $I^2 t \rightarrow 0$  there is no damage to the fuse element, a trivial expression for  $\lambda$  is recommended as

$$\lambda = a_0 (I^x t_{on}^y)^k$$

where  $x > 0$ ,  $y > 0$ ,  $k > 0$  and  $a_0 > 0$ . The physical meaning of this expression is that for any current pulses, fuses have infinite lifetimes as long as either the current  $I$  or the on time  $t_{on}$  is zero.

First, a reference mean value is taken as  $E[\tau_0(I, t_{on})]$  for  $\lambda_0$ . According to the definition of the mean value of the distribution, the ratio of the expected mean value ( $N = E[\tau(I, t_{on})]$ ) for a specific current pulse to the reference mean value  $E[\tau_0(I, t_{on})]$  is given by

$$\frac{E[\tau(I, t_{on})]}{E[\tau_0(I, t_{on})]} = \frac{\lambda_0}{\lambda(I, t_{on})}$$

It follows that the number of current pulses  $N$  can be approximated by

$$\log_{10} N = A_n - k \log_{10} I^n t_{on}^y \quad (3.1)$$

Introducing regression analysis into this expression, coefficients in Eq. 3.1 are found to be

$$x = 11, y = 0.5, k = 2.45, A_n = 9$$

The values of  $k$  and  $A_n$  corresponding to the 90% confidence level are estimated to be

$$k_{min} = 2.4, k_{max} = 2.58, A_{n, min} = 8.8, A_{n, max} = 9.19$$

Comparisons of experimental observations and results of Eq. 3.1 are presented in Fig. 3.6.

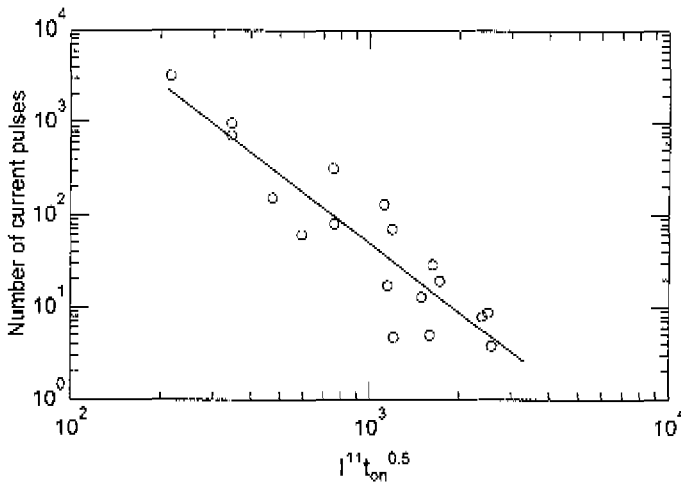


**Figure 3.6** Number of current pulses as a function of a combined parameter  $I^{11} t_{on}^{0.5}$

Because this relationship is derived from the experiments for long time current pulses, therefore predictions from the graph should provide a guidance for practical situations for the on times above 10 seconds. Using Eq. 3.1, the number of current pulses fuses withstood for different current pulses with the on time  $t_{on} = 1$  hour is predicted. Figure 3.7 shows comparisons of predictions with observations from Table 3.1. Mark "x" indicates observations corresponding to 5% value (Table 3.1). Mark "o" indicates observations for  $1.4 I_n$  and  $1.5 I_n$ . Three curves indicate results for 5% values, 95% values and the mean respectively.

However it should be kept in mind that predictions obtained are based on two conditions: the constant slope or shape parameter  $\beta$  and the scale parameter  $\lambda$  can be expressed as a power function of  $I^n t_{on}^y$ . The first condition is supported by experimental results which are shown in Figs. 3.4 and 3.5. The second condition is further derived from Figs. 3.4 and 3.5. Because a comparable constant slope  $\beta$  in Table 3.3 (in accordance with Weibull plots) has been demonstrated for high currents above  $1.5 I_n$ . For the current less than  $1.5 I_n$ , the slope tends to increase (see Table 3.3). This result provides the support for the resistance increase percentages, where the increase tendency has been found to saturate. Nevertheless, it may be clearly seen in

this graph that regression analysis on the basis of lifetime observations for the on time  $t_{on}$  from 10 seconds to 10 minutes may be used to predict lifetimes for much long pulse times (about 1 hour).

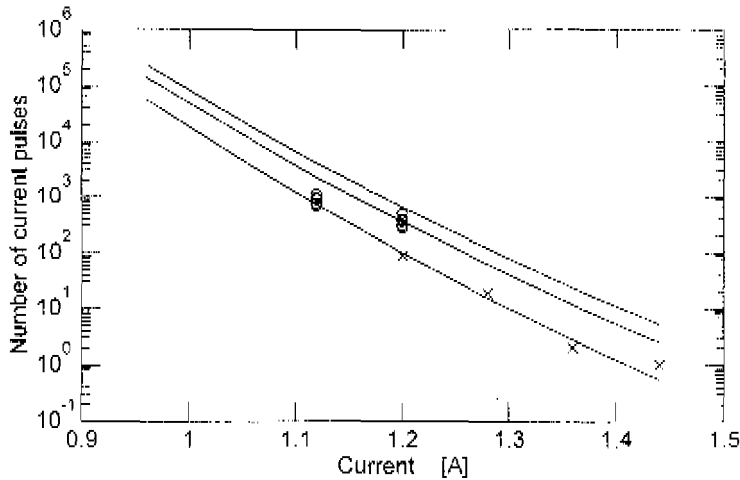


**Figure 3.7** Comparisons of predictions with observations relevant to endurance  
 Mark "x" : observed 5% values from Table 3.1  
 Mark "o" : observations for  $1.4 I_n$  and  $1.5 I_n$

### 3.5 Conclusions

From experimental studies, resistance is found to increase after fuses are subjected to long time current pulses or continuous loading. Observation shows that continuous loadings lead to small resistance increase compared with cyclic loading before fuse blowing. The resistance change before fuse breaking decreases as the magnitude of currents increases and tends to approach a constant value below 1.4 times the rated current for cyclic loading.

This work has proposed a method for combining statistical methods and regression analysis on the basis of observations. Using lifetime observations of different on and off times from 10 seconds to 10 minutes, estimations of lifetimes have been carried out. Based on these results comparison of predictions and observations for the on time 1 hour and off time 15 minutes are made and found to be in reasonable good agreement. This means that the time required to evaluate annoying endurance tests can be greatly reduced based on several short time experiments.

## Chapter 4 Experiments for Notched Strip Fuses

This chapter describes attempts to observe thermal buckling and deformation of notched fuse elements. Using high speed photography, motion of the element was observed and displacements were measured during current pulses. After fuses were subjected to current pulses, the surface of the fuse elements was examined by using electron scanning and optic microscopes.

Concerning previous investigations, ageing related with notched fuse elements may be roughly divided into four types: unreliable contacts [33] due to contact resistance increase; diffusion of metal interactions [13, 14]; thermal fatigue induced by temperature variations [35] (strain cycling) and electromagnetic reaction.

The prime objective of this chapter is to provide quantitative experimental observations for understanding physical phenomena related with lifetime reduction of fuses for silver notched strip elements. Thermal fatigue induced by short current pulses is assumed to be the only ageing mechanism. Three series experiments are intended to be performed: withstand ability of short current pulses, displacement measurements by using high speed photography and deformation studies by applying a scanning electron microscope and an optical microscope.

### 4.1 Experimental set-up

#### 4.1.1 Circuit scheme

To produce a pulsed current, a RLC circuit with ten parallel capacitor branches was realised [66]. Figure 4.1 shows the principle of the test circuit. Basically a capacitor and a thyristor formed a branch, and an inductance was used in series with a test object. First capacitors were charged by connecting them to a d.c. supply. After isolating the d.c. source, capacitors were then discharged by triggering thyristors. Consequently a current pulse was produced.

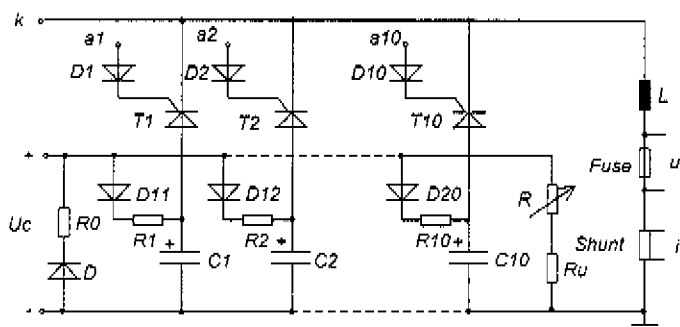


**Figure 4.1** Electrical circuit for producing the pulsed current  
 $L: 78.7 \mu\text{H}$ ,  $C: 114 +30/-10\% \text{ mF}$ ,  $\text{Shunt}: 60\text{mV}/100\text{A}$ ,  $T: T 24 \text{ N}$

Triggering signals of 120 mA were individually exerted on 10 thyristors to provide reliable triggering and to prevent damage of thyristors. The separate triggering circuit [51] is shown in Fig. 4.2.

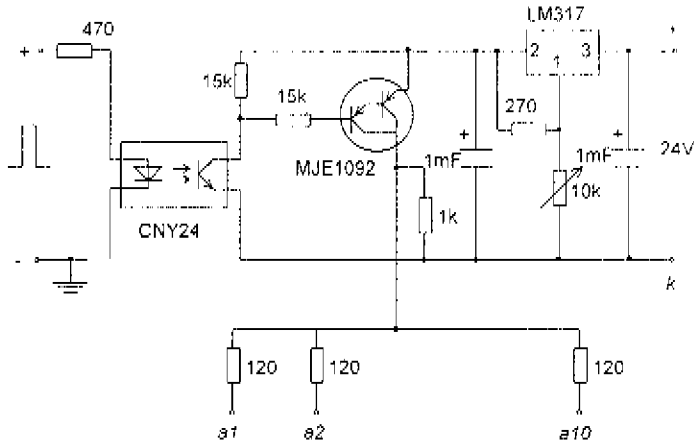


Figure 4.2 Triggering circuit

The test current from the circuit was of a half sinusoidal wave form, which can be characterised by parameters as  $I^2t$ ,  $I_p$ ,  $t_{on}$  (on time) and  $t_{off}$  (off time). The on time  $t_{on}$  is the conducting time for the pulsed current.  $I^2t$  is the integral of the current square over the on time.  $I_p$  is the peak value of the pulsed current. The off time  $t_{off}$  is the time between two successive pulsed currents.

#### 4.1.2 Peak current and $I^2t$ values

With the circuit shown in Fig. 4.1, a current peak value up to 2.8 kA can be produced, dependent on the charging voltage of capacitors. The shortest duration between two pulsed currents was chosen to be about 2 minutes, the on time for each current pulse can be chosen to be 5 ms or 9 ms.

Figure 4.3 shows measured peak currents and  $I^2t$  values as functions of the charging voltage of capacitors. Two curves indicate the peak current and  $I^2t$  value respectively for pulses with a duration of 9 ms.



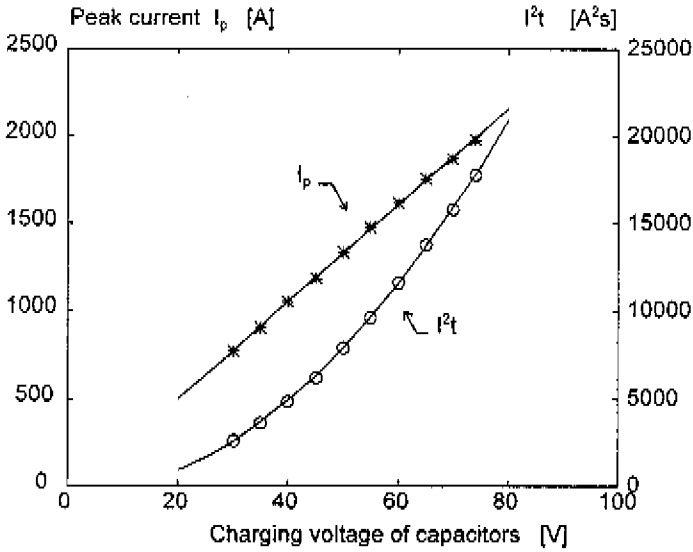


**Figure 4.3** Relationships between peak current,  $I^2t$  and charging voltage of capacitors

#### 4.1.3 Test objects

Commercial fuses (160 A and 660 V) for the semiconductor protection were chosen as test objects. Figure 4.4 shows a typical element geometry, where dimensions are given in millimetres. The thickness was 130  $\mu\text{m}$ . Elements of three typical shapes ("type A", "type C" and "type D") shown in Figs. 4.5, 4.6 and 4.7 were used in the lifetime tests.

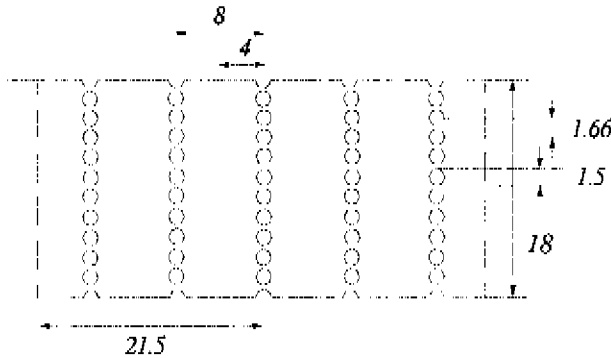


**Figure 4.4** Element geometry for type A, C, D and E

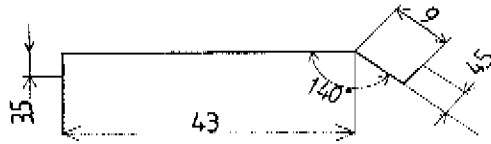


Figure 4.5 Type A

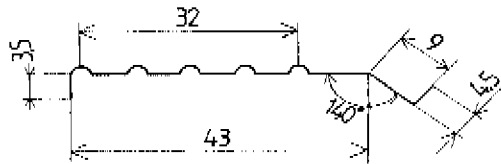


Figure 4.6 Type C

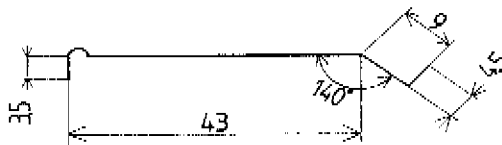


Figure 4.7 Type D

Because the element in commercial fuses for ratings of 160 A and 660 V has five rows of notches (see Fig. 4.4), it is difficult and time consuming to determine the displacement for each row at different currents. For this reason, straight fuse elements with five rows (*type E*) and one row (*type F*) of notches were proposed. Figure 4.8 shows the dimensions of fuse element "type F" composed of only one row of notches in the middle of the element. The overall size was the same as the elements used in commercial products.

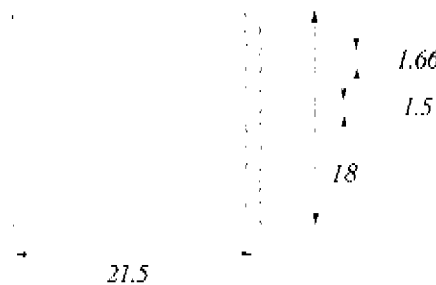


Figure 4.8 Notched element "type F" for displacement measurements

## 4.2 Lifetime experiments with short current pulses

Experiments for lifetimes were performed in Siba GmbH Germany for three types of commercial fuses: *Type A, C and D* (see Figs. 4.5, 4.6 and 4.7). The test circuit was given in Figs. 4.1 and 4.2. Both sand and bound sand were used as arc extinction materials in the ceramic body of fuses. The on time  $t_{on}$  was chosen to be 5 ms or 10 ms.

### 4.2.1 Results of lifetimes

In experiments, current pulses were applied to test objects until fuses blown. The number of current pulses which fuses withstand were obtained and summarised in Tables 4.1, 4.2 and 4.3.

**Table 4.1** Testing results of lifetime for type A fuse elements ( $t_{on} = 10$  ms)

| Filler type                | Sand                                     | Sand   |
|----------------------------|--|--|
| $I^2t \text{ A}^2\text{s}$ | 15800                                    | 14200  |
| Total samples              | 8  | 19   |
|                            | 26, 29, 54, 86,<br>103, 187, 190,<br>326 | 72, 158, 182, 195, 273, 276, 323, 345,<br>372, 383, 508, 621, 741, 939, 969, 1161,<br>1232 |

**Table 4.2** Testing results of lifetime for type C fuse elements

| Filler                     | Sand                      | Bound                        | Sand                                 | Sand   | Sand   | Bound                           | Bound  |
|----------------------------|---------------------------|------------------------------|--------------------------------------|--|--|---------------------------------|--|
| $I^2t \text{ A}^2\text{s}$ | 10735                     | 10961                        | 14280                                | 15082  | 15400  | 15082                           | 15400  |
| $t_{on}$ ms                | 5                         | 5                            | 10                                   | 10   | 10   | 10                              | 10   |
| Samples                    | 4                         | 4                            | 5                                    | 14   | 14   | 4                               | 6  |
|                            | 76<br>299<br>1027<br>1173 | 1328<br>1525<br>1755<br>1811 | 1754<br>1865<br>2732<br>2863<br>3213 | 305, 545,<br>685, 741,<br>753, 795,<br>951, 1060,<br>1197,<br>1284,<br>1374,<br>1399,<br>1530,<br>1901 | 93, 190,<br>223, 457,<br>482, 503,<br>624, 625,<br>737, 860,<br>861, 876,<br>1131,<br>1799 | 2249<br>>5000<br>>5000<br>>5000 | 2794<br>4288<br>>5000<br>>5000<br>>5000<br>>5000 |

**Table 4.3** Testing results of lifetime for type D fuse elements

| Filler                     | Sand                      | Bound                      | Sand  | Sand   | Bound                            | Bound                        |                                  |
|----------------------------|---------------------------|----------------------------|---|--|----------------------------------|------------------------------|----------------------------------|
| $I^2t \text{ A}^2\text{s}$ | 10735                     | 10961                      | 15082   | 15400  | 15082                            | 15400                        |                                  |
| $t_{in} \text{ ms}$        | 5                         | 5                          | 10  | 10   | 10                               | 10                           |                                  |
| Samples                    | 4                         | 4                          | 6   | 15   | 4                                | 5                            |                                  |
|                            | 23<br>460<br>1161<br>2164 | 200<br>225<br>701<br>>5000 | 1934,<br>2438,<br>2722,<br>4410,<br>>5000<br>> 5000 | 1169,<br>1502,<br>1508,<br>1839,<br>2200,<br>3281,<br>3281,<br>3633,<br>4213, >5000,<br>>5000, >5000 | 1248,<br>1649,<br>2261,<br>3424, | 1082<br>1236<br>1843<br>1927 | 231<br>423<br>556<br>767<br>4360 |

#### 4.2.2 Lifetime distribution and prediction

Because so many parameters influence the lifetimes of fuses (see Tables 4.1-4.3), first, statistical approaches are used to find the lifetime distribution. Figure 4.9 shows lifetime distributions on the Weibull paper [63] for a typical fuse element (*type C*) for different  $I^2t$  values, experimental results in Table 4.2 were used. It may be seen that in general the data are well fitted with straight lines on the Weibull probability plot. It is therefore concluded that the lifetime distribution obeys the Weibull distribution.

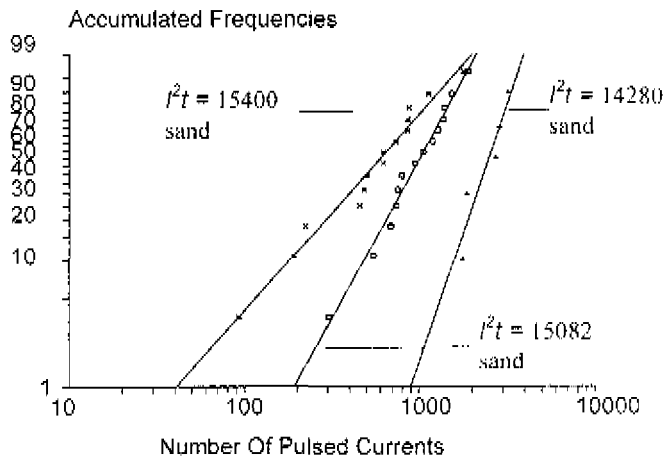


**Figure 4.9** Lifetime distributions on the Weibull probability plot for type C element at different  $I^2t$  values

For different types of fuse elements, the slope parameter of the Weibull distribution are often found to vary with the  $I^2t$  value of current pulses. However, it also has been noticed that for certain experiments, this slope keeps the same, for example, results in Table 4.1. In attempting to present a simple relationship between lifetime and  $I^2t$  value, the slope is assumed to be a constant. From this point, the ratio of mean lifetimes  $E[\tau(I^2t)]$  is given by

$$\frac{E[\tau(I^2t)]}{E[\tau(I^2t_0)]} = \frac{\lambda_0}{\lambda(I^2t)} \quad (4.1)$$

where  $I^2t_0$  is the reference  $I^2t$  value and  $\lambda_0$  is the scale parameter of the Weibull distribution at  $I^2t_0$ . Further the relationship is expressed as

$$\log_{10} N = \log_{10} N_0 - \log_{10} \frac{\lambda(I^2t)}{\lambda_0} \quad (4.2)$$

where

- $N_0$ : the mean value of lifetime at the reference  $I^2t$  value  
 $N$ : the mean value of lifetime ( $N = E[\tau(I^2t)]$ )

Because of no damage to the fuse element for  $I^2t = 0$ , a trivial expression for  $\lambda$  is suggested to be

$$\lambda = a_0 (I^2t)^k \quad (4.3)$$

This implies that for  $I^2t = 0$ , fuses should have infinite lifetimes. It follows that the lifetime  $N$  can be approximated by

$$\log_{10} N = \log_{10} N_0 - \log_{10} \frac{a_0}{\lambda_0} - k \log_{10} I^2t \quad (4.4)$$

Eq. 4.4 provides a linear extrapolation for the lifetime determinations on the double logarithmic scale. However, it should be kept in mind that the result here is obtained based on the assumption that the constant slope or shape parameter and the scale parameter can be expressed as a power function of  $I^2t$  value.

### 4.2.3 Comparisons with literature contributions

Using different expressions of the scale parameter  $\lambda$  leads to the different lifetime relationships:

- (1) assuming  $\lambda$  is dependent on the temperature rise  $\theta$  of the fuse element

$$\lambda = a_0 \theta^k \quad (4.5)$$

- (2) assuming  $\lambda$  is dependent on the temperature rise  $\theta$  and the average temperature  $\theta_{av}$  at the hottest spot of the fuse element

$$\lambda = a_0 (\theta \theta_{av}^x)^k \quad (4.6)$$

where  $a_0$ ,  $x$  and  $k$  are constants.

From Eq. 4.5 the lifetime expression similar to that proposed by Arai [35] can be achieved, while from Eq. 4.6 the lifetime expression similar to that suggested by Wilkins [67] can be obtained.

### 4.3 Motion of notched elements

To understand physical phenomena of lifetime consumption related with motion of elements, quantitative observations of motion are to be provided from experiments.

#### 4.3.1 Set-up for measuring displacements

Figure 4.10 shows an illustration of the experimental set-up for measuring the displacement during a current pulse. Fuse elements are normally surrounded by sand and not visible to the outside. To confirm whether the fuse element moves or not when a current is exerted, a dummy fuse was used for observations. In the dummy fuse, one edge of the fuse element faced a glass plate, the distance between the plate and the element was smaller than the grain size of sand so that the element can be easily monitored. In such a way, the influence of the plate on the possible element motion can be neglected. Sand packing density for fuses is examined to be approximately the same as for commercial products. A high speed camera was located in front of the fuse. A flash light was positioned at an angle of about  $45^\circ$  between the plate. To determine the exact exposure time, a light detector was installed to pick up the light signal. A four channel digital oscilloscope was used to record fuse current, voltage, an opening signal from the camera shutter and a signal related with the exposure period due to a flash light.

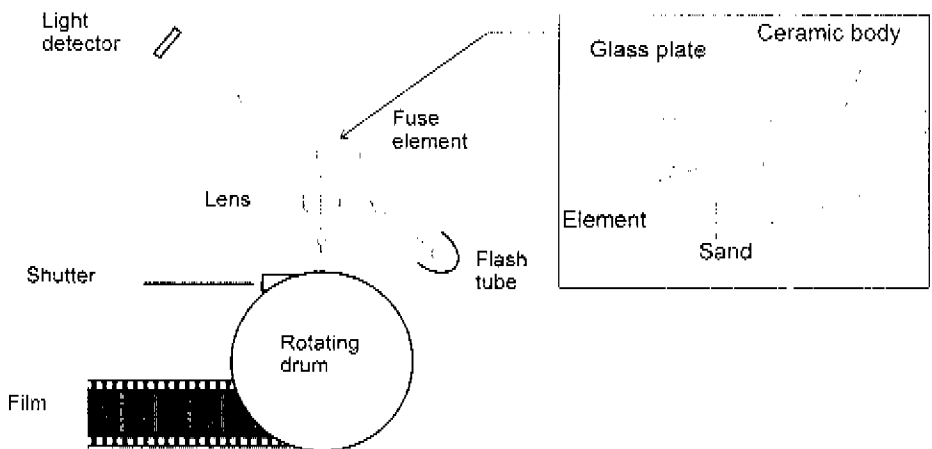


**Figure 4.10** Experimental set-up for measuring displacements

#### 4.3.2 Results

Typical traces recorded by a four channel digital oscilloscope are displayed in Fig. 4.11, the current was produced by charging capacitors to about 70 volts. During a current pulse, the corresponding voltage across the fuse was measured. The closing contact of the high speed camera indicated the shutter release, produced an action signal about 3 ms before current pulses were triggered and this shutter releasing signal was sent to the oscilloscope. An optical sensor was installed to pick up the light signal which indicated film exposure period. The exposure took place about  $900 \mu\text{s}$  before electric current flowed.

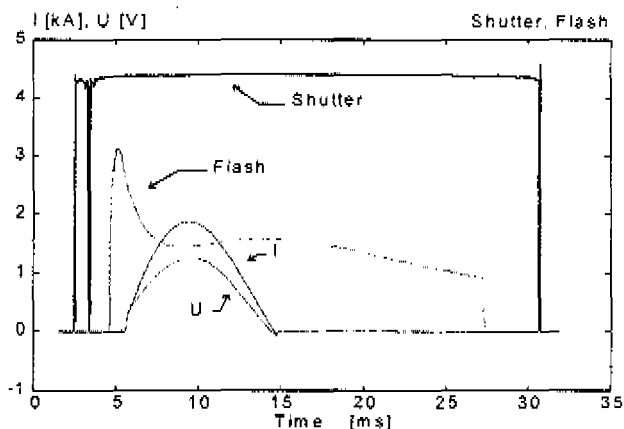


**Figure 4.11** Typical oscilloscope traces for measuring displacements  
*I* : current; *U* : voltage

Displacements at the element notch were measured for different  $I^2t$  values of pulsed currents. The element thickness  $135 \mu\text{m}$  was taken as the measuring reference, measuring accuracy was within  $\pm 8 \mu\text{m}$ . Figure 4.12 shows typical displacements of the element at two locations (point 1 at the notch edge and point 2 at a distance of 1 mm along the strip) together with the pulsed current against time.

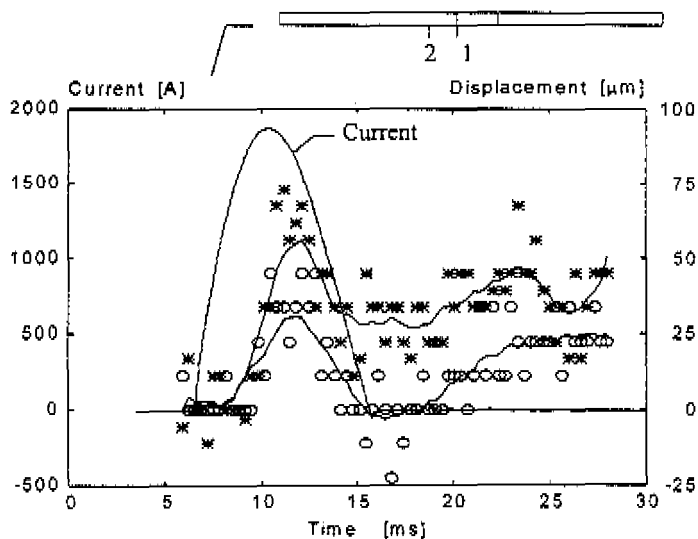


**Figure 4.12** Measured dynamical displacement induced by pulsed current  
 \*—\* : displacement at location 1; o—o : displacement at location 2

As shown in Fig. 4.12, the element started to move in about 2 ms. after the current was exerted. Slightly after the current peak, the element arrived at the maximum displacement in about 7 ms after current conducting. As the current decreased, the element moved gradually backwards. After the current reached zero, the element still needs time (at least 15 ms in this case) to move back to its original position.

In addition to these displacement measurements, two standstill points were found to be spaced about 5 mm across the notch for current pulses with different  $I^2t$  values. For the straight fuse elements with five rows of notches (see Fig. 4.4), high order buckling shapes have been observed. Significant displacements were detected at one or more notch locations. For quantitative analysis, more experiments are needed.

### 4.3.3 Discussion

Thermal expansion is proportional to the temperature rise, thus the compressive force due to expansion in the element increases with temperature. If this compressive force exceeds a certain limit, motion of the element starts. This is similar to the process in miniature fuses to be described in Chapter 7.

The total thermal strain induced is also proportional to temperature rise, so in principle, the maximum displacement as a function of time should have a relation with the temperature trace. Supposing that the maximum displacement is corresponding to the maximum temperature rise of the element notch, then the maximum temperature of the notch may be expected at about 7 ms after current conducting according to Fig. 4.12. Because the displacement at the middle of the notch can not be measured directly, the displacement at the location  $l$  indicated in Fig. 4.12 can provide a rough approximation of the maximum displacement.

For compact sand, elasticity may be assumed. During the motion of the element, sand is compressed, a part of the energy is stored in sand. The compressive force in the element decreases with the temperature. In such a situation, sand acts as a compressed spring due to the movement of the fuse element. When the temperature of the element is below the value corresponding to the compressive force of sand (as a spring), sand pushes the element backwards. This probably explains why after current zero the element slightly oscillates (see Fig. 4.12), only after a rather long time, the element goes back to its original position.

Because of sand grains, one might also expect the element to move among grains, however, such a motion requires very high force in the axial direction. For the commonly used sand sizes (several hundred micrometers in diameter), this condition can not be fulfilled. This is confirmed by observations where the displacement profile has been found rather smooth along the element.

On the basis of observations in Section 4.3.1, the integral of current square and the corresponding time before the motion started can be defined as special parameters similar to the definitions of prearcing time and  $I^2t$ , which are noted as  $I^2t_b$  and  $t_b$  respectively. From measurements for different  $I^2t$  values of current pulses, these parameters at the motion starting moment can also be determined as functions of the  $I^2t$  value of pulsed currents.

Results related with these parameters are given in Figs. 4.13 and 4.14; as the  $I^2t$  value of current pulses increases, the time for motion to begin decreases. This leads to a reduction of the  $I^2t$  value for the motion starting. For the  $I^2t$  value below 3 kA<sup>2</sup>s (the peak current about 800 A), the movement will not start for the object under discussion. Because the maximum  $I^2t$  value in



Fig. 4.14 is near the melting  $I^2t$  for this element type, the maximum displacement for the tested element is limited within about  $100\ \mu\text{m}$  (see Fig. 4.14). This value is in the order of the element thickness ( $130\ \mu\text{m}$ ).

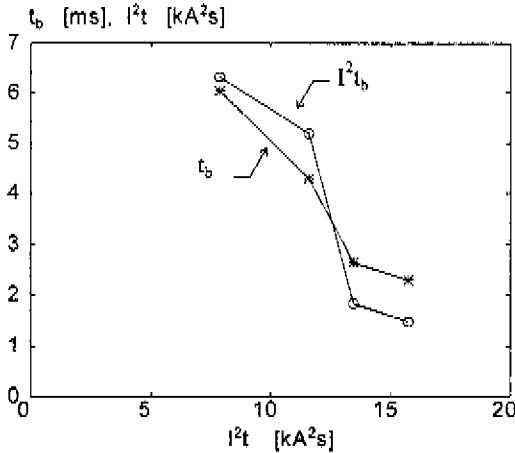


Figure 4.13 Motion starting time  $t_b$  and starting  $I^2t_b$  against  $I^2t$  of current pulses

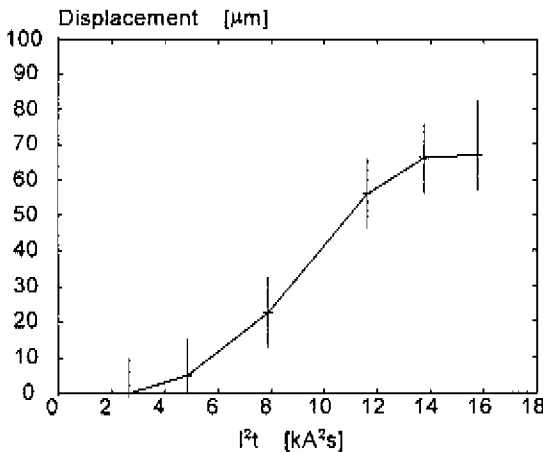


Figure 4.14 Measured maximum displacements as a function of the  $I^2t$  value of current pulses at the location 1 indicated in Fig. 4.12

#### 4.4 Minimum melting $I^2t$ value

As it has been introduced in Chapter 1 that the use of the minimum melting  $I^2t$  value can avoid unexpected interruptions in service. In addition, this criteria will be used in the lifetime

estimation in Chapter 9. This section describes efforts for determining the minimum melting  $I^2t$  values and presents experimental results.

Experimental set-up described in Section 4.1 was used to determine the minimum  $I^2t$  values for the two types ("type F" see Fig. 4.2 and "type E") of elements. Figure 4.15 shows measured results of the melting  $I^2t$  values for two types of elements.

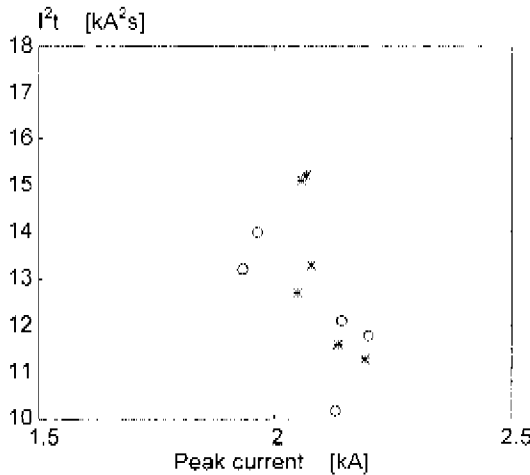


**Figure 4.15** Determination of the minimum melting  $I^2t$  value:  
 \* : Melting  $I^2t$  values type C  
 o : Melting  $I^2t$  values type F

In this graph, mark "\*" and mark "o" depict the melting  $I^2t$  values corresponding to different peak currents (or melting times). As the peak current increases above 2.1 kA, commercial fuses will blow. The melting time decreases with the peak current. For elements with one row of notches, similar results were obtained. It is therefore confirmed the minimum melting  $I^2t$  value is about 17 kA<sup>2</sup>s (see Fig. 4.15).

## 4.5 Microscopic study of deformation

After fuses were submitted to current pulses, notches were examined by a scanning electron microscope and an optical microscope. This section presents deformation studies for elements in commercial fuses ("type E" and "type C") with ratings of 160 A and 660 V.

### 4.5.1 Microscope view

After 100 pulsed currents with  $I^2t$  value of 14.7 kA<sup>2</sup>s, the fuse element was taken out from the ceramic body and put under the scanning electron microscope. Typical views of the new fuse element and the element after test are given in Figs. 4.16 and 4.17, where 150 amplification was used.

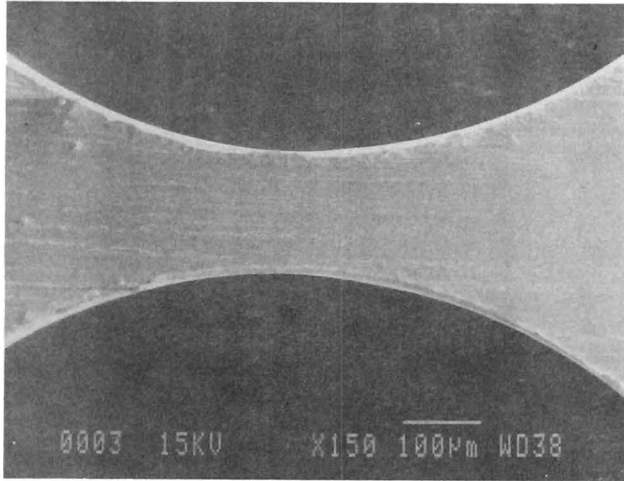


**Figure 4.16** SEM photo of a new element notch (type E)

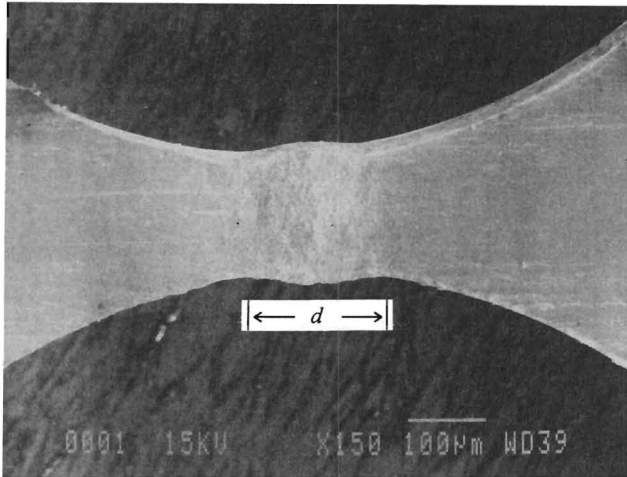


**Figure 4.17** SEM photo of an element notch after tests (type E)

From Fig. 4.16 it can be seen that scratches exist even for new fuse elements. After fuses are subjected to current pulses, plastic deformation is situated in the notch region and the surface becomes rough (see Fig. 4.17). The damage can be characterised by a length parameter  $d$  shown in Fig. 4.17 ( about 0.16 mm ).

### 4.5.2 Damage length distribution

For 22 samples "type C", the damage length of the middle row notches was measured by an optical microscope. The damage length  $d$  is described with the Weibull distribution, its density function  $f(d)$  ( $d > 0$ ) is expressed as

$$f(d) = \lambda^\beta \beta t^{\beta-1} \exp(-(\lambda d)^\beta) \quad (4.7)$$

Figure 4.18 presents experimental results of the damage length with calculated values for the density function of the Weibull distribution (the scale parameter  $\lambda = 1.38$ , the shape parameter  $\beta = 3.7$ ). The mean damage length is estimated to be 0.7 mm with the confidence interval [0.3, 1.0] at 10% confidence level.

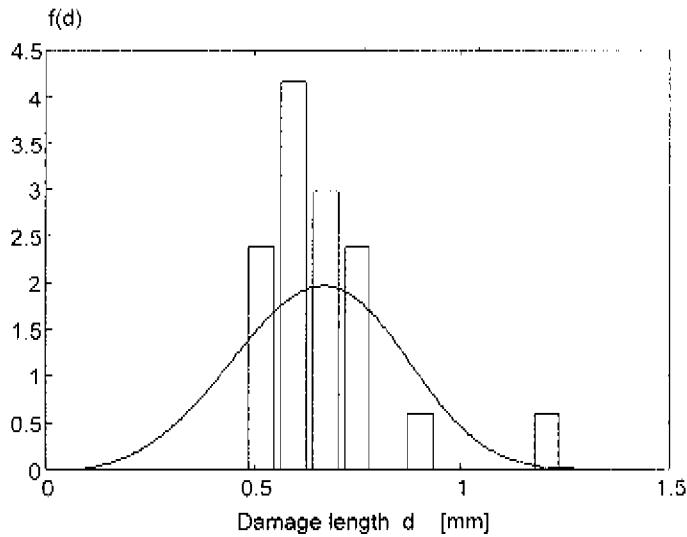


**Figure 4.18** The density function of the damage length (type C)  
*Bar* : observations;  
*Curve* : estimation

On the basis of Figs. 4.17 and 4.18, it is clear that the damage length increases after fuses are subjected to current pulses. This suggests resistance change of fuses during their life. However, prior to fuse breaking very small increase of resistance has been detected to be within the resistance spread of new products. It is therefore concluded that resistance measurements during the service of semiconductor protection fuses can not indicate the lifetime consumption before fuse breaking.

## 4.6 Conclusions

From the present studies, following main points are concluded:

- (1) The number of current pulses which fuses withstand is described with the Weibull distribution; it is also approximated as a linear function of  $I^2t$  value on the double logarithmic scale.
- (2) As fuses with sand fillers are subjected to current pulses, displacements of the fuse elements may take place during the fuse element heating up.
- (3) The maximum displacement of tested elements has been found to increase with the  $I^2t$  value of current pulses. However, experiments show that the maximum value is limited within  $100\mu\text{m}$  (in the order of the element thickness and notch width).
- (4) The minimum melting  $I^2t$  value of the tested objects has been found to be  $17 \text{ kA}^2\text{s}$ .
- (5) After flow of pulsed currents, plastic deformation is accumulated in the notch region. Scanning electron microscope pictures show that surface of the fuse element becomes rough as compared with new fuse elements. The damage length increases with the number of current pulses.
- (6) Existing methods for resistance measurements can not provide replacement information for semiconductor protection fuses in service.

## **Part III Thermal Modelling**

## Chapter 5 Nonlinear Thermal Modelling for Miniature Fuses

This chapter presents an electrical thermal analogue method for the heat transfer problems in miniature fuses. As in the foregoing, it has been stated that  $I^2t$  is a dominant factor for fuse ageing, therefore the related temperature change is. Numerical solutions of temperature distributions of the fuse element are found by solving the equivalent electrical network relations. Heat conduction, convection and radiation are considered for the fuse element. Non-linear behaviour related with material properties and heat convection are introduced. The thermal analysis is considered as the basis to enable cyclic stress determinations which on their turn are related directly to fuse ageing.

Because temperature values of thin fuse wire elements during the normal load are extremely difficult to measure, temperature changes should be calculated. During the last 20 years, several calculating methods have been proposed [6, 7, 8, 9, 10, 11, 12]. It has been demonstrated that the thermal problem can be modelled by its electrical equivalent [11]. Among many advantages, components in the networks have clear physical meaning. The convergence of numerical solutions is guaranteed [12] because of the existence of real components and their physical behaviour. Linear or constant material properties are normally used, effects of end caps are often omitted. For miniature fuses, a special request should be fulfilled for solving non-linear problems due to element materials and heat convection [25, 52].

To fulfil the task of simulating the temperature variations due to electric currents, in this chapter a thermal model will be developed on the basis of a thermal and electrical analogue scheme. It starts from the description of physical models according to the thermal process. Afterwards corresponding networks are described. A software package used for the electronic circuit analysis, is chosen to simulate networks because of its possibility to model components with lookup tables. In the simulation, heat conduction and storage within the end cap are considered. In addition, non-linear behaviour related with material properties and heat convection are used.

### 5.1 Thermal models

To be general, commercial miniature fuses with straight fuse wires were chosen as studying objects. The wire was positioned along the middle axis of a glass tube. To describe the thermal process of fuse wires due to electric currents, the fuse wire was divided into several axial segments between end caps. The diameters of the wire elements are  $50\ \mu\text{m}$  (nickel wire element) and  $103\ \mu\text{m}$  (silver clad wire element). The number of segments  $n$  can be arbitrary. In the thermal modelling, the following temperature can be distinguished:  $T_w$  (wire temperature),  $T_{wg}$  (temperature inside the glass tube) and  $T_a$  (air temperature outside the glass tube). The temperature at the same axial position  $z$  inside the wire element was assumed to be the same because the heat transfer in the element is much better than in air. Figure 5.1 shows geometry notations.

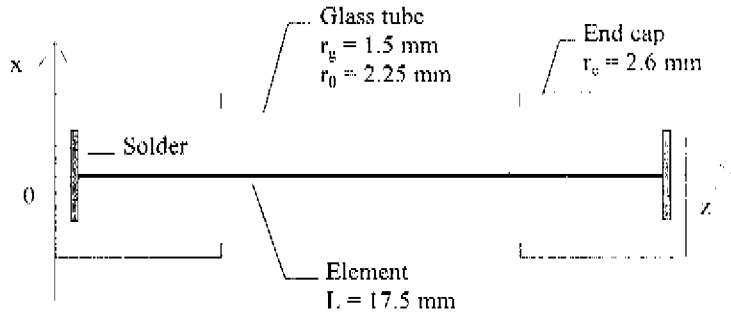


**Figure 5.1** Geometry notations of a miniature fuse

Basic thermal analysis used in the following can be found in literature [68, 69, 70]. For heat transfer due to the forced convection in the tube, the natural convection was assumed.

### Energy input

The Joule heating due to electric current  $i(t)$  within each segment obeys

$$P = i^2(t) \rho L / (n\pi r_d^2)$$

### Heat dissipation

The heat dissipation is contributed to the temperature rise of the wire, which is determined by the rate of temperature change, mass density, specific heat and the volume to be

$$q_s = \gamma c \Delta V \frac{\partial T}{\partial t}$$

### Heat conduction

The heat conduction along the wire is determined by the product of the temperature gradient along the wire, thermal conductivity and cross sectional area of the wire. It may be expressed by

$$q_z = -\lambda A \frac{\partial T}{\partial z}$$

### Heat convection

Heat loss caused by convection is determined by

$$q_c = hS(T_w - T_{mc})$$

The effect of heat convection [71, 72, 73, 74] can be represented by a resistance

$$R_{conv} = \frac{1}{Sh}$$

The cooling effect of convection is usually expressed by the Nusselt number  $Nu$

$$Nu = \frac{hx_f}{\lambda}$$



for a cylinder  $x_c$  is the diameter. Other relevant dimensionless numbers for the convection are the Prandtl number  $Pr$

$$Pr = \frac{c_p \mu}{\lambda}$$

and the Grashof number  $Gr$

$$Gr = g \beta (T_w - T_\infty) \frac{x_c^3}{\nu^2}$$

The Rayleigh number  $Ra$  is defined as

$$Ra = Pr * Gr$$

The Nusselt number is expressed as

$$Nu_w = 0.36 + 0.048 (Gr Pr)^{0.125} + 0.52 (Gr Pr)^{0.25}$$

under the following conditions:

- ◇ horizontal cylinder in geometry
- ◇ natural convection
- ◇ wire in air and with small diameter ( in order of 50  $\mu\text{m}$ )
- ◇  $10^{-7} < Gr Pr < 10^8$

### Heat radiation

The heat loss due to radiation may be approximated by [68, 69]

$$q_r = \sigma \varepsilon S (T_w^4 - T_\infty^4)$$

## 5.2 Analogies and circuits

On the basis of the descriptions in the above section for heat transfer, the thermal model can be rewritten in terms of electrical components by using the following analogues:

|                    |                       |
|--------------------|-----------------------|
| heat flow          | electric current      |
| temperature        | voltage               |
| thermal resistance | electrical resistance |
| thermal capacity   | electrical capacity   |

Table 5.1 shows equivalent expressions which represent electrical components according to the analogue [52, 75]. All parameters are temperature (voltage) dependent. In Table 5.1,  $T_\infty = 300$  K.

To establish a simulating scheme, the fuse was divided into similar axial segments between the end caps. Because of symmetry, only half of the element was necessary to be simulated. Figure 5.2 shows subcircuits of one segment and one half segment. The subcircuit of the half segment was connected to the subcircuit of the end cap. Component parameters were determined by reorganising the thermal expressions, equivalent resistance and capacitance.

The end cap is assumed to be of a room temperature (typically 20 °C) during short current pulses (in order of 10 ms), because the end caps have a massive volume as compared with the wire element. It was represented by a fixed voltage source, in this situation the source was the circuit earth. For d.c. current or long time current periods, heat storage and conduction within the end

caps should be considered. This suggested that thermal behaviour of the end caps can be simulated by capacitors and resistors. Capacitors represented heat dissipation in the end caps, and resistors represented the conduction and convection loss in the end caps. The complete circuit for the simulation was formed by connecting all the sub circuits. The reference point in the electrical network for the 0 volt was chosen to be corresponding to 300 K.

**Table 5.1** Thermal and electrical analogues

|                 |  |
|-----------------|--|
| P               | $i^2(t) \frac{\rho(V) L}{n \pi r_d^2}$   |
| $R_{th, e}$     | $\frac{L}{2 \pi r_d' n \lambda(V)}$  |
| $R_{th, glass}$ | $\frac{n}{\lambda_{glass} * 2 \pi L} \ln \left( \frac{r_o}{r_i} \right)$             |
| $R_{rad}$       | $\frac{n}{\epsilon \sigma 2 \pi r_d L} \frac{1}{((V + T_a)^4 + T_a^4)(V + 2 * T_a)}$ |
| $R_{conv}$      | $\frac{n}{2 \pi r_d L h(V)}$   |
| $C_e$           | $\gamma_c \frac{L \pi r_d^2}{n} c_e(V)$  |
| $C_{air}$       | $\gamma_{air} \frac{L \pi (r_o^2 - r_i^2)}{n} c_{air}(V)$                            |
| $C_{glass}$     | $\gamma_{glass} \frac{L \pi (r_o^2 - r_i^2)}{n} c_{glass}(V)$                        |

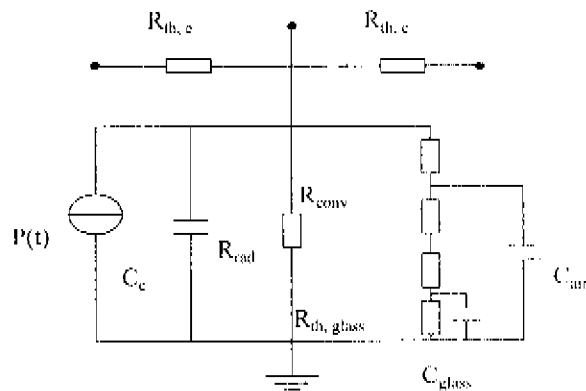


**Figure 5.2** Black box model for a segment and a half segment

To simulate the transient behaviour, an extra subcircuit for the time dependent current source is often necessary. In practice, electric current exerted to fuses does not always follow a well defined wave shape. For this reason, the digital values of current should be taken to form the subcircuit. Electric current is expressed as a function of time in a lookup table (time and current pairs). To introduce this table into the network, a piece wise linear function is used to convert time into voltage. Therefore numerically speaking, current as a function of time is equal to the voltage control current source in this subcircuit.

### 5.3 Applications

In Sections 5.1 and 5.2, descriptions for solving heat transfer problems related with miniature fuses have been provided. In the following, applications will be illustrated for two typical commercial miniature fuses. The first one is a fast acting fuse for a rated current of 315 mA, its element was made of pure nickel (length = 17.5 mm, radius  $r_d = 25 \mu\text{m}$ ). The second is a typical time delay fuse of which the element was made of silver clad wire (length = 17.5 mm, radius  $r_d = 51.5 \mu\text{m}$ ), the rated current was 800 mA. Simulated results of current - time characteristics, voltage response and resistance increase due to current pulses will be compared with experimental determinations.

#### 5.3.1 Fast acting fuses (Nickel element)

The technical data of fuses are as follows: Littelfuse type 217.315; rated voltage : a.c. 250 V; rated current : 315 mA; the melting  $I^2t$  value:  $0.13 \text{ A}^2\text{s}$ .

Temperature dependency of electrical resistivity  $\rho$  of nickel was used [52, 76]. For the heat storage within the nickel wire and the air inside the tube, temperature dependent values [68, 76] were used for the specific heat. For the thermal conduction in the axial direction along the wire and in the radial direction across the air, temperature dependent values of conductivity [68, 76] were used. For the glass tube, constant values [77] were used for the thermal conductivity ( $\lambda_{\text{glass}} = 1.95 \text{ W}\cdot\text{m}^{-1}\cdot\text{K}^{-1}$ ) and the specific heat. The emissivity for nickel was taken to be 0.23. Component parameters for  $n = 7$  in the simulation circuit were determined by introducing the material properties. Figures 5.3 to 5.8 show their numerical results of components as functions of the segment temperature.

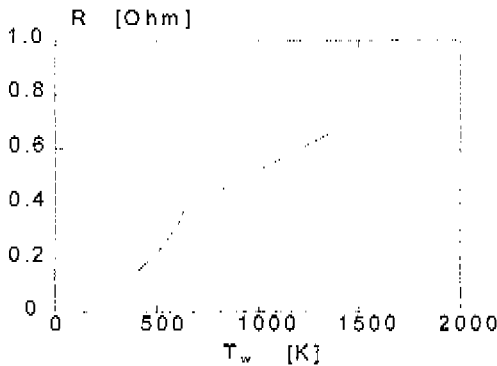
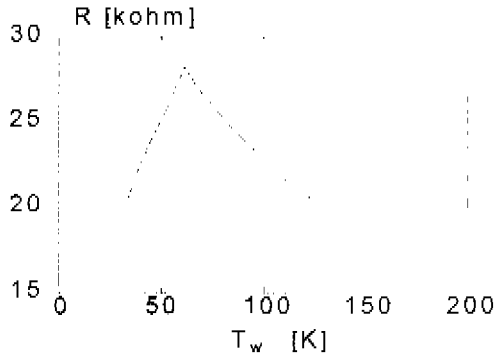
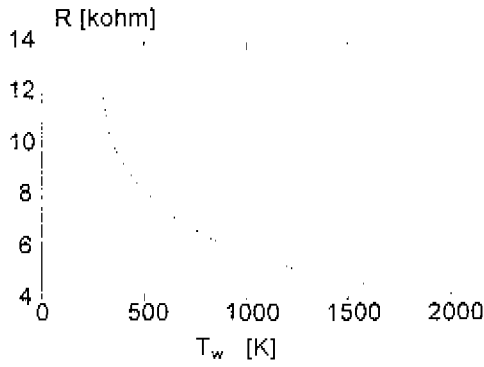


Figure 5.3 Electrical resistance of nickel wire as a function of temperature ( $n=7$ )



**Figure 5.4** Thermal resistance of nickel wire as a function of temperature ( $n=7$ )



**Figure 5.5** Convection resistance of nickel wire as a function of temperature ( $n=7$ )

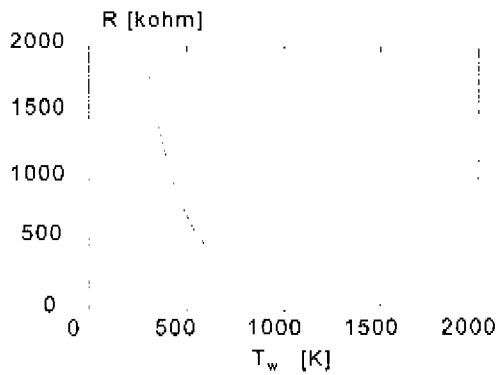


**Figure 5.6** Radiation of nickel wire as a function of temperature ( $n=7$ )

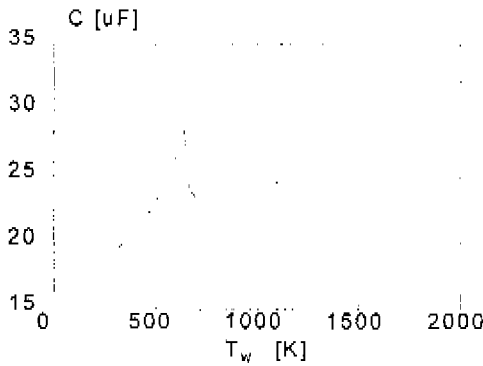


**Figure 5.7** Heat capacity of nickel wire as a function of temperature ( $n=7$ )

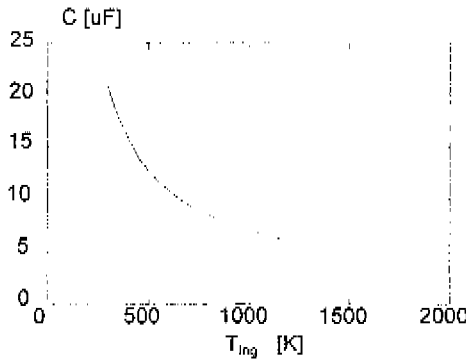


**Figure 5.8** Air capacity as a function of air temperature ( $n=7$ )

The whole model in the above is strongly dependent on a number of assumptions for the heat flow behaviour and material properties. As a check of the validity, the  $I-t$  characteristic of nickel fuses which is well documented experimentally and also determined with our thermal models. Figure 5.9 shows a comparison of simulated results and the manufacturer limits. Apparently, a rather good agreement has been achieved with respect to the temperature of the wire elements, which encourage us to use the thermal modelling for temperature determinations during pulse load.

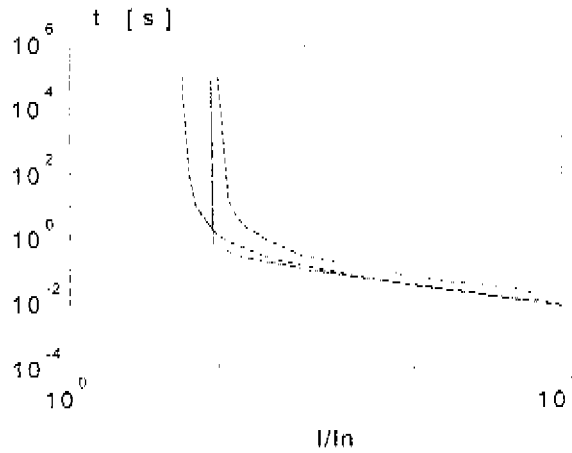


**Figure 5.9** Comparison of  $I$ - $t$  characteristics of nickel fuse wires  
Dashed line : manufacturer limits; solid line : simulation

Further the measured voltage response for a given current pulse with a peak value of 4 A was compared with simulation results. Figure 5.10 shows the measured voltage and the simulations for the current pulse together. The graph indicates that theoretical values are slightly below the measurements.

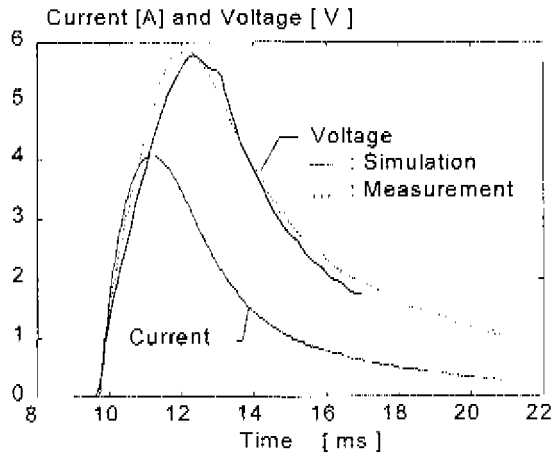


**Figure 5.10** Voltage response of a current pulse with a peak value of 4 A  
— : Simulation; ... : Measurement

From the current and voltage measurements, the resistance was obtained as a function of time. For the same current pulse, the calculated resistance was also obtained, the results are compared in Fig. 5.11. For both resistance determinations the initial resistance was reasonable in accordance with the cold fuse resistance (about 800 m $\Omega$ ). During the current peak, both simulations and derived resistance from measurements were similar. After the current peak, simulated values are below those determined from voltage and current measurements. One of the possible reasons is that as current decreases, the accuracy in the ratio of voltage to current becomes low.

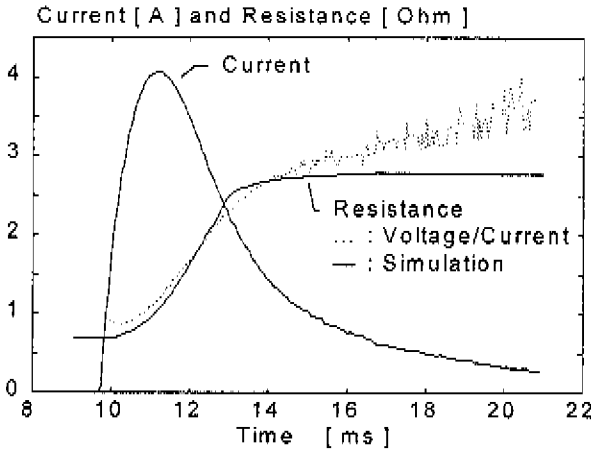


**Figure 5.11** Comparisons of nickel wire element resistance for a given current pulse  
 ... : Determination from voltage and current ratio; — : Simulation

### 5.3.2 Time delay fuses (Silver clad wire)

Element composition of this fuse wire was 50% silver and 50% tin - zinc alloy by weight. Tin -zinc alloy was composed of 85% tin and 15% zinc. Technical data arc: Littelfuse type 218.800; rated voltage : a.c. 250 V; rated current : 800 mA and the minimum melting  $I^2t_{min}$  : 1.3 A<sup>2</sup>s.

The electrical resistivity  $\rho$  and temperature coefficient of resistivity  $\alpha$  were determined from measurements by using the four terminal method. Because of the obvious difficulty in determining material properties, mass density  $\gamma$ , specific heat  $c$  and thermal conductivity  $\lambda$  were estimated according to their composition and wire construction. In the simulation, the following values were used:  $\rho = 3.7 \cdot 10^{-8}$  ohm.m,  $\alpha = 4.5 \cdot 10^{-3}$  K<sup>-1</sup>,  $c = 254$  J.kg<sup>-1</sup>.K<sup>-1</sup>,  $\gamma = 8.6 \cdot 10^3$  kg.m<sup>-3</sup>,  $\lambda = 220$  W.m<sup>-1</sup>K<sup>-1</sup>. Resistivity and its temperature coefficient [55] are in accordance with manufacture data. Specific heat  $c$  and thermal conductivity  $\lambda$  are evaluated according to wire compositions, which might contribute the deviations to simulations. Specific heat  $c$  is also in accordance with the value suggested by manufacturer.

For a given pulsed current, the voltage across the fuse and the temperature distribution ( $n=7$ ) were calculated. Figure 5.12 illustrates the simulated fuse voltage from the model and the measured voltage corresponding to a pulsed current with  $I^2t = 0.6$  A<sup>2</sup>s. On the other hand, from voltage and current measurements, resistance values were found. Because the initial resistance before current flowing was known, the average temperature rise can be determined by using the

relationship between temperature and resistance. Figure 5.13 displays a typical trace of the average temperature rise from the simulation, where the temperature rise derived from the measured voltage - current values is also presented. In this graph, the delay of temperature profile is clearly identified referring to the current pulse. The maximum temperature rise is reached after the current pulse started about 5 ms.

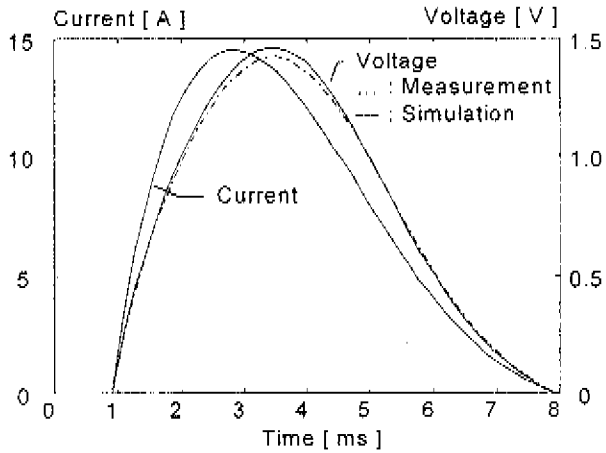


**Figure 5.12** Comparison of the simulated and experimental fuse voltage for a current pulse  $I^2t = 0.6 \text{ A}^2\text{s}$  (silver clad wire)

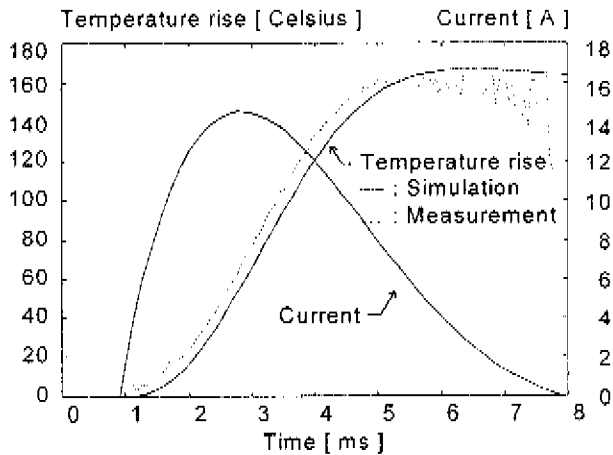


**Figure 5.13** Comparison of the average temperature rise of the fuse (silver clad wire) for a current pulse  $I^2t = 0.6 \text{ A}^2\text{s}$



From a previous study [55], the maximum displacement in the middle of the wire element was found to be 300  $\mu\text{m}$  for a constant current of 1.3 A. By using a well defined relationship [55] between displacement and the average temperature rise, the corresponding temperature rise was found to be 70 Celsius. To study the influence of end caps and further to examine the analogue method, the temperature distribution for a current of 1.3 A is calculated and shown in Fig. 5.14. The average temperature rise is about 60 Celsius.

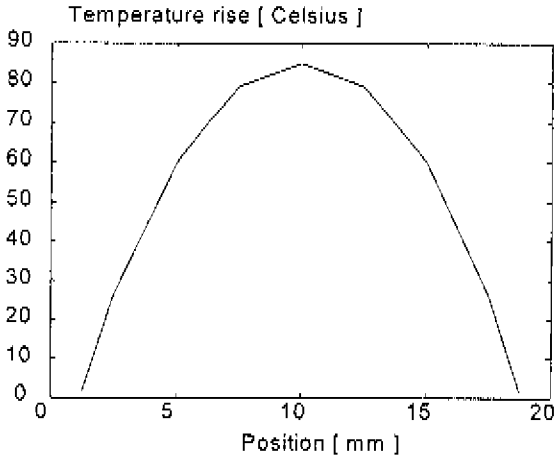


**Figure 5.14** Temperature distribution for a current of 1.3 A

While Fig. 5.14 is related with a constant current of 1.3 A, Table 5.2 also presents temperature values for current pulses with a duration of about 7 ms (see Fig. 5.13).

**Table 5.2** Average temperature rise corresponding to different  $I^2t$  values of pulsed currents

|                               |      |      |      |      |      |
|-------------------------------|------|------|------|------|------|
| $I^2t$<br>$\Lambda^2\text{s}$ | 0.22 | 0.37 | 0.60 | 0.78 | 0.98 |
| $\frac{I^2t}{I^2t_{min}}$     | 0.17 | 0.28 | 0.46 | 0.60 | 0.75 |
| $T_{exp}$ [°C]                | 52   | 101  | 164  | 205  | 284  |
| $T_{ad}$ [°C]                 | 60   | 111  | 207  | 301  | 431  |
| $T_{sim}$ [°C]                | 50   | 93   | 169  | 218  | 328  |

In Table 5.2,  $T_{ad}$  is the temperature rise under the adiabatic assumption,  $T_{sim}$  is the value from network simulations, and  $T_{exp}$  is the temperature rise determined from voltage and current

measurements.  $I^2t_{min}$  indicates the minimum melting  $I^2t$ . Comparison between the calculated temperature rises is made in Fig. 5.15 with the temperature values obtained by measuring voltage and current. This graph indicates that as  $I^2t$  values increase, the simulation results move up and above the results determined from voltage and current measurements. Figures 5.10 to 5.15 show a deviation of about 10 % between simulations and experimental results.

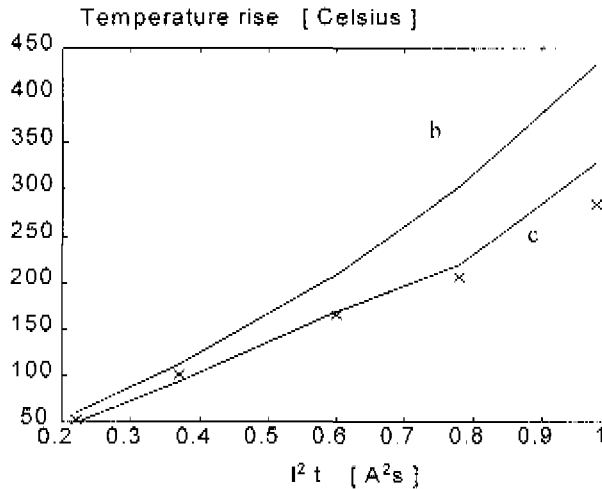


**Figure 5.15** Comparisons of temperature rises  
*x* : Values from voltage - current measurements  
*b* : Calculated results under adiabatic assumption  
*c* : Simulation results

To examine the simulation, the average temperature rise for wire elements has been determined from the resistance measurements, namely, from the voltage and current measurements. For the uniform distribution of the temperature along the fuse element, this method is always valid. For the circumstances where the electric resistivity of the fuse element is a linear function of the temperature rise, the validity can also be proved to be independent of the temperature distribution. The resistivity of silver clad wire has been experimentally determined, results indicate that the resistivity can be approximated by a linear function ( $\alpha = 4.5 \cdot 10^{-3} \text{ K}^{-1}$ ). For the nickel wire, as the temperature is above 600 K, because of nonlinearity of resistivity the accuracy of this method relies on its temperature distribution. The temperature rise determined from the resistance is slightly higher than the real average temperature rise, and the deviation can be evaluated to be within 13%.

## 5.4 Conclusions

Because both melting characteristics and voltage - current relations predicted by the thermal analysis are reasonable in accordance with experimental results, the thermal analogue method can be considered as a tool for stress analysis which is essentially based on thermal behaviour.

## Chapter 6 Thermal Modelling for Semiconductor Fuses

The primary objective of the fuse reliability project is to understand fuse ageing mechanisms and to provide application guidance for industries. This chapter describes a method to simulate three dimensional transient thermal responses of semiconductor fuses stimulated by electric current. The results will be used for thermal stress determinations related with fuse lifetimes.

For miniature fuses, because of their simple construction, thermal modelling could be performed with electrical analogue techniques. However, for semiconductor protection fuses, because of nonuniform current density distribution and complex of the construction, more sophisticated programming techniques are needed.

For thermal simulations of fuses, the finite different method [6, 7] and the finite element method [8, 9, 10] and the network analogue method [11, 12] may be applied. To find the solution of the three dimensional thermal problems of semiconductor protection fuses, EMTP [54] (Electro-Magnetic Transient Program) as a tool is chosen in this work. EMTP has been widely used for simulating electrical transients in networks. EMTP, compared with other available software packages, such as PSPICE and MICROCAP, is capable of handling very large networks (more than 10000 components) for Apollo workstation with 4 MB memory. EMTP allows various components which cover TACS (Transient Analysis of Control Systems), models, switches, resistors, capacitors, controlled voltage or current sources, look up tables (point by point function) and sub circuits (including files). Additionally, students in power engineering can get the knowledge of EMTP for huge electrical network simulations [78, 79, 80].

Two dimensional electric current distribution within the notched fuse element is numerically resolved by using resistive networks. Thermal behaviour of fuses has been simulated in EMTP (Electro-Magnetic Transient Program) by using the thermal electrical analogue method. The problem of three dimensional heat transfer within fuses is converted into electrical modelling where relevant electrical components represent heat conduction, generation and dissipation. The validity of the thermal model has been checked by comparison of the resulting melting characteristic with the manufacture curve; however, the final purpose is to use EMTP for lifetime determinations.

### 6.1 Considerations for thermal modelling

#### 6.1.1 Geometry of the fuse element

Commercial power fuses for semiconductor protection are chosen as simulation objects, with ratings of 160 A, 660 V and breaking capacity 120 kA. Figure 6.1 shows a typical element geometry, where dimensions are given in millimetres.

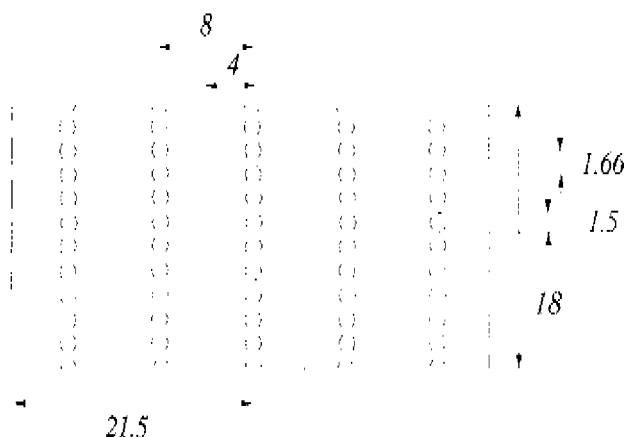


**Figure 6.1** Element geometry

The fuse element made of silver without M-spots consists of five rows of notches and each row has 10 holes. The hole has a diameter of 1.5 mm. The overall element size is 43mm\*18mm\*0.135mm.

The fuse element is surrounded by sand with an average grain size diameter of 0.36 mm. The sand packing density is about 1.79 g/cm<sup>3</sup>. The thickness of the surrounding ceramic body is about 5 mm. The distance between the body and the element is about 9 mm.

### 6.1.2 Thermal behaviour of fuses

In order to find the temperature distribution, two equations should be solved.

$$\nabla \nabla \phi = 0 \quad (6.1)$$

$$\gamma c \frac{\partial T}{\partial t} = \nabla \lambda \nabla T + \rho j^2 \quad (6.2)$$

The first is the field equation, which describes the electric potential distribution. The second is the energy balance equation. It states that the input energy due to joule heating is balanced by the heat conduction and the energy to raise the temperature of the object. The boundary conditions are specified as

$$T = T_0 = 20 \text{ } ^\circ\text{C}$$

$$\phi = \phi_0 = 0$$

$$\phi = \phi_1$$

$\phi_1$  is a known constant at one boundary.

Regarding fuse ageing and thermal behaviour, simulations for both long time and short time current conduction are required. To get an insight of heat transfer, it is easy to start with the idea of thermal diffusion depth (or the penetration depth). This concepts states that the distance

depends on the heat conducting time and the thermal diffusion coefficient. An approximation of the diffusion depth [68] is given by

$$\delta(t) = \sqrt{12\alpha t} \quad (6.3)$$

The diffusion coefficient is given by

$$\alpha = \frac{\lambda}{\gamma c} \quad (6.4)$$

To understand the heat transfer process in the fuse, the middle row of the notch is considered only, because it has the highest temperature as electric current flows.

Using the fuse element dimensions and the expression of diffusion depth, the following time limits are established. For times less than 0.3 ms, heat conduction is limited within the notch zone (0.75mm), hence adiabatic heating is suggested. Diffusion depth is about 4 mm in the silver element for 9 ms. Diffusion depth in sand is equal to the thickness of the element (0.13 mm) for 7 ms. These two time limits give an impression of the adiabatic heating. After about 150 ms, diffusion depth reaches 4 mm in sand. From 150 ms to 300 ms both heat conduction in the element and sand have the influence. After about 300 ms, heat conduction from the central notch reaches the end contacts. Heat transferred to contacts can not be neglected. After about 30 seconds, heat conduction reaches the ceramic body. Therefore in this range contacts and sand are heat transfer media. Heat convection and radiation of the ceramic body take place. As a consequence, all possible heat transfer factors should be considered above this time limit.

Within 300 ms, heat energy conducts in the silver element and sand. There is no heat conduction in the ceramic body for this period. Figure 6.2 shows relevant dimensions for this simulation. Because of geometric symmetry, only a small region of the total fuse element is required to be simulated. Above 300 ms, to simplify the simulation, the contact temperature and the outer surface temperature of the ceramic body are assumed to be the same as the surrounding temperature. Figure 6.3 shows the simulation region of the fuse element for longer time studies.

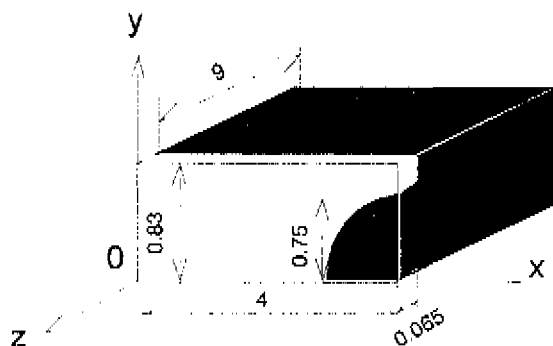
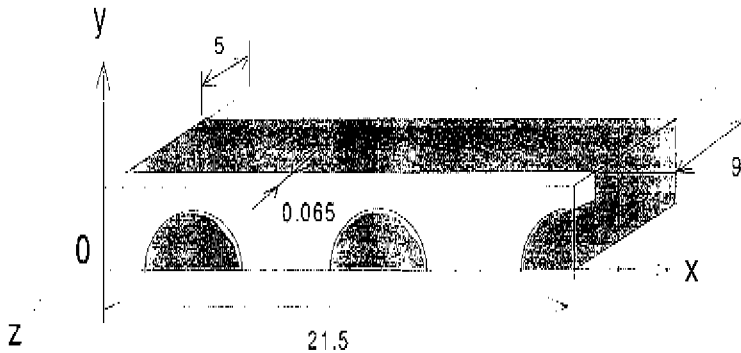


Figure 6.2 Simulation region for times shorter than 300 ms



**Figure 6.3** Simulation region for times between 300 ms and 30 s

### 6.1.3 Electrical equivalents

To realise the electrical analogue method, the simulation region is divided into small sub volumes. Electrical equivalents are network components transformed from the thermal and electrical problems, like already discussed in Chapter 5. Quantities of electrical components are defined according to Eqs. 6.1 and 6.2.

## 6.2 Network representation

In the previous section, general forms of component representations have been discussed. In this section, sub circuits corresponding to subvolumes will be represented.

### 6.2.1 Sub-volume generation

To achieve high resolution, small subvolumes are necessary. Figure 6.4 shows a typical subvolume and its dimensions.

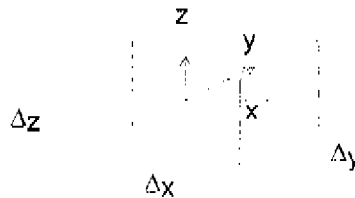


**Figure 6.4** Co-ordinates and subvolume dimensions

### 6.2.2 Sub circuits

Corresponding to Fig. 6.2 and 6.3, the area for the electric current flow simulation in the silver can be divided into small sub-volumes. For a subvolume, electrical behaviour is represented by

four resistances,  $R_{el}^j$  ( $j=1, 2, 3, 4$ ). A two dimensional representation is adequate here because of the small thickness of the metal strip. The corresponding subcircuit is represented in Fig. 6.5. Four measuring switches (type 91 device in TACS) are used to obtain the electric current in the network.

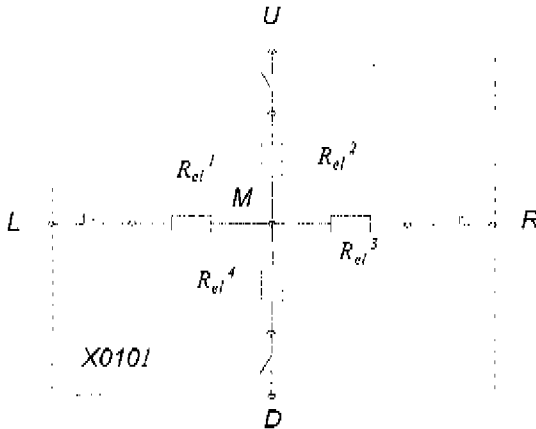


**Figure 6.5** Subcircuit for electric current flow

The resistance values are determined by subvolume dimensions and its resistivity. The length is from the centre point of the subvolume to the boundary surface. It is assumed that the current direction is perpendicular upon the relevant cross section. The resistivity of silver is dependent on the temperature of the subvolume which is represented by a type 98 device in TACS as a look up table.

For heat transfer, three dimensional modelling is necessary. Heat conduction is represented by six equivalent resistances,  $R_{th}^j$  ( $j=1, \dots, 6$ ). Resistance values depend on the thermal conduction coefficient. Energy due to electrical current flow is represented by injecting an equivalent thermal current. Energy used to increase the subvolume temperature is represented by charging an equivalent capacitor. Figure 6.6 shows the equivalent subcircuit for thermal simulation. Temperature coupled to a type 90 device in TACS is also measured by using a measuring switch and introduced into a type 98 device. In this way, a injected current source (type 60 device) is realised with the resistivity dependence of temperature in thermal network.

Component parameters for the sand and the ceramic body can be obtained in a similar way. Of course, no branches exist in the subcircuit for the electric current flow in sand. The complete circuit consists of all sub circuits. From this circuit, temperature values at different nodes are obtained.

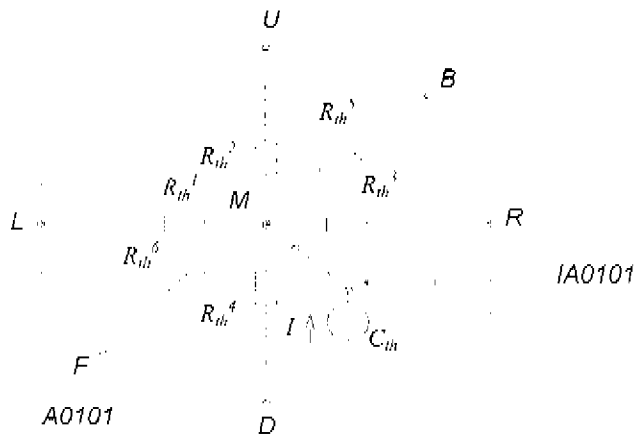


**Figure 6.6** Equivalent subcircuit of heat conduction

For decoupled solutions, current distribution and temperature distribution are obtained separately. However, for the coupled solutions, two networks have to be solved simultaneously. In the subcircuit for simulating current flow, the temperature dependent resistance is represented as a current source and a constant resistance together. Consequently, the subcircuit shown in Fig. 6.7 is used to simulate the electric current flow. Output of current is realised by a type 33 device. Figure 6.8 presents the coupled subcircuit for the heat transfer in the silver strip (see Fig. 6.7).

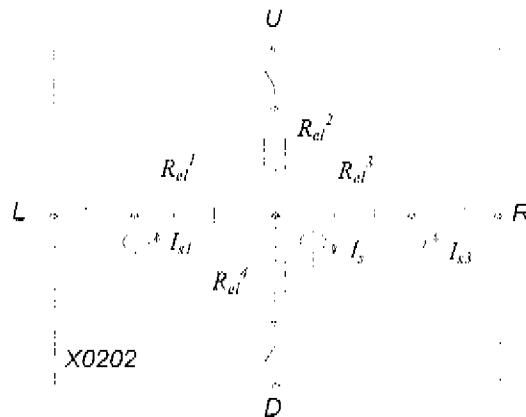


**Figure 6.7** Subcircuit for electric current flow including temperature dependence



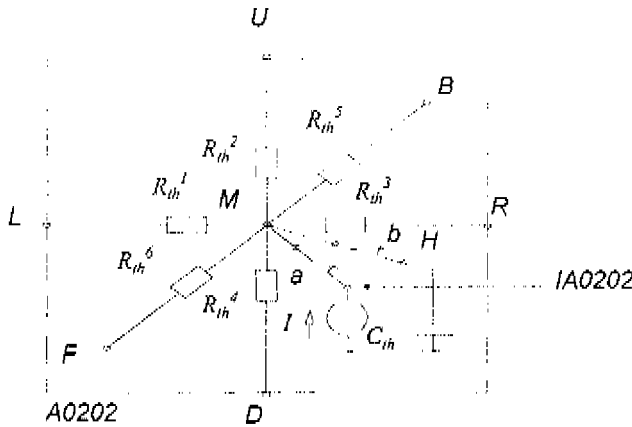


**Figure 6.8** Coupled equivalent subcircuit for the heat conduction in the silver strip (see Fig. 6.7)

In Fig. 6.8, two TACS controlled switches are used to couple the electric and thermal networks. A sample and hold function is introduced to keep the capacitor voltage. Two type 23 devices are used as triggers which control two switches represented as type 23 devices. To solve the complete network, an iteration procedure has to be applied. This is shown in Fig. 6.9, where  $T$  is the period for the coupled network simulation. The process is realised by exerting two triggering signals to switches  $a$  and  $b$  (TACS controlled switches). First, two switches are closed by trigger 1. Temperature values at all nodes are calculated. The temperature of the silver strip is measured by the measuring switch  $b$  in one time step. These two switches are opened by trigger 2. Consequently, temperatures at all nodes are hold. New electric current distribution is calculated during two time steps because of nonlinearity. As the stable state is reached, two switches are closed again and then temperatures at the next instant can be calculated.

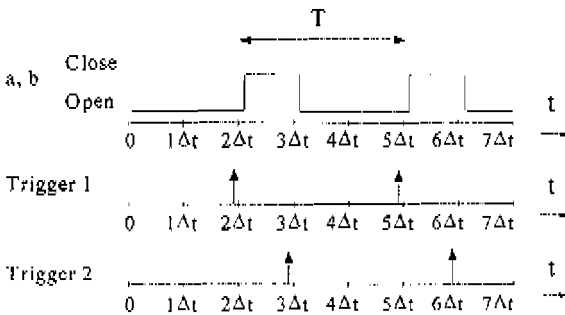


**Figure 6.9** Iteration scheme for the coupled non-linear network

### 6.2.3 Boundary conditions

In the simulation, the last sand layer and the network nodes at the end contact are connected to the thermal network ground. The temperature of the layer is at a room temperature. Heat conduction through the narrow edges of the silver strip into sand is assumed to be neglected.

### 6.3 Data input and output files

For the network, a program (SEMIFUSE.PAS) is used to generate data input files for EMTP. All resistances, capacitors, switches, current sources and TACS (Transient Analysis of Control Systems) are connected according to the subvolume representation.

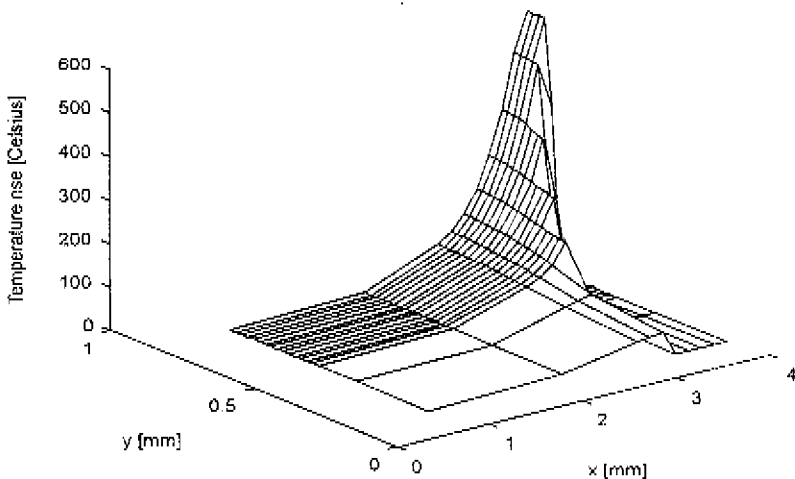
Resistivity as a function of temperature, thermal conductivity, specific heat and mass density of silver were taken from the literature [81]. For sand and ceramic, the commonly used values were introduced. Some properties are given in Table 6.1.

**Table 6.1** Material properties in the simulation

|         | $\lambda$ W/mK | $\gamma$ kg/m <sup>3</sup> | $c$ J/kgK |
|---------|----------------|----------------------------|-----------|
| silver  | 391            | 10492                      | 276       |
| sand    | 0.3            | 1670                       | 800       |
| ceramic | 1.46           | 2200                       | 670       |

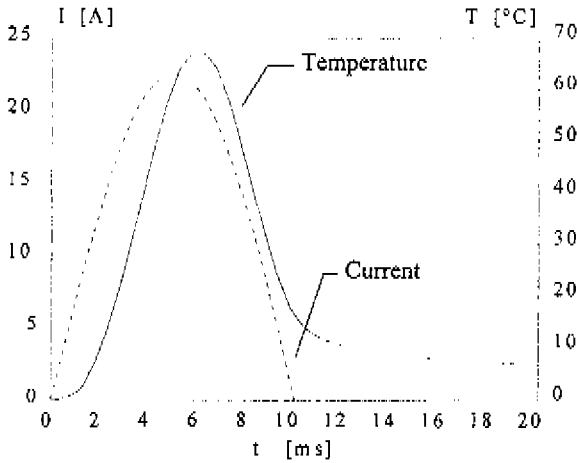
### 6.4 Results and discussion

Figure 6.10 shows a typical temperature distribution near the notch (the maximum temperature 574 °C) at the time instant of 7 ms for a sinusoidal current pulse of 1250 A. This graph indicates the most heated location is around the notch within about 1 mm.



**Figure 6.10** Three dimensional temperature distribution at 7ms for a 10 ms current pulse of 1250 A

Figure 6.11 shows simulation results of the maximum temperature rise for a current pulse of 700 A. The current indicated in the graph is 1/44 value of the total current through the fuse element. The graph indicates the simulated temperature profile as a function of time. After the current flows, the temperature rises up with a time delay. The maximum temperature of the element is reached after the current peak, the temperature delays about 2 ms. As the current decreases, the temperature falls down.



**Figure 6.11** Simulation for current pulses

To examine the current - time ( $I-t$ ) characteristics in the long time range, measurements of melting times for 300 A, 400 A and 600 A were performed. Experimental results from measurements are summarised in Table 6.2.

**Table 6.2** Measurements for checking  $I-t$  characteristics

| $I$ [A] | $t_m$ [s] | $I$ [A] | $t_m$ [s] |
|---------|-----------|---------|-----------|
| 300     | 220       | 400     | 20        |
| 300     | 154       | 600     | 2.8       |
| 300     | 220       | 600     | 2         |
| 400     | 10        | 600     | 1.8       |
| 400     | 15        | 600     | 2         |
| 400     | 19        | 600     | 1.8       |

From manufacturer data of  $I^2t$  values for the time range within 10 ms, the prospective current  $I_p$  and the virtual current  $I_v$  [82] was obtained for the corresponding melting times. The results are presented in Table 6.3.

**Table 6.3** Prospective current  $I_p$ , virtual current  $I_v$  and  $I^2t$  values

| $I^2t$ $\Lambda^2s$ | $t_m$ ms | $I_p$ $\Lambda$ | $I_v$ s |
|---------------------|----------|-----------------|---------|
| 7600                | 1        | 10854           | 2756    |
| 10200               | 4        | 1824            | 1579    |
| 11300               | 5        | 1503            | 1503    |
| 15870               | 10       | 1260            | 1260    |

Comparison of the manufacturer  $I-t$  characteristic, the measurements and calculated results from EMTP is made in Fig. 6.12. The minimum fusing current from the simulation was found to be 205 A.

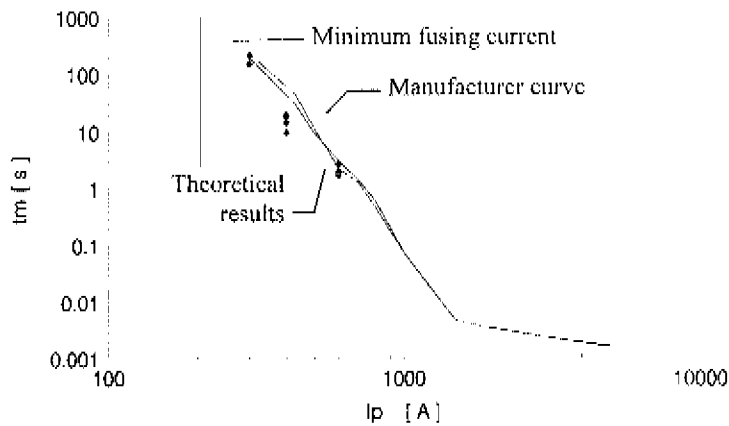


**Figure 6.12** Comparison of theoretical results with manufacturer curve and measurements "♦"

This graph shows that measured values ("♦") are slightly below the manufacture curve as well as the simulated results. In general, it can also be seen that calculations are in agreement with both results from the fuse manufacturer and the measurements.

## 6.5 Conclusions

As before, the proposed analogue method proved to be a powerful tool for simulating thermal transient responses. EMTP numerical results of current - time characteristics of fuses show reasonable agreement with both manufacturer curve and measurements. Numerical calculations have been conducted for current pulses. This study shows that the proposed EMTP modelling method can be used to predict thermal responses of fuses, as it will be necessary for the lifetime analysis.

## **Part IV Thermal Buckling and Lifetime Predictions**

## Chapter 7 Thermal Buckling of Wire Elements

As stated in Chapter 1, to predict fuse lifetimes, thermal response and displacement of the fuse element should be known first. This chapter describes efforts to solve the thermal post buckling problem of thin metal columns which carry electric current. The solution of analytical studies is based on the principle of the minimum potential energy. Besides, the effect of temperature is included in a theoretical finite element formulation. Both methods have taken vertical displacements into account in contrast to existing methods. Mechanical material properties are considered to be temperature independent. Also edge conditions are assumed to be immovable. Numerical results of displacements are compared with measurements from a microscope and high speed photography. In the present investigation, these two methods are used to analyse motion of wire elements subjected to thermal loads.

### 7.1 Buckling concept

Thermal buckling due to electric current may be of interest in many areas such as printed circuit boards, connections of electronic components, overhead lines and cables [83]. For fuse wire elements, because they are fixed onto end caps, the thermal expansion due to electric heating is suppressed. As a result, temperature change produces thermal strain that leads to thermal stress. This may bring about strain cycling and changes in material properties. Consequently, it can result in thermal fatigue and lifetime reduction of wire elements.

In 1983, Arai [35] conducted both experimental and analytic studies to determine lifetime of notched fuse elements. Motion of the fuse element was shown and suggested to be related with lifetime, however, without any quantitative models. The objective of the present study is to provide a quantitative description.

Figure 7.1 gives a schematic view to illustrate the motion of wire elements. The motion is simplified to be one dimensional in the  $y$ - $z$  plane and the magnitude is only dependent of one spatial variable  $z$ . When wire elements are subjected to electric current, temperature rises. As a consequence, thermal stresses are built up,

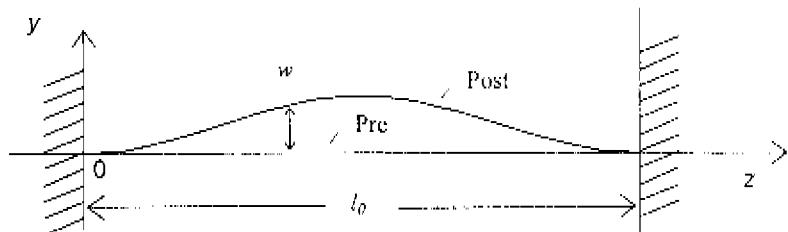


*Figure 7.1 Buckling geometry and sign notation*

The thermal strain corresponding to the thermal stress induced in the wire element is proportional to the thermal expansion coefficient and the temperature rise of fuse wire without end constraints. It is expressed as

$$\Delta \epsilon_{th} = \beta T \quad (7.1)$$

Because the wire is fixed at the ends, temperature rise results in stress. The wire keeps its original position; this process is called *pre buckling*. As the thermal stress exceeds a certain value, the wire element starts to move. The start of the motion is called *buckling*. The complete movement is called *post buckling*. During the post buckling, one part of the thermal strain is contributed to the motion of the wire element, another part is converted into compressed deformation. Timoshenko [84] proposed a function to describe the displacement (see Fig. 7.1) as

$$y(z) = 0.5 D_{max} \left( 1 - \cos \frac{2\pi z}{l_0} \right) \quad (7.2)$$

For the determination of the maximum displacement  $D_{max}$ , no valid theoretical method was available. Further literature [85, 86, 87, 88] shows that most methods are based primarily on linear structural theory with empirical corrections to account for non-linear behaviour. Namely, most investigations are limited to displacements comparable with the thickness of plates or the diameter of columns. In our situation, however, the maximum displacement of wire elements can be up to 10 times the diameter of the wire and even more. A suitable solution for thermal post buckling of fuse wire elements has therefore not been found yet.

This chapter describes the mechanical response of a fuse wire element during thermal buckling for miniature fuses subjected to electric current. Two methods will be addressed to find the post buckling solution for thin columns. The first attempt is to present an analytic study which describes the process in terms of energy [55]. The second describes efforts to develop a finite element formulation by using the virtual work principle [85]. Numerical results from these methods will be compared with experimental observations.

## 7.2 Analytical study

This section introduces an analytic method [55] for solving thermal buckling problems. Deformation causes are limited to thermal origins, oxidation and creep are neglected. In addition, temperature rise along the column is assumed to be constant.

To describe buckling, Eq. 7.2 still can be used as one of the possibilities of curved forms in equilibrium [55, 84] in the neighbourhood of the bifurcation point. This point is referred to the location of the maximum load without causing displacement perpendicular to the load in the load - displacement curve. Using the  $y(z)$  function, the increase of fuse wire length after buckling follows

$$\Delta L = \int_0^{l_0} \left\{ \sqrt{1 + \left( \frac{dy}{dz} \right)^2} - 1 \right\} dz = K_o D_{max}^2 l_0$$

$$K_o = \frac{\pi^2}{4 l_0^2}$$

For a linear spring with the actual elongation  $d_s$ , the stored energy is expressed to be  $W_s = 0.5 k_s d_s^2$ . With the analysed system, the total energy consists of the deformation energy, bending energy and energy due to the actual elongation in the post buckling. The deformation energy due to the compression is

$$W_d = \frac{l}{2} EA (\beta T - K_s D_{max}^2)^2 l_0 \quad (7.3)$$

The energy due to the actual elongation in motion is

$$W_b = \frac{l}{2} EA (K_s D_{max}^2)^2 l_0 \quad (7.4)$$

The bending energy to keep the buckling takes

$$W_m = \frac{1}{16} EI_m l_0 D_{max}^4 \left( \frac{2\pi}{l_0} \right)^4 \quad (7.5)$$

The total potential (elastic energy) consists of  $W_d$ ,  $W_b$  and  $W_m$ . Denoting by  $U_T$  the total potential, one may write

$$U_T = W_d + W_b + W_m \quad (7.6)$$

The total potential energy has to be minimum for realising a possible buckling mode and therefore the derivative of  $U_T$  to a position variable  $\eta$  is zero. It follows

$$\frac{dU_T}{d\eta} = 0 \quad (7.7)$$

where  $\eta$  is equal to  $D_{max}^2$ .

The maximum displacement can be obtained from Eq. 7.7 to be

$$D_{max} = \frac{2l_0}{\pi} \sqrt{\frac{l}{2} \beta \star T - \frac{2\pi^4}{l_0^2} \frac{I_m}{A}} \quad (7.8)$$

Substitution of Eqs. 7.8 into 7.2 leads to an expression of the buckling shape for the static condition. According to Eq. 7.8, let  $D_{max} = 0$ , the critical temperature rise is found to be

$$T_{cr} = \frac{4\pi^4}{L^2} \frac{I_m}{\beta A} \quad (7.9)$$

The deflection factor  $\gamma$  is defined as

$$\gamma = \frac{\Delta \varepsilon_m}{\Delta \varepsilon_{th}} = 1 - \frac{\Delta \varepsilon_n}{\Delta \varepsilon_{th}} \quad (7.10)$$

It means physically that the mechanical strain is a fraction of the thermal strain expressed in Eq. 7.1 during the post buckling. Before the buckling occurs, the wire is motionless, thermal stress is equal to mechanical stress ( $\gamma=1$ ). During the buckling, the factor is calculated from

$$\gamma = \frac{l}{2} + \frac{2\pi^4}{l_0^2} \frac{I_m}{A} \frac{l}{\beta T} \quad (7.11)$$



### 7.3 Finite element formulation

In Section 7.2, the analytic approach has been presented to determine the displacement response due to temperature rise, where the temperature rise along the column is taken as a constant. In practical situations, temperature decreases as the location is near the fixing ends. This motivates a more accurate simulation method for the mechanical response concerning arbitrary temperature distribution along the column. In 1991, Locke [85] conducted studies of thermal buckling for beams, the description is considered to be useful and relevant with this work. The following presents an extended description to enable analysis of large deflections of thin columns.

#### 7.3.1 Physical models

The principle of virtual work [85, 89] states that for a column in equilibrium under the action of internal and external forces, in undergoing an infinitesimal virtual displacement [90] the work done by the external forces is equal to the work done by the internal forces. This can be written as

$$\delta W_{int} = \delta W_{ext} \quad (7.12)$$

To describe the formulation, Fig. 7.1 shows sign notations for a column (fuse wire), where the undeformed co-ordinates are applied. Suppose that the damping and acceleration are neglected, because the external work is zero during the thermal post buckling, the left side remains to be zero. The virtual work of the internal forces is written as

$$\delta W_{int} = \int (\delta \epsilon N + \delta k M + \delta \epsilon_s E A \epsilon_s) dz \quad (7.13)$$

The first and second terms describe the virtual work in the axial direction. *The third term represents the virtual work needed for the vertical displacement, which is not present in Locke's work [85].* Possibly because this term is small and thus it can be neglected. For fuse wire elements, the vertical displacement  $w$  can be many times the wire diameter during the post buckling. Therefore this term can no longer be neglected.

The large deflection strain - displacement relation [85] for an initially deflected beam is given by

$$\epsilon = \epsilon_m + \epsilon_b \quad (7.14)$$

where

$$\begin{aligned} \epsilon &= \epsilon_m + \epsilon_b \\ \epsilon_m &= u_z \\ \epsilon_b &= \frac{1}{2} w_z^2 + w_z w_{0z} \\ k &= - w_{zz} \end{aligned} \quad (7.15)$$

In an initially straight column,  $w_0$  is zero. For an uniform column, subjected to a temperature rise  $T(z)$ , the in-plane force  $N$  and moment resultant  $M$  are given by

$$\begin{aligned} N &= E A \epsilon + N_0 - E A \beta T(z) \\ M &= E I k + M_0 \end{aligned} \quad (7.16)$$

In this work, the initial moment  $M_0$  and the initial in-plane force  $N_0$  are assumed to be zero.

### 7.3.2 Formulation

To describe the virtual work, the column is divided into a number of segments or subvolumes  $N_{seg}$ . For each subvolume ( $[z_j, z_{j+1}]$ ,  $j = 0, \dots, N_{seg}$ ), the principle of virtual work may be applied. Summarising the virtual work in each subvolume leads to the total virtual work in the column. Figure 7.2 shows notations of the nodal displacements for a subvolume.

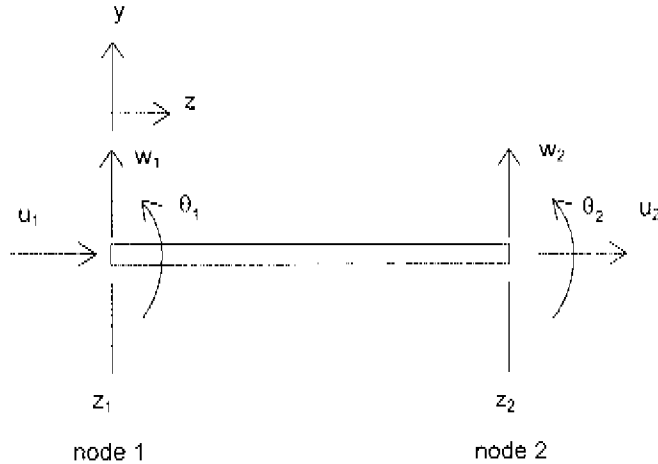


**Figure 7.2** Nodal displacements for a subvolume

At two nodes, displacement  $w$  and its derivative, displacement  $u$  and temperature rise  $T$  give the nodal values as follows

$$\{a_s\}^T = [w_1, \theta_1, u_2, \theta_2] \quad (7.17)$$

$$\{a_u\}^T = [u_1, u_2]$$

$$\{T_s\}^T = [T_1, T_2] \quad (7.18)$$

Displacement functions  $w$  and  $u$  at any locations are represented by node values and expressed as

$$\begin{aligned} w &= \alpha_1 + \alpha_2 \xi + \alpha_3 \xi^2 + \alpha_4 \xi^3 \\ u &= \beta_1 + \beta_2 \xi \end{aligned} \quad (7.19)$$

where the co-ordinate  $\xi$  is transformed from

$$\xi = \frac{2}{h} (z - z_m) \quad (7.20)$$

$$z_m = \frac{1}{2} (z_1 + z_2), \quad h = z_2 - z_1$$

Accordingly,  $\alpha_1$ ,  $\alpha_2$ ,  $\alpha_3$ ,  $\alpha_4$ ,  $\beta_1$  and  $\beta_2$  are found as functions of nodal values. By using Hermit's high order functions, displacement  $w$  and  $u$  can be rewritten as

$$\begin{aligned} w &= \alpha_1 + \alpha_2 \xi + \alpha_3 \xi^2 + \alpha_4 \xi^3 = [N] \{a_s\} \\ u &= \beta_1 + \beta_2 \xi = [N_u] \{a_u\} \end{aligned} \quad (7.21)$$

where  $N$  and  $N_u$  are Hermit's shape functions. Their expressions are

$$\begin{aligned} N(1) &= \frac{1}{4}(2 - 3\xi + \xi^3) \\ N(2) &= \frac{h}{2} \frac{1}{4}(1 - \xi - \xi^2 + \xi^3) \\ N(3) &= \frac{1}{4}(2 + 3\xi - \xi^3) \\ N(4) &= \frac{h}{2} \frac{1}{4}(-1 - \xi + \xi^2 + \xi^3) \end{aligned} \quad (7.22)$$

$$\begin{aligned} N_u(1) &= \frac{1}{2}(1 - \xi) \\ N_u(2) &= \frac{1}{2}(1 + \xi) \end{aligned} \quad (7.23)$$

In a similar way, the temperature rise in a subvolume is defined as

$$T = \{N_T\} \{T_n\} \quad (7.24)$$

where  $N_T = N_u$ .

For the column, the nodal displacements  $\{q\}_j$  in a subvolume ( $j = 0, \dots, N_{seg}$ ) and the nodal displacements  $\{Q\}$  are respectively defined as

$$\begin{aligned} \{q\}_j^T &= [\{a_b\}_j^T, \{a_w\}_j^T] \\ \{Q\}^T &= [\{q\}_0^T, \dots, \{q\}_j^T, \dots, \{q\}_{N_{seg}}^T] \end{aligned} \quad (7.25)$$

Introducing Eqs. 7.17-7.24 into Eqs. 7.14-7.16, the virtual work (see Eqs. 7.12 and 7.13) reads in general

$$A(Q)\delta Q = \sum_{j=1}^{N_{seg}-1} a_j(q_j) \delta q_j \quad (7.26)$$

Because this expression holds for arbitrary variations  $\delta Q$ , according to the strain-stress definitions, the element equations in matrix form can be expressed further as  $a_j(q_j) = 0$ , and the corresponding system equations can be reorganised as

$$A_\theta Q = F \quad (7.27)$$

where  $A_\theta$  is a matrix,  $F$  is the right hand vector. The vector  $Q$  represents complete nodal displacements. Both  $A_\theta$  and  $F$  are functions of nodal displacements.

### 7.3.3 Programming and numerical solution

A finite element program was developed based on the previous formulation. The program was coded with Maple [64] which is a symbolic mathematics package. One of the advantages is that variables involved can be easily changed, for example, the matrix calculations. At the time being, initial deflection and moment were not considered in the calculation.

The resulting equations of motion represented by Eq. 7.27 were solved by using Newton's iteration technique [91]. For any  $Q$ , a vector function  $G$  is defined as

$$G(Q) = A_0(Q)Q - F(Q)$$

For the system equation Eq. 7.27, the Newton's method defines a sequence  $Q^0, Q^1, Q^2, \dots$ , then

$$\begin{aligned} G^{k+1} &= G^k + H^k \\ G(Q^k) + J(Q^k)H^k &= 0 \end{aligned}$$

where the Jacobean matrix  $J(Q^k)$  contains the partial derivatives of the vector function  $G(Q^k)$ . The  $i$ -th equation of the system is given by

$$G_i(Q^k) + \sum_{j=1}^{N_{eq}-1} \frac{\partial G_i(Q^k)}{\partial Q_j^k} H_j^k = 0$$

for  $i = 1, \dots, 3*(N_{seq} - 1)$ . The iteration continues until  $\|G(Q^k)\| \leq \epsilon_n$ , where  $\epsilon_n$  is related with the required iteration accuracy.

The iteration requires the initial values of nodal displacements which were given in two ways. The first method is based on Eq. 7.2 which describes the column shape in the neighbourhood of the bifurcation point [92, 93]. The maximum displacement value  $D_{max}$  from Eq. 7.8 (for the known average temperature rise) is used. As an alternative, arbitrary values smaller than the wire diameter, for example 10 percent value of the wire diameter, can also be used without influencing the final solution for the buckling. The second method uses the idea that if the imperfection of the column tends to zero and then the solution is considered approximately as the real solution. The imperfection in the iteration scheme was represented by different small nodal displacements. Both methods for giving initial iteration nodal displacements were tested, results show no significant difference.

## 7.4 Displacement measurements

A miniature fuse is composed of a fuse element or wire, end caps and a glass tube. The straight fuse element can be positioned inside the tubular visible glass body. The element is fixed onto two end caps. Therefore, the fuse wire can be assumed to be a column with two fixed ends. Column dimensions are simplified to be diameter and length.

As fuses are exposed to electric currents, thermal expansion of the element occurs. In attempting to observe the buckling effects and verify the proposed numerical scheme, experiments for both d.c. current and current pulses were performed for two types of fuses (Littelfuse type 217.315 and 218.800). Their elements were made from pure nickel wire and silver clad wire (*Ag/Sn-Zn*) respectively. The later consisted of 50% silver, 50% tin-zinc alloy (85% tin and 15% zinc) in weight.

### 7.4.1 DC current

Before measuring displacements of fuse wires due to d.c. current, to check whether the glass tube has influence on the measuring accuracy, the displacements were measured with and without current flowing for fuses. These two measurements did not show difference for the same sample. During experiments, the test current up to 10 A can be supplied, which was measured by a Fluke 8000 digital multimeter. The voltage across the tested fuse was measured by a Keithley 179 digital TRMS multimeter. The displacements in the two perpendicular directions of the fuse wire were measured by using a NIKON microscope [55].

### 7.4.2 Current pulses

For measuring the displacements of fuse wires, an *LC* circuit was constructed to generate current pulses. A thyristor was used to switch on and off the current through the tested fuse. A high speed camera was used to measure the displacement. To get enough illumination for filming, a flash tube was installed. Images were produced with the help of achromats and micro zoom lens. The wire diameter was taken as a reference for determining the displacement. During the experiment, fuse current and voltage were recorded by a digital 12 bit oscilloscope. An optical sensor reacted to the flash tube and produced the exposure signal. In the meantime, the camera shutter release signal and the exposure signal were also obtained and written down in the oscilloscope. For determining the maximum displacement, a spatial resolution of 10  $\mu\text{m}$  per mm was achieved.

### 7.5 Results and discussion

Table 7.1 summarises material properties used in the displacement calculations for *Ag/Sn-Zn* fuses and Nickel fuses.

**Table 7.1** Material properties and dimensions

| Element type                  | Ni                                    | Ag/Sn.Zn                              |
|-------------------------------|---------------------------------------|---------------------------------------|
| Length of fuse element        | $l_0=17.5 \text{ mm}$                 | $l_0=17.5 \text{ mm}$                 |
| Diameter of fuse element      | $d=50 \mu\text{m}$                    | $d=103 \mu\text{m}$                   |
| Thermal expansion coefficient | $\beta=13.3 \cdot 10^{-6}$            | $\beta=22.1 \cdot 10^{-6}$            |
| Elasticity                    | $E=199.5 \cdot 10^9 \text{ Pa}$       | $E=61 \cdot 10^9 \text{ Pa}$          |
| Cross sectional area          | $A=1.96 \cdot 10^{-9} \text{ m}^2$    | $A=8.33 \cdot 10^{-9} \text{ m}^2$    |
| Area moment of inertia        | $I_m=3.07 \cdot 10^{-18} \text{ m}^4$ | $I_m=5.52 \cdot 10^{-18} \text{ m}^4$ |

In the table, diameter and elasticity were measured values. In theoretical calculations elasticity does not influence the displacement as long as the deformation can be assumed to be elastic. Length was evaluated according to the fuse manufacturer's requirements for the element, which was also examined by the resistance measurements. Thermal expansion coefficient in the literature [76] was used for nickel wire, while the data for *Ag/Sn.Zn* wire was taken from the manufacturer's information.

During the experiment for d.c. current, voltage, current and displacements were measured. On the basis of temperature dependency of resistivity, the temperature rise of fuses was determined. Theoretical values of displacements were found by substituting these experimentally determined temperature rises into Eq. 7.8. Figure 7.3 and Fig. 7.4 show comparisons of theory with observations of the displacements for nickel fuses and *Ag/Sn.Zn* fuses. Because of the nonlinearity of resistivity of nickel due to temperature rise, the average temperature rise determined from the voltage and current measurements may not represent the real average temperature rise of the wire element. For the existing element configuration, the inaccuracy is within 13% for d.c. currents and 7% for short current pulses. In addition for the average temperature rise above the magnetic

transition point (about 630 K), the evaluated value from the resistance measurement is higher than the real average temperature rise. This means that experimentally evaluated results in Fig. 7.3 fit calculations (Eq. 7.8) better if this nonlinearity of resistivity is taken into account.

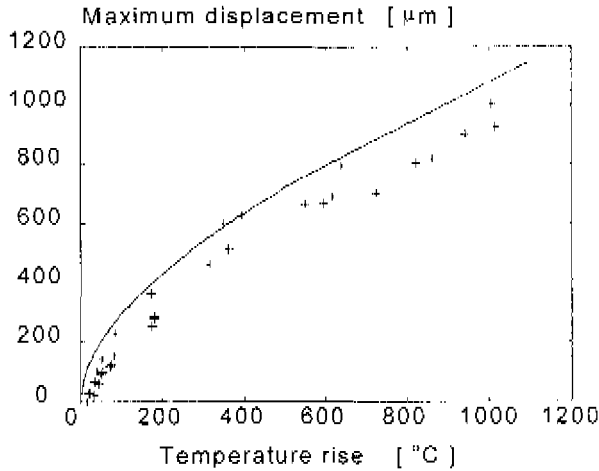


**Figure 7.3** Dependence of displacements on temperature rise (nickel wires)  
 "+" : microscope observation; "-" : theory (Eq. 7.8)

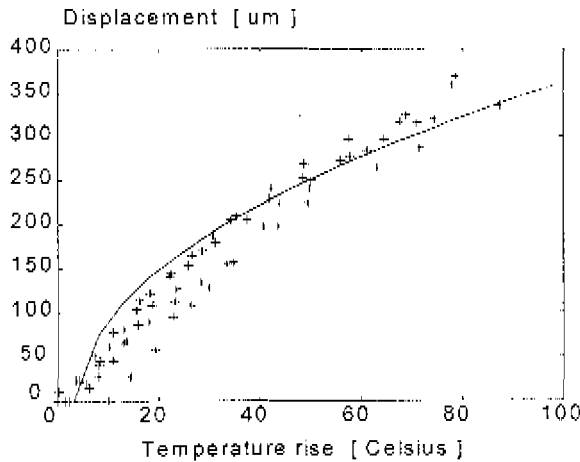


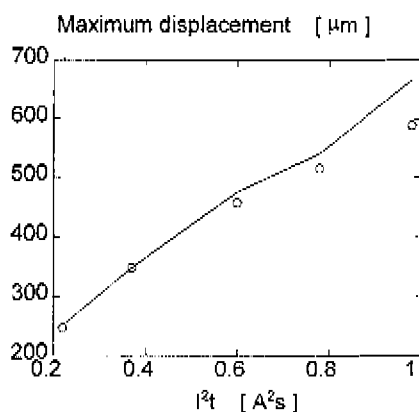
**Figure 7.4** Dependence of displacements on temperature rise (Ag/Sn.Zn wires)  
 "+" : microscope observation; "-" : theory (Eq. 7.8)

By introducing the measured current into thermal modelling, the average temperature rise was found for different  $I^2t$  values of current pulses. Using the displacement - temperature rise relation in Section 7.2, theoretical displacements were obtained. Table 7.2 lists experimental results from high speed photography and temperature calculations from thermal modelling.

**Table 7.2** Results of measurements and calculations for different  $I^2t$  values of pulsed currents

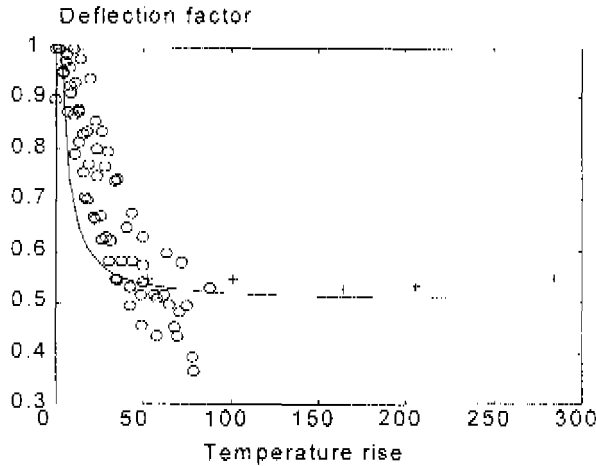
|                              |      |      |      |      |      |
|------------------------------|------|------|------|------|------|
| $I^2t$<br>$A^2s$             | 0.22 | 0.37 | 0.60 | 0.78 | 0.98 |
| $\frac{I^2t}{I_{t_{min}}^2}$ | 0.17 | 0.28 | 0.46 | 0.60 | 0.75 |
| $T_{exp}$                    | 52   | 101  | 164  | 205  | 284  |
| $D_{max}$                    | 247  | 349  | 458  | 516  | 590  |
| $\Delta\varepsilon_{th}$ %   | 0.11 | 0.22 | 0.36 | 0.45 | 0.62 |
| $\Delta\varepsilon_g$ %      | 0.05 | 0.10 | 0.17 | 0.21 | 0.28 |
| $\Delta\varepsilon_m$ %      | 0.06 | 0.12 | 0.19 | 0.24 | 0.34 |
| $T_{ad}$                     | 60   | 111  | 207  | 301  | 431  |
| $T_{sim}$                    | 50   | 93   | 169  | 218  | 328  |
| $D_{sim}$                    | 250  | 349  | 475  | 541  | 665  |

Figure 7.5 shows that theoretical calculations and results determined by using high speed photography for *Ag/Sn.Zn* fuses; in agreement with experimental observations.



**Figure 7.5** Displacement as a function of  $I^2t$  value for current pulses (*Ag/Sn.Zn* wires) "o": observation from high speed photography; "—": theory (thermal modelling, Eq. 7.8)

According to Table 7.2, the deflection factors were calculated and shown in Fig. 7.6. The average value was about 0.54 for  $Ag/Sn.Zn$  fuse elements during current pulses. For d.c. currents, as temperature rise increases, the deflection factor decreases down to a value small than 0.5.



**Figure 7.6** Relationship between deflection and temperature rise ( $Ag/Sn.Zn$  fuse wires)  
 "o": d.c. current; "+" : pulse current; "-" : theory (Eq. 7.8)

To examine the influence of temperature distribution on the displacement, profile of vertical displacements is compared with measurements for a d.c. current of 960 mA. First, the temperature distribution for the current was simulated, the results are shown in Fig. 7.7.

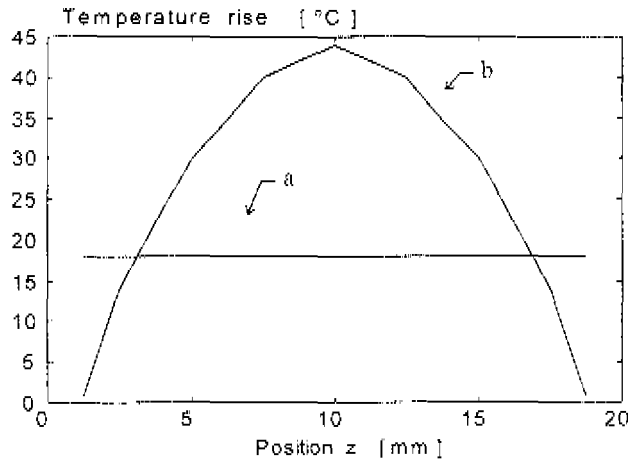
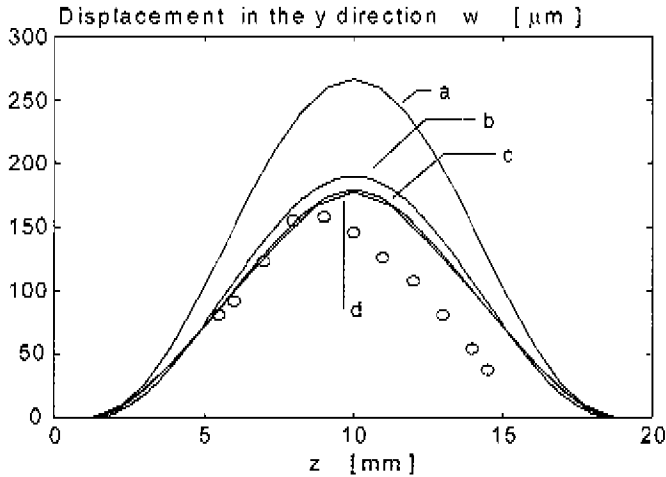


**Figure 7.7** Temperature distribution for a d.c. current of 960 mA  
 a : average temperature rise 18 °C from voltage current measurements  
 b : thermal modelling



In Fig. 7.7, curve "a" indicates the average temperature rise from the voltage and current measurement. Curve "b" indicates the distribution obtained from the thermal modelling.

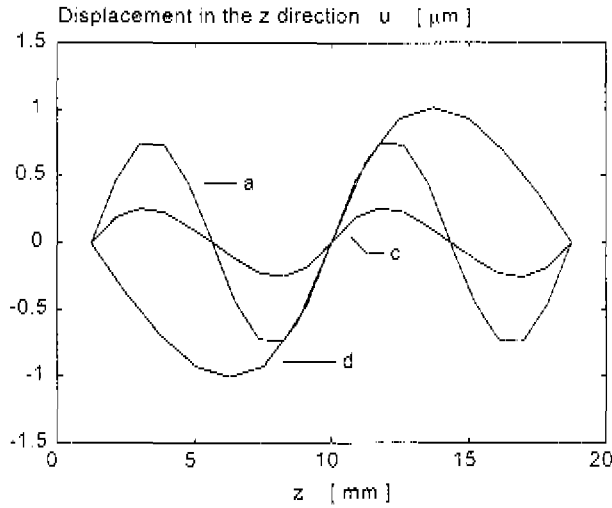
Figure 7.8 shows the displacement  $w$  as functions of position  $z$  obtained from different simulation methods.



**Figure 7.8** Displacement for Ag/Sn.Zn fuse wires  
*a* : Locke's method; *b* : Eq. 7.8; *c* : FEM at 30 Celsius;  
*d* : FEM with temperature distribution (see Fig. 7.7)

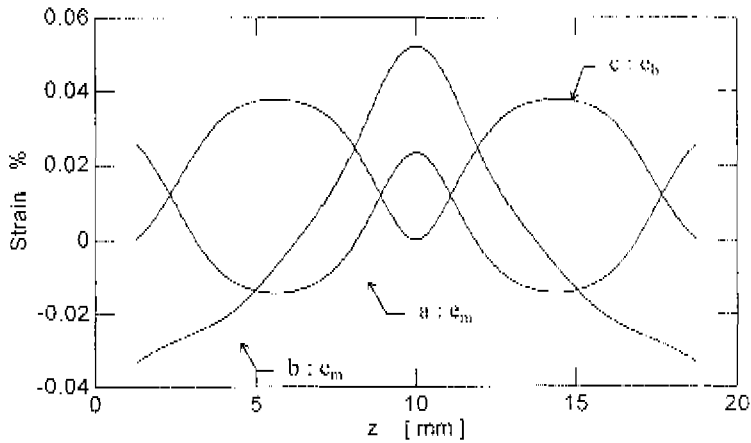
In Fig. 7.8, curve "a" indicates the results obtained by using the literature method [85]. Curve "b" gives the results from Eq. 7.8. Curve "c" presents the results from the finite element method, where the average temperature rise was used. Curve "d" presents the results from the finite element method, where the temperature distribution in Fig. 7.7 was used. Mark "o" displays the observed displacements due to the d.c. current. This graph shows that the biggest deviation between curve "a" and the observations exists. Therefore, methods presented in this work offers a better solution than that in literature [85].

Figure 7.9 shows the displacement  $u$  as functions of position  $z$ . Curve "a" indicates the results obtained by using the literature method [85]. Curve "c" presents the results from the finite element method, where the average temperature rise was used. Curve "d" presents the results from the finite element method, where the temperature distribution in Fig. 7.7 was used. Concerning the temperature distribution during the d.c. current below the minimum melting current, the displacement  $u$  takes the direction towards two end caps. As the temperature is near the uniform distribution (constant temperature rise), the displacement acts as curve "a" and "c".



**Figure 7.9** Axial displacement for Ag/Sn.Zn fuse wires  
*a* : Locke's method; *c* : FEM at a temperature rise 30 Celsius;  
*d* : FEM with temperature rise in Fig. 7.7

Figure 7.10 shows the FEM numerical solutions of the strains  $e_m$ ,  $e_z$  and  $e_b = 0.5e_z^2$  corresponding to Eq. 7.15 based on different temperature distributions.



**Figure 7.10** FEM solution of strains  $e_m$  and  $e_b$  for Ag/Sn.Zn fuse wires  
*a* :  $e_m$  at a temperature rise 30 Celsius; *b* :  $e_m$  temperature rise in Fig. 7.7;  
*c* :  $e_b$  for both temperature distribution (see Eqs. 7.14 and 7.15)

In Fig. 7.10, Curve "a" gives the results by assuming the uniform temperature distribution, while curve "b" gives the results corresponding to the temperature distribution in Fig. 7.7. Curve "c" displays the strain  $e_b$  for both temperature distributions.

Figure 7.11 shows the relative stress as a function of position axial  $z$ . The stress is equal to the ratio of the in-plane force  $N$  (see Eq. 7.15) and the average thermal force stress  $E\beta T$ .

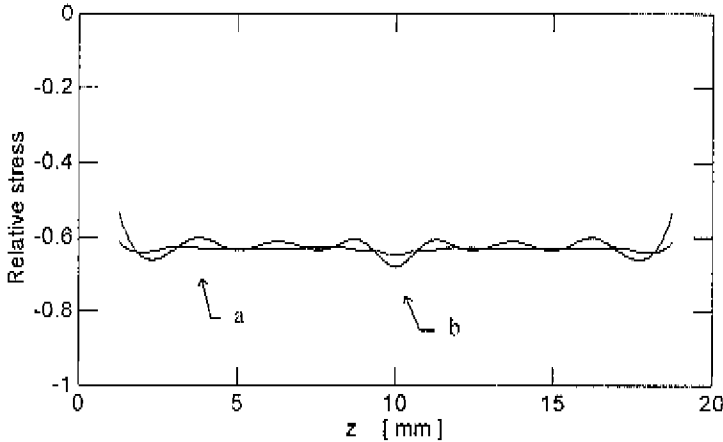


**Figure 7.11** FEM solution of relative stress for Ag/Sn,Zn fuse wires (Eq. 7.15)  
*a* : at a temperature rise 30 Celsius; *b* : temperature rise in Fig. 7.7

Temperature rise  $T$  takes the average value of the whole wire element. Similar to Fig. 7.10, curve "a" gives the results obtained by assuming the uniform temperature distribution, while curve "b" gives the results corresponding to the temperature distribution in Fig. 7.7. This graph indicates that the in-plane force is compressive (negative) along the wire element. For the uniform temperature distribution, the in-plane force is almost a constant. The breaking location is expected to be at the middle point, or/and at the soldering position (near end caps) as a result of the bending stress. Curve "b" indicates three points (one at the middle point and other two near end caps) subjected to larger stresses. Between the point near the end cap and the middle point, additional two points also have relatively high local stress.

As the heat transfer increases along the wire element, the extension in the middle of the wire element increases and the extension near the end caps decreases. It is concluded that the particles with high temperature attempt to move towards the location where the temperature is low. Because the stress due to the bending reaches the highest value in the middle and at the end caps, the maximum deformation depends largely on strain  $e$  which includes the contribution of  $e_m$  and  $e_b$ . Again because of bending, the breaking possibility at the middle point is the largest. These explain why the fuse element breaks in the middle region for current pulses and for short time d.c. currents.

However, for long cyclic loading, creep takes place, after motion the wire element may have difficulty to come back to its original position. In this case, if the deformation is assumed to be controlled by the strain  $e_h$  (see Fig. 7.10), then breaking locations can be expected at the place where  $e_h$  is the maximum. This assumption is supported by the results of lifetime experiments for long current pulses, where the breaking location is verified.

Figure 7.11 also shows that the relative stress is approximately a constant about 0.6 along the wire element. If the maximum temperature rise in Fig. 7.7 is used, the relative stress will decrease to about 0.4. Because the deflection factor in Section 7.2 is related with this relative stress, comparison of the deflection factor in Fig. 7.7 with the relative stress becomes obvious.

## 7.6 Conclusions and future work

Analytic solutions and the finite element formulation are presented for the buckling of thermally stressed wire elements under assumption of the elastic deformation. The analytical approach assumes the uniformly distributed temperature. The in - plane stress along the middle plane of the element is also evaluated to be the same. From the finite element formulation, displacements of wire elements are calculated and presented for both the uniform temperature distribution and arbitrary temperature distributions. The analytic approach provides a simple solution for the vertical displacement. The finite element formulation offers both vertical and axial displacements with consumption of numerous computer time. The breaking locations of the wire element is also discussed.

For the practical interest, this work can be improved in two aspects in the future. The first is to extend the finite element formulation of thermal post buckling problems for a strip fuse element. The second task is to include the initial deflection for designing the optimal shape of the fuse element.

## Chapter 8 Lifetime Predictions

This chapter presents physical models of lifetime predictions for electric fuses, when fuses experience current pulses. Commercial miniature fuses and semiconductor protection fuses have been used to verify the proposed models. For short current pulses, lifetimes are estimated based on the elastic fracture mechanism, while for long current pulses the combination of Manson - Coffin law and the creep process is used. After determination of material and design properties, lifetime predictions are finally obtained from theory, in agreement with experimental observations. Consequently, change of current - time characteristics is indicated by using results of lifetime predictions. Recommendations are also made to reduce the experiments needed for determination of fuse lifetimes in practice.

### 8.1 Introduction

Engineering materials are normally subjected to stresses in the temperature dependent environment, consequently, components show a limited lifetime. Because of the importance of engineering reliability, extensive studies of metal deformation and fatigue [94, 95, 96] have been performed in this century.

Before the lifetime of fuse is determined, main contributions to the element damage should be defined. When fuses are subjected to current pulses, temperature rise brings about thermal strain due to thermal expansion. The strain produces stress due to the constraints of fuse elements. A cyclic thermal stress is applied to the fuse. The thermal stress fatigue is only of cyclic nature, as long as the time period for each current pulse is short enough. At the time being, this time limit is assumed to be in several milliseconds, later this limit will be discussed again. For long current pulses, in addition to the cyclic strain, thermally activated creep may play a role. For continuous loading, thermally activated creep is the main origin for the damage.

As it has been discussed in the first chapter, previously proposed methods in lifetime determination [35, 79, 97] are based on curve fitting of experimental results; lifetime relations are purely empirical either without statistical analysis or clear physical meaning. Existing standards for fuses also do not provide enough information for lifetime expectancy. This means for the prediction of lifetime that many experiments are required for each design again, above all, methods are not general, they can not give an overview for fuse ageing.

Chapters 2, 3 and 4 have extended the study to improve lifetime estimation by using statistical methods. The objective of this chapter is to develop physical models for lifetime predictions for fuses in general. This work is concerned with cyclic thermal fatigue for both short and long current pulses. Besides, creep during long current pulses and continuous loading is also discussed. In the description of this chapter, a typical time lag fuse [47] is used as an example. Afterwards, the theory is applied to semiconductor protection fuses. Results of high voltage fuses and low voltage power fuses from literature are also presented by using the methods proposed in this thesis.

## 8.2 Lifetime prediction for short current pulses

During thermal buckling, a part of the thermal strain contributes to mechanical strain to result in stress. This mechanical strain may be divided into elastic strain and plastic strain. Based on the relationship between stress and strain, the number of current pulses which fuses can withstand will be predicted, following physical modelling.

### 8.2.1 Physical models

Although less general modelling of fuse lifetime behaviour has been published up to now, enormous work has been conducted since 50's on lifetime modelling of mechanical components [46, 57, 98, 99, 100, 101]. This section attempts to make connection between general mechanics studies and specific fuse behaviour.

#### Lifetime for the elastic strain range

In terms of the number  $N$  of cycles to failure, the modulus of elasticity  $E$  and the monotonic fracture strength  $\sigma'_f$ , the elastic strain can be expressed [46, 99]

$$\frac{\Delta \varepsilon_e}{2} E = \sigma_a = \sigma'_f N^b \quad (8.1)$$

where

|                          |   |
|--------------------------|---|
| $\Delta \varepsilon_e/2$ | elastic strain amplitude                      |
| $E$                      | modulus of elasticity                         |
| $\sigma_a$               | stress amplitude                              |
| $\sigma'_f$              | fatigue stress coefficient                    |
| $N$                      | number of current pulses to blowing           |
| $b$                      | fatigue strength exponent from -0.07 to -0.15 |

#### Lifetime for the plastic range

In 1954, Manson and Coffin [98] have made two important contributions on the subject of metal thermal fatigue at the same time independently. These contributions propose a relationship between the plastic strain and the number of cycles to failure which have formed foundations for thermal fatigue studies up to now. This relationship is named as Manson - Coffin law [46, 98, 99]. With this relationship, the plastic part of the strain is related with the number of cycles to failure

$$\frac{\Delta \varepsilon_p}{2} = \varepsilon_f N^c \quad (8.2)$$

where

|                          |  |
|--------------------------|--|
| $\Delta \varepsilon_p/2$ | plastic strain amplitude                     |
| $\varepsilon_f$          | fatigue ductility coefficient                |
| $N$                      | number of current pulses to blowing          |
| $c$                      | fatigue ductility exponent from -0.5 to -0.7 |

#### Thermal buckling for wire elements

Thermal strain induced in the fuse element due to a current pulse is given by

$$\Delta \varepsilon_{th} = \beta T$$

where  $\beta$  is temperature coefficient for the thermal expansion and  $T$  is temperature difference. Thermal buckling occurs (see Chapter 7) for the temperature rise above the critical limit. Only a part of this thermal strain contributes to the actual mechanical strain. In Chapter 7, the deflection factor is derived as

$$\gamma = \frac{1}{2} + \frac{2\pi^2 I_m}{l_0^2 A \beta T} \quad (8.3)$$

For intermediate and high  $I^2t$  values of current pulses, the deflection factor  $\gamma$  is almost a constant, the mechanical strain is

$$\Delta\varepsilon_m = \gamma \Delta\varepsilon_\theta \quad (8.4)$$

According to the discussion above, the mechanical strain amplitude  $\Delta\varepsilon_m/2$  is generally given by

$$\frac{\Delta\varepsilon_m}{2} = \frac{\Delta\varepsilon_c}{2} + \frac{\Delta\varepsilon_r}{2}$$

### 8.2.2 Results of lifetime predictions for miniature fuses

To demonstrate the validity of our models, comparisons will be presented by using both predictions based on measurements of displacements and predictions purely from simulations. For the lifetime predictions, material properties listed in Table 8.1 are used. The values directly measured or derived are indicated in the source item as TUE. The values from fuse manufacturer and from the literature are also indicated. In addition, diameter, resistivity, temperature coefficient of resistivity, fracture stress and elasticity have also been measured.

*Table 8.1 Material properties in the modelling*

| Properties                                      | Source         | Values   | Units             |
|---|----------------|----------|-------------------|
| wire diameter $d$                               | Littelfuse     | 0.103E-3 | m                 |
| fatigue strength exponent $b$                   | Hertzberg [46] | -0.08    |                   |
| fatigue stress coefficient $\sigma'_f$          | Littelfuse     | 115E6    | Pa                |
| thermal expansion coefficient $\beta$           | Littelfuse     | 22.1E-6  | m/mK              |
| modulus of elasticity $E$                       | Littelfuse     | 61E9     | Pa                |
| equivalent mass density $\gamma$                | TUE            | 8.6E3    | kg/m <sup>3</sup> |
| equivalent specific heat $C$                    | TUE            | 254      | J/kgK             |
| resistivity at 20 °C $\rho_0$                   | Littelfuse     | 3.48E-8  | W.m               |
| fatigue ductility exponent $c$                  | Hertzberg[46]  | -0.5     |                   |
| temperature coefficient of resistivity $\alpha$ | TUE            | 4.5E-3   | 1/K               |
| deflection factor $\gamma$                      | TUE            | 0.5      |                   |

### Predictions based on measurements of displacements

From displacement measurements, mechanical strains were determined [55, 57] as presented in Table 8.2. The mechanical strain  $\Delta\varepsilon_m$  was considered as the difference between the thermal strain  $\Delta\varepsilon_{th}$  contributed by the temperature rise and the apparent strain  $\Delta\varepsilon_a$  determined from the maximum displacement by the high speed films. Results related with different  $I^2t$  values of current pulses are summarised in Table 8.2 with the calculated lifetime  $N$  for the elastic relationship (see Eq. 8.1).

**Table 8.2** Lifetime predictions based on elastic strain ranges

| $I^2t_{pulse}$ $\Lambda^2s$ | $T$ $^{\circ}C$ | $\Delta\varepsilon_{th}$ % | $\Delta\varepsilon_a$ % | $\Delta\varepsilon_m$ % | $N$              |
|-----------------------------|-----------------|----------------------------|-------------------------|-------------------------|------------------|
| 0.22                        | 52              | 0.11                       | 0.05                    | 0.06                    | $9.5 \cdot 10^9$ |
| 0.37                        | 101             | 0.22                       | 0.10                    | 0.12                    | $1.6 \cdot 10^6$ |
| 0.60                        | 164             | 0.36                       | 0.17                    | 0.19                    | $5.2 \cdot 10^3$ |
| 0.78                        | 205             | 0.45                       | 0.21                    | 0.24                    | 283              |
| 0.98                        | 284             | 0.62                       | 0.28                    | 0.34                    | 3.6              |

Figure 8.1 compares these calculated lifetimes (see Table 8.2) with experimental results, where  $I^2t_{min}$  is the minimum  $I^2t$  value corresponding to current - time characteristics at the same time as the pulse time for a current pulse.

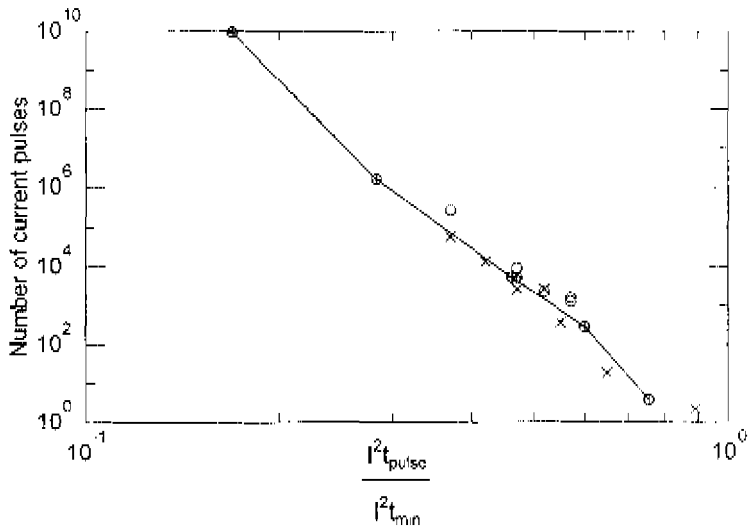


**Figure 8.1** Comparisons of experimental results with lifetime predictions "⊕" based on displacement measurements for different current pulses  
"x": sinusoidal (exp.); "o": rectangular (exp.)



In this graph, Mark "o" indicates the observations for rectangular current pulses and mark "x" depicts the results for sinusoidal current pulses. The curve with mark  $\oplus$  gives the predicted values of lifetimes based on the elastic strain relationship.

#### Purely theoretical lifetime predictions

In order to estimate lifetimes without use of any empirical relation, later on the temperature rise and the resulting mechanical strain have been simulated by using PSPICE. By introducing the material properties listed in Table 8.1, lifetimes of fuses for pulsed currents were computed with Eq. 8.1 and tabulated in Table 8.3, where  $T_{sim}$  is the calculated temperature rise from the thermal modelling.

**Table 8.3** Theoretical lifetime for pulsed currents

|                                       |                  |                  |                  |      |      |      |
|---------------------------------------|------------------|------------------|------------------|------|------|------|
| $I^2 t_{pulse} \text{ A}^2 \text{ s}$ | 0.38             | 0.50             | 0.63             | 0.78 | 0.95 | 1.04 |
| $\frac{I^2 t_{pulse}}{I^2 t_{min}}$   | 0.29             | 0.38             | 0.48             | 0.60 | 0.73 | 0.80 |
| $T_{sim} \text{ } ^\circ\text{C}$     | 83               | 114              | 156              | 208  | 276  | 318  |
| $N$                                   | $4.7 \cdot 10^7$ | $8.9 \cdot 10^5$ | $1.8 \cdot 10^4$ | 487  | 14   | 2.4  |

Figure 8.2 compares observed lifetimes with predictions from Table 8.3. The solid line presents the lifetime calculated by using the temperature rise obtained from the thermal modelling [52].

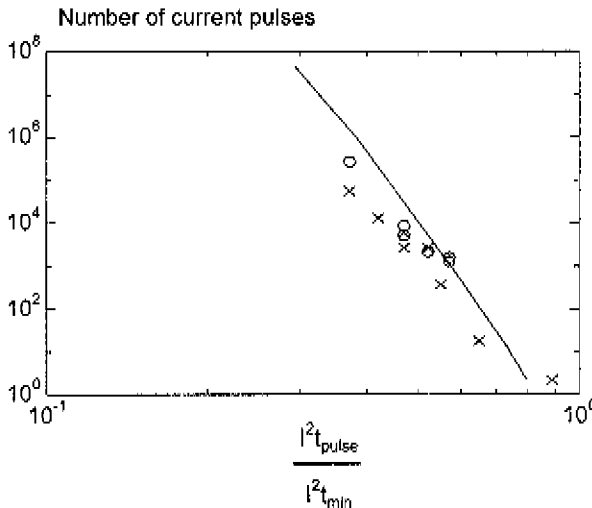


**Figure 8.2** Comparisons of lifetime predictions (Eq. 8.1) and experimental results "o": rectangular; "x": sinusoidal

### 8.2.3 Discussion

Both Figs. 8.1 and 8.2 show that the number of current pulses which fuses withstand increases as the  $I^2t$  value decreases, predictions are well fitted with lifetime observations, supposing that elastic strain is dominant. Because temperature rise  $T$  is approximately proportional to  $I^2t$ , so the number of current pulses  $N$  is approximately a linear function of  $I^2t$  on the double logarithmic scale.

Theoretically, the elastic strain is of the most significance for the high cycle fatigue, while for low cycle fatigue, the plastic strain will be the dominant item. The takeover point is situated at lifetimes about 1,000 corresponding to the strain amplitude 0.01 [46, 99]. Pao [100] and Logsdon [102] studied the thermal fatigue of solder joints. Pao suggested that the elastic fracture is also dominant for low cycle fatigue for thin layers with thickness of 0.254 mm, because there is insufficient thickness to accommodate the plastic information. This is in accordance with our experimental observations (see Figs. 8.1 and 8.2), where wires with diameters in order of 0.1 mm are used.

Although agreement has been found between lifetime predictions and actual values, it should be aware that for a fuse element, the deformation can be developed in the axial direction and in the radial direction. The stress in the radial direction depends on the thermal expansion coefficients of silver, tin-zinc alloy and the temperature rises. In the prediction above, the radial strain and stress are not concerned. Besides, the ductility coefficient, oxidation in the element, the connection technology and the local temperature rise may also have influences on lifetimes. In Chapters 2 and 3, the resistance increase has been reported during the fuse life, however, no use of resistance change has been made for the lifetime determinations.

## 8.3 Lifetime prediction of miniature fuses for long current pulses

After fuses are subjected to a number of long time current pulses, the position of elements changes. Additionally, after breaking longitudinal cracks can also be found on the element surface for long current pulses, in contrast to the radial cracks for short current pulses. This suggests that the plastic deformation is induced. Because of cyclic nature, the lifetime is suggested to follow Manson - Coffin law. In this process, the steady creep strain rate is taken for the determination of plastic strains.

### 8.3.1 Temperature relationship

Temperature rise for long current pulses can be determined both by simulations and experiments. Two experimental methods have been applied to determine the average temperature rise of fuse wire elements. The first method is based on the measurement of the voltage and current, from which resistance is determined. As the resistivity dependence of material on temperature is known, the average temperature rise can be calculated.

The second procedure [55] is derived from the buckling theory proposed in Chapter 7. When electric currents are applied to fuses, thermal buckling takes place. Both currents and displacements may be measured. As it has been proved that the maximum displacement has a well defined relationship with the average temperature rise, the relationship between the temperature rise and the current is found.

Figure 8.3 shows results of average temperature rises obtained from measurements of displacements. The experimental relation between the average temperature rise  $T$  and the d.c. current  $I$  is determined from curve fitting to be

$$T = 10^{3/2} I^3$$

This suggests a general expression for the temperature rise  $T$  which can be described by

$$T \propto I^{a_1}$$

where  $a_1$  is a constant.

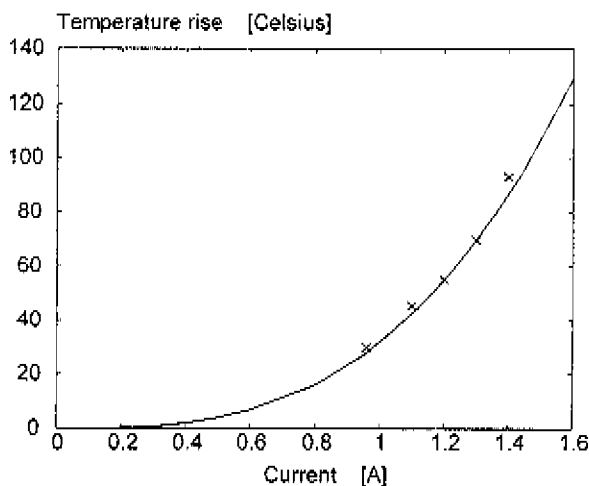


**Figure 8.3** The average temperature rise determined from displacement measurements as a function of d.c. current

### 8.3.2 Creep rate

The creep rate is related to stress, temperature and time in general. Various relationships based on experiments have been proposed in the past. One of the common used relationships is the power law creep [45, 46] for the steady state creep rate.

This states that at intermediate to high stresses and at temperature above  $0.5 T_m$ , where the thermally activated creep process is dominated by the activation energy for self-diffusion, the creep rate is given by

$$\dot{\epsilon}_s \propto \sigma^{a_2}$$

where  $a_2$  is a constant ( $a_2 = 4-5$ ). This stress dependency has been demonstrated and holds for pure metals and their solid solutions (silver, copper, aluminium, nickel and etc.). If  $\sigma \propto T$ , the creep rate is rewritten as

$$\dot{\epsilon}_s \propto T^{a_2} \propto I^{a_1 a_2}$$

For the determination of creep, the relationship with time is essential. Concerning time influence, during each period, the creep rate may be assumed to be

$$\dot{\epsilon}_p \propto I^{a_1 t^{a_2}} t^m \quad (8.5)$$

where  $m$  is a material constant.

### 8.3.3 Lifetime relationship

If the plastic strain is assumed to be equal to creep strain contributed by the steady state creep rate, it follows

$$\begin{aligned} \Delta \epsilon_p &= \dot{\epsilon}_p t \\ \Delta \epsilon_p &= A_0 I^{a_1 t^{a_2}} t^{m+1} \end{aligned} \quad (8.6)$$

Combination of Eqs. 8.2 and 8.6 leads to the relationship for the number of current pulses for fuses to blow

$$N = \left[ \frac{A_0 I^{a_1 t^{a_2}} t^{m+1}}{2 \epsilon_f} \right]^{1/c} = K_0 I^{a_1 t^{a_2/c}} t^{(m+1)/c} \quad (8.7)$$

where  $A_0$ ,  $K_0$ ,  $a_1$ ,  $a_2$ ,  $\epsilon_f$  [98, 103] and  $m$  are constants. The relation between  $K_0$  and  $A_0$  reads

$$\frac{A_0}{2 \epsilon_f} = K_0$$

Finally, the relationship for the number of current pulses which fuses withstand is defined.

### 8.3.4 Determination of parameters

For the time delay fuses in discussion, the value  $a_1 = 3$  can be obtained from Fig. 8.3. The value of  $a_2$  is given by  $4 < a_2 < 5$  according to the power law creep, a trial value  $a_2 = 4.5$  is suggested therefore. Manson - Coffin law states that the fatigue ductility exponent  $c = -(0.5 - 0.7)$ , in this work,  $c = -0.5$  is suggested.

For the determination of the material constant  $m$ , experiments were carried out for the same current but with different on times. The number of current pulses which fuses withstand and the on time should have a linear relation on a double logarithmic scale; the slope of the relation is a measure for the value of  $m$ .

From the experimental results listed in Table 3.3 of Chapter 3, three series of experiments were used for this purpose. Their values are given in Table 8.4.

**Table 8.4** Data used for the determination of material constants

| $I$    | $t_{on}$ | $t_{off}$ | 5%  | mean $N$ | 95%  |
|--------|----------|-----------|-----|----------|------|
| 1.52 A | 1min     | 1min      | 20  | 80       | 158  |
| 1.52 A | 5min     | 5min      | 3.8 | 19.7     | 42.4 |
| 1.52 A | 10min    | 1min      | 2.1 | 7.9      | 15   |

According to this table, Fig. 8.4 gives the results for the time slope.  $m$  is found to be -0.5, therefore the exponential component for time is -1 in the lifetime relation. Another feature of this evaluation is that the determination of constant  $K_0$ . From Fig. 8.4, the value of  $K_0$  for the mean [63] is found to be  $3.6 * 10^8$  (the 5 % value is  $7.8 * 10^7$ ).

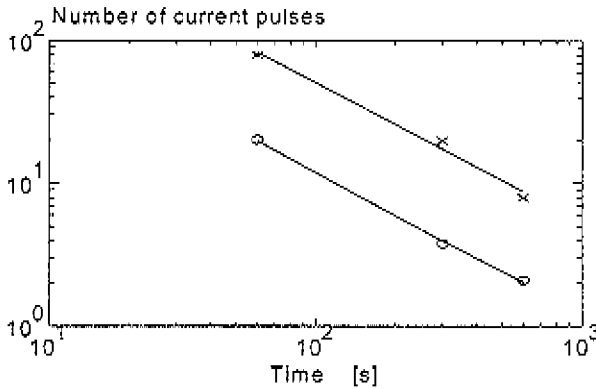


**Figure 8.4** Determination of material constants  $m$  and  $K_0$   
 "x—x": mean values; "o—o": 5% values

### 8.3.5 Discussion

As a final expression for the lifetime consumption by plastic strain, it follows from Eq. 8.7

$$N = K_0 I^{-27} t^{-1} \quad (8.8)$$

with  $K_0 = 3.6 \cdot 10^8$ ,  $a_1 = 3$ ,  $a_2 = 4.5$ , and  $m = -1/2$ . In Fig. 8.5, the relation Eq. 8.8, based on limited data from Table 8.4 are compared with the whole set of experimental lifetimes from Tables 3.1 and 3.2.

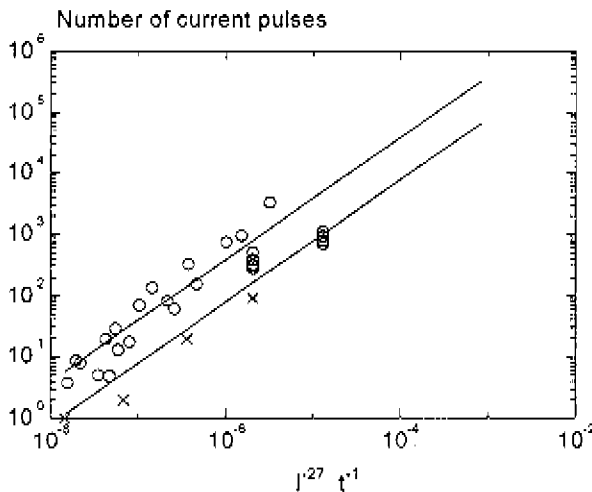


**Figure 8.5** Comparisons of predicted lifetimes and observations  
 "o": for the on time from 10 seconds to 1 hour (see Table 3.3)  
 "x": 5% values for the on time of 1 hour (see Table 3.1)

Considering the experimental lifetimes in Table 3.3, showing such a wide range of values for current  $I$ , on time  $t_{on}$  and off time  $t_{off}$ , it is remarkable that the lifetimes can be related with only one expression, even when some parameters were determined by using a part of this table.

For the diffusion dominant situation, diffusion thickness is known to be proportional to the square root of time and diffusion coefficient. The diffusion coefficient [46] is related with the activation energy  $Q$  and temperature rise  $T$ . Combining the diffusion with the power law creep, the creep rate can be approximated by

$$\dot{\epsilon}_c \propto \exp\left(-\frac{Q}{2RT}\right) I^{1/2} \sigma^{1/2}$$

where  $Q$  is the activation energy for diffusion,  $R$  is gas constant. This means that as temperature rise  $T$  decreases, the lifetime increases with  $K_\theta$  also.

#### 8.4 Lifetime prediction for a continuous loading

For continuous loading, the creep accumulation may be different from creep with cyclic loading. However, considering the plastic strain relation proposed in Section 8.3, the lifetime reads

$$N = 1 - K_0 I^{0.5} t^{0.5} I^{(1+0.5n)}$$

resulting in a rupture time  $t$

$$t = K_0^{-1/n} I^{-0.5/n} \quad \text{or} \quad t = 3.6 \cdot 10^8 I^{-2.2} \quad (8.9)$$

Figure 8.6 shows comparisons of predictions from Eq. 8.9 and observations from Fig. 3.3.

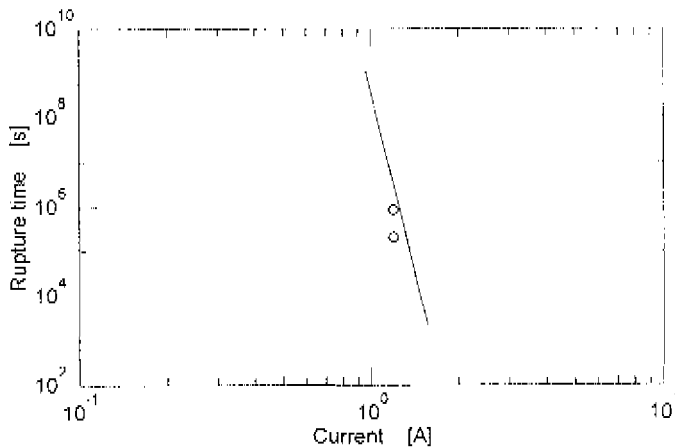


**Figure 8.6** Comparisons of predictions (Eq. 8.9) and observations for a d.c. current  $I = 1.5 \cdot I_n$

It shows that indications for the minimum melting current which is normally determined after several hours has lost their relevance in the very long time.

### 8.5 Change of current - time characteristics

Up to now, extensive studies have been performed for lifetime determinations for short current pulses and long current pulses. It is clear that fuses age if creep of the fuse element happens or elastic fracture is involved.

Because of ageing, current - time characteristics change. They shift to faster operating curves. If a fuse breaks after a number of current pulses, the  $I^2t$  value of the last current pulse before breaking is the momentary  $I^2t$  value of the fuse. This means that Eq. 8.7 can be used to determine the whole shifted  $I - t$  curve of fuses with the number of long current pulses  $N$  as a parameter. For short current pulses, Eq. 8.1 can be used for determining the shift of  $I - t$  curve. For the transition from the creep dominant interruption to the elastic fracture, the number of current pulses for fuses to withstand will be the same. From Fig. 8.2 and Eq. 8.7, for different current magnitudes, the on time for the transition is estimated to be about 5 seconds for the time lag fuses under discussion. Figure 8.7 shows comparison of current - time characteristics for new products and fuses after subjected to 10000 current pulses. Curve "a" indicates the shifted  $I - t$  characteristic calculated by creep dependent part and the elastic fracture determined part.

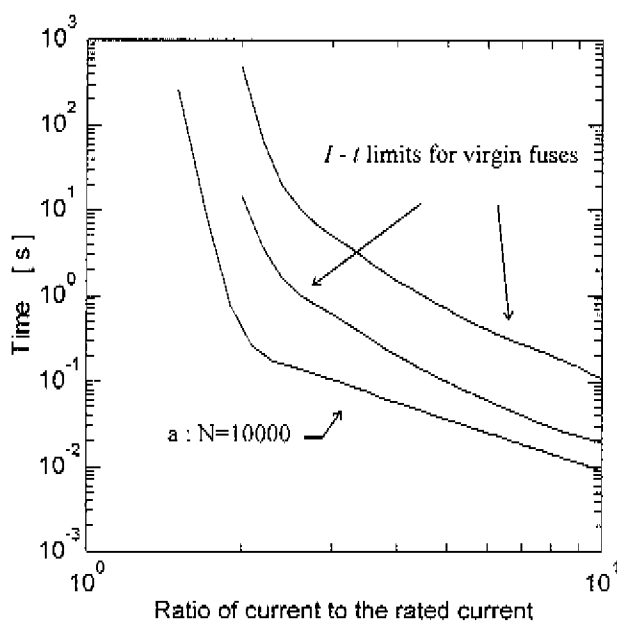


**Figure 8.7** Comparison of current - time characteristics of virgin fuses (before current pulses) with that after current pulses ( $N=10000$ )

Physically, the shift of current - time characteristic is also directly related with the increase of resistance of fuses. In the adiabatic heating, the  $I^2t$  for the melting is a constant which is proportional to the inverse of resistivity (or resistance). However, the minimum fusing current is proportional to the inverse square root of the resistivity. Considering the fact that resistance increases after use indicated in Chapters 2 and 3, the more shift of  $I - t$  curve in the adiabatic range will be expected as compared with the shift in the range of the small currents for the same amount of resistance increase. In other words, for the same amount of current pulses, the shift of  $I - t$  curve is larger for small currents. This is not significant in Fig. 8.7.

Previous researchers considered that the fatigue of fuse element was mainly controlled by the plastic strain range. In Section 8.2, lifetimes are predicted according to the elastic fracture for short current pulses. If the relative  $I^2t$  value of the pulsed current is smaller than 0.7, elastic strain plays an important role. In the range of large relative  $I^2t$  value  $> 0.7$ , plastic strain exists, cracks propagate in a more or less brittle fashion [100] for wire elements with small diameters (corresponding to the plate with a thickness of 0.254 mm), Eq. 8.1 can still be used for the fuse lifetime prediction. In Sections 8.3 and 8.4, the lifetimes are determined with the plastic strain (creep) for long current pulses and continuous loading. At this moment the reason is still not clear why not all processes follow the elastic fracture.

From Fig. 8.7, it is also clear that the proper protection provided by new fuses may be not valid for fuses after use because of the shift of current - time characteristics. For this reason, it is recommended that fuse manufacturers should provide the information of shift in current - time characteristics to avoid unexpected interruption due to ageing. This requirement is still not yet specified in IEC Publications for fuses.

## 8.6 Lifetime prediction for notched strip fuses

In the previous sections, lifetime predictions have been presented where typical commercial miniature fuses have been taken as examples. This section describes efforts to apply the method of lifetime predictions for semiconductor protection fuses subjected to short current pulses. Thermal buckling of the element due to electric currents is discussed, and thermal fatigue is considered as the main reason for ageing.

For the commercial semiconductor protection fuses in test, the rated current of silver fuse elements was 160 A. The fuse construction was shown in Fig. 1.1, the element shapes and dimension were shown in Figs. 4.4 - 4.7.

### 8.6.1 Comparisons of calculations and observations

When fuses are subjected to current pulses, temperature rise brings about thermal stress due to thermal expansion. As the thermal stress is above a certain value, the fuse element tends to move and leaves its previous position. During post buckling, only a part of the thermal strain is contributed to the mechanical strain to produce stress. Therefore, to predict the lifetime, the temperature distribution and the thermal buckling behaviour were studied and described in Chapters 4 and 6.

Thermal strain induced in the notch region of the fuse element due to a current pulse is proportional to the temperature rise. The total thermal strain can be obtained by integrating from  $x = l_1$  to  $l_2$  and is approximated by



$$\Delta \varepsilon_{th} = \sum_{x=l_1}^{l_2} \beta T(x) = A_0 \beta T_{max} \quad (8.10)$$

where  $\beta$  is the thermal expansion coefficient of silver ( $20 \times 10^{-6}$ ),  $A_0$ ,  $l_1$ , and  $l_2$  are constants.

The mechanical strain is only a fraction of the thermal strain, it is similar to that for fuses with wire elements in air. Based on the relationship between stress and strain in the elastic range ( $\Delta \varepsilon_e = \Delta \varepsilon_m$ ), the number of current pulses  $N$  which fuses can withstand may be predicted [46, 97] according to Eq. 8.1.

For silver fuse elements, modulus of elasticity  $E = 71 \times 10^3 \text{ MPa}$ , fatigue stress coefficient  $\sigma_f = 130 \text{ MPa}$  can be used. Fatigue strength exponent  $b = -0.08$  was assumed. For elements with five rows of notches, parameters  $A_0$ ,  $l_1$ ,  $l_2$  in Eq. 8.10 were determined from the simulation to be  $A_0 = 0.23$ ,  $l_1 = 1.5 \text{ mm}$ ,  $l_2 = 4 \text{ mm}$ . However, the deflection factor  $\gamma$  in Eq. 8.4 is not known. To formulate the calculations, this factor was assumed to be the same as for the elements with one row of notches shown in Fig. 4.5. Based on the experimental observations presented in Chapter 4,  $\gamma = 0.88$  was found.

As it has been indicated in Chapter 4, to study the deformation mechanism of semiconductor fuses, lifetime tests were performed with different types of fuse elements (*type A*, *type C* and *type D*). From the experiments, the number of current pulses which fuses withstood and their mean values were obtained. Comparison of predictions and the mean values of observations is shown in Fig. 8.8. This figure clearly shows that for pulsed currents with a duration of about 10 ms, lifetimes of fuses with sand decrease as the  $I^2 t$  value increases, predictions are in the conservative side of the number of current pulses which fuses withstand.

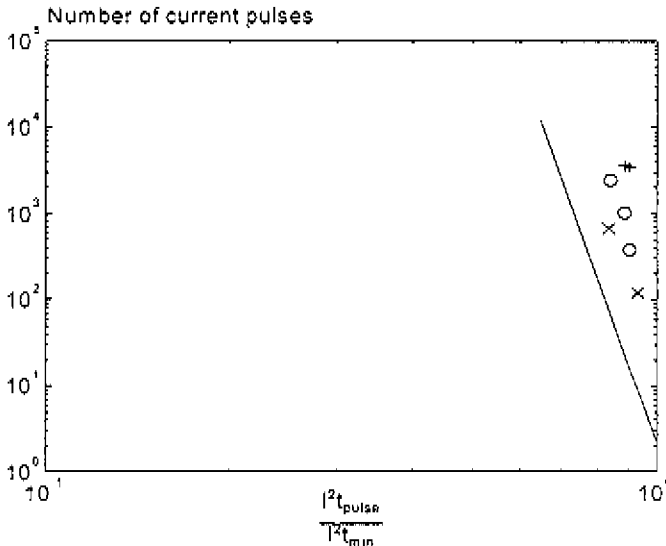


**Figure 8.8** Comparisons of predictions and observations  
 "x": type A; "o": type C; "+": type D; —: Calculation

In Fig. 8.8, the number of current pulses that fuses withstand has been presented together with experimental results for short current pulses of about 10 ms. For real semiconductor fuse applications, cycles are often with on times of around 5 seconds (motor starting) or several minutes (traction). From the discussion in Section 8.5, it is known that the elastic fracture mechanism mainly determines lifetimes for the time lag fuses for on times smaller than 5 seconds. Because the silver element creeps slower than the element for the time lag fuses, the time limit for the elastic fracture mechanism is expected to be larger than 5 seconds, suppose that fuses are properly designed. Therefore, the results here are still valid for this situation. For on times in the range of several minutes, a further examination is needed to consider the competition between creep and elastic fracture.

### 8.6.2 How to reduce ageing

Ageing is a time dependent process. Effects of long time loads on the lifetime consuming are mainly to be of creep nature (including diffusion and oxidation). For short time loads, lifetimes are considered to be consumed due to cyclic fatigue related with strain variations [57].

As ageing due to temperature rise is concerned, perhaps the maximum temperature can be proposed as one factor for design and application of fuses. According to the deformation mechanism map [46], for temperature below 200 °C there will be no plastic deformation for silver elements. On this basis, fuses should be designed to carry currents which do not produce overheating. For the commercial fuses under investigation, when with the rated current of 160 A is exerted, the corresponding temperature rise is found to be 200 °C from the FEMTP simulation. Therefore, in theory this means the designed fuses will have infinite lifetimes if the current flows through these fuses without switching off.

The argument here is that deformation mechanism maps are established at a rather slow heating up process, is the result relevant to fuse applications? According to observation provided in [32], during the rapid heating up diffusion may occur on the grain boundaries, because of inhomogenous material construction. It means that the criteria from the deformation map is only valid for the small current carrying ability and constant loads which do not always reflect reality.

Because of cyclic effects, temperature variations produce deformation even at the lower temperature, as a consequence, lifetime reduction can not be avoid. The question is how to design an element shape with the optimal lifetime.

Straight fuse elements provide a relative high stress during current flowing, because thermal expansion can not be released easily. In practice, often originally bent or waved fuse elements are used. In the most situations, the element notch has to withstand the maximum stress because of the highest temperature rise and the smallest cross sectional area. The local stress in the fuse element notch is determined by thermal expansion, strain due to the displacement in the axial direction and strain due to the displacement in the perpendicular direction. Another factor is the curvature at the notch due to the vertical displacement. On the one hand, the vertical displacement will release part of thermal expansion, stress decreases. On the other hand, bending will increase the stress on the outer surface. The final situation depends on the compensation of two factors.

The breaking location of fuse elements is situated at the place where maximum deformation is induced. Experiments indicate the breaking usually occurs at the notch near end caps. As

temperature rises near end caps are not the highest, stress release is expected to be less at these locations due to the element design.

For very short pulse times, lifetime difference due to element shapes, sand and bounded sand will decrease in theory because of the delay in displacement. The maximum stress imposed depends mainly on thermal expansion caused by joule heating.

### 8.7 Application of the method to results from literature

In this section, results presented in several literature for different types of fuses will be examined with the proposed lifetime determination method for miniature fuses. For the power law of creep rate,  $a_2 = 4 \sim 5$ , the exponent in Eq. 8.7 can thus be from 24 to 30, if  $T \propto I^2$ . Because of heat transfer in sand,  $a_2 < 3$  can be expected in the expression  $T \propto I^{a_1}$  for low voltage power fuses. Consequently, the exponent of current in the lifetime relation can be below 24. Stevenson [97] obtained experimental results for semiconductor protection fuses with on times from 5 seconds to 10 minutes. The curve slope in the fitted function can be found to be 0.045 on a double logarithmic scale. This value is very close to  $1/24$  and comparable to the slope  $1/27$ . This encourage further practice of using physical models presented in Section 8.3

In 1972, Sletterink [104] conducted experiments for determining the number of current pulses that fuses withstood. The tested fuse links were made of silver, a spot of pure tin was positioned between two rows of notches of the fuse link. The rated current of these fuse links was 100 A. The number of current pulses with on times from about 10 seconds to 1000 seconds was presented for different current values between 160 A and 400 A. From the experimental results, the current - time characteristics of fuse links were evaluated with the number of current pulses as parameter. As discussed in Section 8.3, for the pure diffusion controlled ageing, the exponent of time is about -1 for the lifetime relation (see Eq. 8.7). Because of stress concentration near the notch, it may be expected that creep increases faster for the notched element than for the uniform element due to diffusion. For the same reason as indicated in Section 8.3, this time exponent has to be determined from experimental values. The exponent of on time  $t$  was found to be -4. Following this scheme, calculations were made in use of

$$N = k_0 \frac{10^{16}}{t^4} \left( \frac{I_n}{I} \right)^{25.5} \quad (8.11)$$

where  $k_0 = 2.51$ ,  $I_n = 100$  A. Results from the literature are presented with calculations from Eq. 8.11 in Fig. 8.9, where marks represent the observations for different currents and lines give the corresponding calculations. From this, again one may conclude that from the determination of one set of ageing results, all data can be related with the same expression.

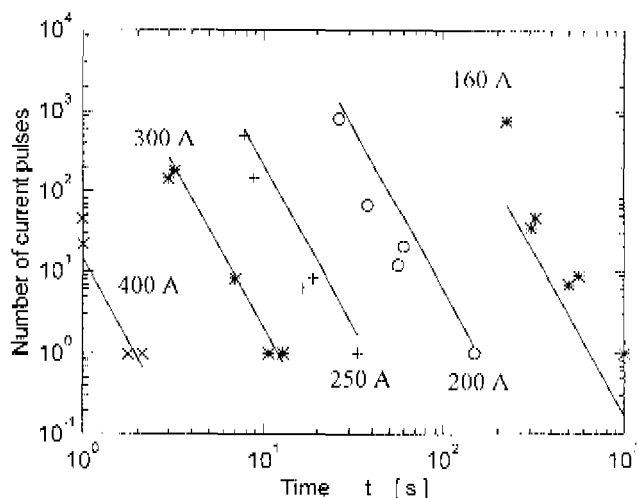


**Figure 8.9** Comparisons of calculations (Eq. 8.11) and observations after Sletterink [104]  
 — : Calculation; x, \* + o : Observations

For the h.v. motor protections, Ossowicki [105] presented experimental results of copper fuse elements for cyclic loading. In a similar way, results there can also be extrapolated on the basis of elastic fracture mechanisms.

## 8.8 Recommendations

In the existing standard IEC Publication 127, pulse tests and endurance tests have been specified for small amounts of cyclic currents. A very limited number (1000 pulses in IEC 127) of pulsed current is applied to the fuse to examine the quality of fuses. On the one hand, the magnitude of pulsed current will be too low to give a indication of pulse withstand ability of fuses; on the other hand, from this investigation it is clear that fuses may withstand some thousands of pulsed currents, but they may still fail after a long run in service. Results from the tests can not give expectations how long fuses operate according to their characteristics. The only thing known is that fuses can withstand the specified numbers of current pulses. Nevertheless, this measure indeed is effective to remove the initial manufacturing failures of the products. Therefore, the requirement in IEC is unsure to guarantee the long term behaviour of fuses, more specific values of lifetime should be carried out as a guidance of selectivity.

In contrast to these, for both pulse tests and endurance tests it is suggested that fuses are tested for two values of specific current pulses until their operation. High current values may be used to reduce the testing time. For long current pulses according to Eq. 8.7, constant  $K_0$  and  $m$  can be determined. Based on these known factors, lifetimes can be predicted for general conditions. For short current pulses, because the slope is approximately constant for different  $I^2t$  values of current pulses, lifetimes can also be determined as a linear function of the relative  $I^2t$

value. On the basis of lifetime information, the shift of current - time characteristics can be determined. The similar issues can be made also for semiconductor protection fuses.

## 8.9 Conclusions

In this chapter, physical models for lifetime predictions have been established for short current pulse and long current pulses. Possibilities to extend the model for continuous loading are also discussed. Predictions for typical time lag fuses have been demonstrated and compared with experimental observations; agreement has been found. The work is developed purely on the physical basis and results obtained so far therefore provide a significant understanding of fuse ageing problems compared with previous investigations. Methods proposed are also supported by previous contributions which cover topics of semiconductor protection fuses, low voltage fuses and high voltage fuses. For short current pulses, the exponent of  $I^2t$  in lifetime relation depends on the element materials, typically -12.5. For long current pulses, the exponent of current  $I$  is from 24 - 30 and the exponent of time  $t$  may vary from -1 to -4. In general applications of the methods, only a few of experiments are needed to determine fuse lifetimes for cyclic loading. Therefore, it assists the evaluation of commercial products, new developments and applications of fuses. Also this work offers a basis for more powerful tests for detecting fuse ageing.

## **Part V General Conclusions**

## Chapter 9 Conclusions

This thesis deals with ageing problems of electric fuses in service and describes methods to predict lifetimes for these fuses. Typical miniature fuses and semiconductor protection fuses are used as examples to demonstrate the application of proposed methods. This work has been carried out in co-operation with SIBA GmbH, Lünen, Germany and Littelfuse BV, Utrecht, the Netherlands. In particular, attention has been paid to relations between motion and lifetime for different types of fuse elements. Simulations of non-linear thermal and mechanical responses due to electric current are performed. Deformation is studied for notched fuse elements by using a scanning electron microscope and an optical microscope.

### 9.1 Main results

- (1) During the lifetime of miniature fuses, measured resistance shows a gradual increase for short, long current pulses and continuous loading. As a measure for the reached lifetime consumption, it is recommended to check the voltage drop.  
After semiconductor protection fuses subjected to current pulses, damage of the fuse elements has been examined by using a scanning electron microscope and an optical microscope. Significant deformation was found in the notch of the element. However, resistance remains more or less the same. Resistance measurements can only indicate the spread of new products and provide a little guidance for the lifetime consumption for short current pulses.
- (2) The temperature distribution within a fuse is simulated by using the electrical analogue method for both miniature fuses and semiconductor protection fuses. Voltage responses of current pulses and current - time characteristics have been found in agreement with experimental observations. For semiconductor protection fuses, numerical results of the current density distribution can also be obtained with EMTP from three dimensional non-linear transient simulations.
- (3) For straight wire elements, the average temperature rise can be obtained from resistance determinations for arbitrary temperature distributions with an acceptable accuracy. From the average temperature rise or the temperature distribution, the displacement and corresponding stress are calculated on the basis of thermal post buckling analysis. The displacement perpendicular to the element is proportional to the square root of the average temperature rise. The stress along the element is approximately the same and proportional to the total thermal expansion.
- (4) The previously suggested empirical value of the deflection factor for considering fuse element buckling has been determined experimentally and given a theoretical basis for both miniature fuses and semiconductor protection fuses.

- (5) For short current pulses, the lifetime is predicted based on the elastic fracture mechanism in agreement with experiments. The lifetime can be approximated as a linear function of the  $I^2t$  value of a current pulse on the double logarithmic scale for miniature fuses and semiconductor protection fuses.
- The exponent in the lifetime function may vary from -8 to -20 for different types of miniature fuses; the wave form of the current pulse has a secondary influence on the lifetime.
- For the practical interest, combination of good heat conduction from the element to its surrounding and the stress release due to element wave shapes may significantly increase the fuse lifetimes.
- (6) For long current pulses, the lifetime of miniature fuses is predicted by considering the thermally activated creep process. The lifetime can be represented as an exponential function of current and on time. Exponents of current and on time depend on designs and materials of the fuse element; they can be determined by a few experiments. This function has been confirmed by experimental results for a typical time lag miniature fuse. Application of the lifetime relation is also addressed for other types of fuses with and without M-effects.
- (7) For continuous current, the lifetime of miniature fuses is approximated on the basis of the thermally activated creep model for long current pulses.
- (8) In existing standards related with fuses, there are no systematic methods for determining the fuse lifetime or the number of current pulses that fuses withstood and the deterioration of current - time characteristics. If the lifetime is required, a lot of experiments should be realised.

In this work, after lifetime determinations for short and long current pulses, the shift of current - time characteristics can be determined either experimentally or theoretically with the number of current pulses as parameter. This has been demonstrated for a typical time lag miniature fuse. Use of the methods proposed here will therefore be able to provide the information for replacing aged fuses in the installations and greatly reduce unexpected interruptions in the systems.

## 9.2 Suggestions for future work

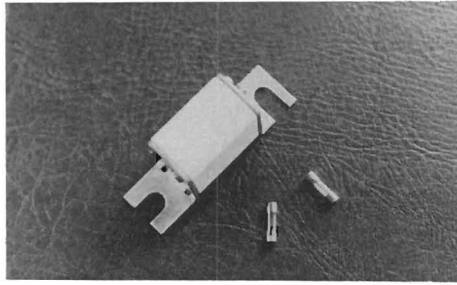
- (1) For fuses subjected to short current pulses, lifetime predictions have been presented. The graphic presentation uses the minimum melting  $I^2t$  value of fuses at 10 ms as a base. In theory, this minimum melting  $I^2t$  value can be replaced at different melting times to provide guidance for practice as long as the pulse time is within a certain limit (about 5 seconds for *Ag/SnZn* wire elements).
- For silver elements used in high voltage, low voltage and semiconductor protection fuses, no enough experimental data of lifetimes are available at this moment for different pulse times. Precautions should be taken for using this limit. In addition, some more experiments are still needed to solve the problem of lifetime prediction in continuous loading.
- (2) To improve reliability of fuses, both good heat transfer and stress release are required. For example, substrate fuses may provide excellent heat transfer media. Because of mismatch



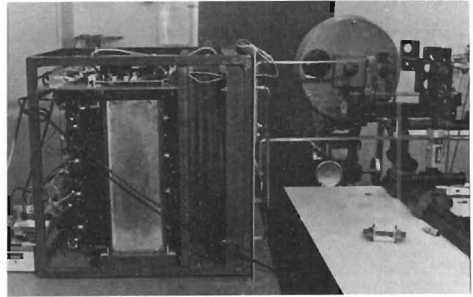
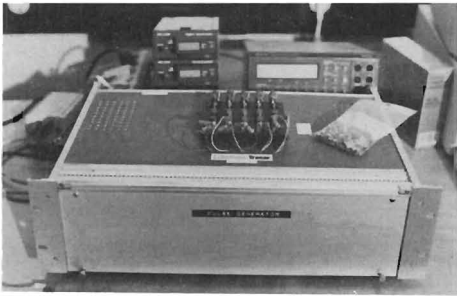
of thermal expansion, however, extra stress can be induced for current pulses and lead to cracks in the interface between conducting materials and the silver base. Therefore further studies are desired.

- (3) For designing optimal shapes of fuse elements, the proposed finite element formulation can be extended to include the influence of sand, element notches and the initial shape of the element.
- (4) To assist applications of fuses, the work of this thesis can be further implemented into a software to help application engineers to control and examine reliability of fuses.

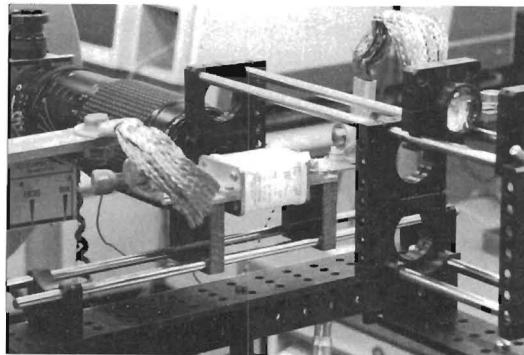
## Appendix Photos of Fuses and Experiment Setup



*Fuses used in experiments*



*Test circuits a : for miniature fuses ; b : for semiconductor protection fuses*



*Experimental setup for measuring displacements*

## Reference

- [ 1 ] A. Wright and P.G. Newbery, "*Electric fuses.*" London: Peter Peregrinus Ltd, 1984.
- [ 2 ] H. Johann, "*Electrical fuses for low voltage,*" Berlin: Springer, 1982.
- [ 3 ] J.M. Wang, "*Low voltage fuses.*" Beijing: Machinery industry, 1983.
- [ 4 ] J.G.J. Sloot, "*Progress in the field of arc extinction in fuses,*" Proc. ICSAP (int. conf. on switching arc phenomena), Lodz, Part 2, pp. 86-100, 1989.
- [ 5 ] E.F. Veverka, H.L. Hess and A.K. McCabe, "*Bibliography of switchgear literature, IEEE committee report,*" IEEE Trans. Power Delivery, Vol. 5 No. 1 Jan. 1990.
- [ 6 ] J.G. Leach, P.G. Newbery and A. Wright, "*Analysis of hrc fuselink prearcing phenomena by a finite difference method,*" Proc. IEE, Vol. 120, No. 9, pp. 987-993, 1973.
- [ 7 ] R. Wilkins and P.M. McEwan, "*AC short circuit performance of notched fuse elements,*" Proc. IEE, Vol. 122, No. 3, pp. 289-292, 1975.
- [ 8 ] X.Z. Meng and J.M. Wang, "*The simulation of prearcing characteristics of fuse elements in the finite element method,*" Proc. ICEFA (int. conf. on electric fuses and their applications), Eindhoven, pp. 24-29, 1987.
- [ 9 ] M. Hofmann and M. Lindmayer, "*Pre calculation of time current characteristics of M-effect fuse elements,*" Proc. ICEFA, Eindhoven, pp. 30-39, 1987.
- [ 10 ] J.C. Gomez, D. Tourn and P.M. McEwan, "*Investigation of the pre-arcing behaviour of dissimilar uniform double element filled fuses, using FE CAD techniques,*" Proc. ICEFA, Nottingham, pp. 65-67, Sept. 1991.
- [ 11 ] J.G.J. Sloot, "*Analog simulations of the heat flow in a high voltage fuse,*" Proc. ICEFA, Eindhoven, pp. 7-11, 1987.
- [ 12 ] L.A.V. Cheim and A.F. Howe, "*Calculating fuse prearcing times by transmission-line modelling (TLM),*" Proc. ICEFA, Nottingham, Sept. 1991.
- [ 13 ] J.E. Daalder, J. Kulsetas and W.G.J. Rondeel, "*Aging in fuses with M-effect,*" Proc. ICSAP, Lodz, pp. 295-299, 1981.
- [ 14 ] M. Hofmann and M. Lindmayer, "*Ageing of fuse elements due to cyclic overloads,*" Proc. ICSAP (int. conf. switching arc phenomena), Lodz, pp. 346-351, 1985.
- [ 15 ] D.A. Beaujean, P.G. Newbery and M.G. Jayne, "*Long term operation of high breaking capacity fuses,*" IEE Proc. A Science, Measurement and technology, Vol. 140, No. 4, pp. 331-337, July 1993.
- [ 16 ] S. Gnanalingam and R. Wilkins, "*Digital simulation of fuse breaking tests,*" IEE Proc. Vol. 127, Part C, No. 6, pp. 434-440, 1980.

- [ 17 ] J.E. Daalder and E.F. Schreurs, "Arcing phenomena in high voltage fuses." EUI Report 83-E-137. Eindhoven: Eindhoven University of Technology, 1983.
- [ 18 ] L.A.V. Cheim, A. F. Howe, "Spectroscopic measurement of fuse arc temperature." Proc. ICEFA, Ilmenau, pp. 251-258, 1995.
- [ 19 ] T. Lipski, "Application of the arc pinch forces interaction theory to the calculation of striation modulus of the strip hbc fuse," Proc. ICEFA, Trondheim, pp. 52-59, 1984.
- [ 20 ] B. Breen, "Thin film surface mount fuses," Proc. 41st Electronic Components and Technology Conference, New York, pp. 428-430, 1991.
- [ 21 ] M. Nishio, H. Kurihara, F. Ono, A. Fujii and K. Sawada, "Development of ultra-fine fuse wires," Sumitomo Electric Technical Review, No. 32, pp. 81-85, 1991.
- [ 22 ] M. Lindmayer and M. Luther, "Fusing and short circuit interruption behaviour of metal film fuses," Proc. ICEFA, Nottingham, pp. 107-113, Sept. 1991.
- [ 23 ] J.M. Wang, "Research on horse shoe core type axial magnetic field vacuum fuse," Proc. ICEFA, Nottingham, pp. 33-36, 1991.
- [ 24 ] D. Brechtken and D. König "Time / current characteristics and breaking capacity of experimental vacuum fuses," IEEE Trans. on Electrical Insulation, Vol. 28, No. 4, pp. 642-649, 1993.
- [ 25 ] D. Brechtken, D. König and B. Müller, "Thermal processes in SF<sub>6</sub> field fuses below the minimum melting current," Proc. ICEFA, Nottingham, pp. 7-12, 1991.
- [ 26 ] D. Denison, "Electronic fuses protect cable, network transformers," Electrical world, Vol. 208, No. 1, pp. 39-41, 1994.
- [ 27 ] R. Ranjan, E.W. Kalkstein, "Design, development and application of smart fuses I," IEEE Trans. on Industry Applications, Vol. 30, No. 1, pp. 164-169, 1994.
- [ 28 ] F.B. Golden, "Ratings & applications of power thyristors for resistance welding," IEEE Conf. Rec. of 4th Annual meeting of industry and general applications group, pp. 507-515, 1969.
- [ 29 ] W.J. Huber, "Transformer inrush considerations for current limiting fuses," IEEE PES (Power Engineering Society) Summer Meeting, Paper C74-386-9, July 1974.
- [ 30 ] G. Stevenson, "Cyclic loading of fuses for the protection of semi-conductors," Proc. ICEFA, Liverpool, pp. 276-283, 1976.
- [ 31 ] E.H. Williams, S.J. Battel, "Incremental failure mechanism in subminiature hermetically sealed fuses," ISTFA (int. symposium for testing and failure analysis), San Jose, pp. 26-38, 1981.
- [ 32 ] E.H. Williams, S.J. Battel, "Study to establish limits for reliable fuse application in transient environment," Proc. ISTFA (int. symposium for testing and failure analysis), San Jose, pp. 111-114, Oct. 1982.
- [ 33 ] G.Klepp, "Contact resistance behaviour of DO fuses," ETZ, Vol. 107, No. 4, pp. 164-166, 1986.

- 
- [ 34 ] J.D. Kueck and D. W. Brinkley, "Improving fuse reliability in critical control circuits," IEEE Trans. on Energy Conversion, Vol. 5, No. 3, pp. 603-606, Sept. 1990.
- [ 35 ] S. Arai, "Determinations and cycles to failure of H.V. current-limiting fuses subjected to cyclic loading," Proc. ICEFA, Trondheim, pp.252-261, 1984.
- [ 36 ] P.R. Mocarzel and V.L.A. Da Silveira, "Proposed test method for distribution fuselinks," Proc. ICSAP (int. conf. on switching arc phenomena). Lodz, pp. 218-222, Sept. 1989.
- [ 37 ] S.F. Costa and L.P. Rangel, R.G. Bastos, "Overload tests for fuses in rolling-mills," Proc. ICEFA, Nottingham, pp. 17-22, 1991.
- [ 38 ] R. Wilkins and A. Wilkinson, C. Cline. "Endurance of semiconductor fuses under cyclic loading," Proc. ICEFA, Nottingham, pp.43-48, Sept. 1991.
- [ 39 ] A.C. Westrom, S.W. Law, R.J. P. Mckenzie, R.C. Patterson and B.R. Livesay., "Field service evaluation of distribution fuse links," IEEE Transactions on Power Delivery Vol. 5, No. 4, Oct. 1990, pp. 1855-1865.
- [ 40 ] A. Hamel, G. St-Jean and M. Paquette, "Nuisance fuse operation on MV transformers during storms," IEEE Transactions on Power Delivery Vol. 5, No. 4, pp. 1866-1874, Oct. 1990.
- [ 41 ] D.E Parrish, "Lightning-caused distribution transformer outages on a Florida distribution system," IEEE Transactions on Power Delivery Vol. 6, No. 2, pp. 880-887, April 1991.
- [ 42 ] M. Darveniza, "Lightning protection of power systems," Journal of Electrical and Electronics Engineering, Australia, Vol. 11, No. 3, pp. 201-209, Sept. 1991.
- [ 43 ] G. Nutsch and W. Rother, "Investigation for the use of copper as an element material in HV HBC fuses," Proc. ICEFA, Nottingham, pp.68-73, Sept. 1991.
- [ 44 ] A. Dasgupta and M. Pecht, "Material failure mechanisms and damage models," IEEE Trans. on Reliability, Vol. 40, No. 5, pp. 531-536, Dec. 1991.
- [ 45 ] J. Li and A. Dasgupta, "Failure mechanism models for creep and creep rupture," IEEE Trans. on Reliability, Vol. 42, No. 3, pp. 339-353, Sept. 1993.
- [ 46 ] R.W. Hertzberg, "Deformation and fracture mechanics of engineering materials." New York: Wiley, 1989.
- [ 47 ] IEC Publication 127 ( 1- 7 ) : miniature fuses, 1988.
- [ 48 ] IEC Publication 269: low voltage fuses, 1986.
- [ 49 ] IEC Publication 644: Specification for high voltage fuselinks for motor circuit applications, 1979.
- [ 50 ] D. Moulin, A. Combescure and D. Acker, "Nuclear engineering and design 116 (a review of thermal buckling analysis methods, pp. 255-263)." Amsterdam: Elsevier, 1989.

- [ 51 ] X.Z. Meng, J.G.J. Sloot and H.U. Haas, "Ageing mechanism of fuses for semiconductor protection," Proc. ICEFA, Ilmenau, pp. 180-187, Sept. 1995.
- [ 52 ] J.G.J. Sloot, J. van Herel and X.Z. Meng, "Thermal modelling of a miniature fuse with PSPICE," Proc. ECAAA (int. conf. electrical contacts, arcs, apparatus and applications), Xi'an, pp. 244-247, 1993.
- [ 53 ] X.Z. Meng, J.G.J. Sloot and H. Rijanto, "Modelling of semiconductor fuses in EMTP," Proc. Int. Conf. Power Systems Transients, Lisbon, Sept. 1995.
- [ 54 ] K.U. Leuven EMTP center, "Alternative transient program, rule book," Heverlee, Belgium, 1987.
- [ 55 ] X.Z. Meng and J.G.J. Sloot, "Thermal buckling behaviour of fuse wires", EUT report 94-E-283, Eindhoven: Eindhoven University of Technology, 1994.
- [ 56 ] X.Z. Meng, P. van Rietschoten, L. Vermij and J.G.J. Sloot, "Pulsed current withstand ability of miniature fuses," Proc. ECAAA, Xi'an, pp. 110-114, 1993.
- [ 57 ] X.Z. Meng, J.G.J. Sloot and G.C. Damstra, "Experimental evaluation of fuse lifetimes for the pulsed current," Proc. ICSSAP, Lodz, pp. 236-240, 1993.
- [ 58 ] X.Z. Meng, J.G.J. Sloot, P. van Rietschoten and H. Rijanto, "A reliability study of miniature fuses," Proc. ICEFA, Ilmenau, pp. 115-121, Sept. 1995.
- [ 59 ] P. H. Sydenham, "Wiley series in measurement science and technology," Chichester: Wiley, 1988.
- [ 60 ] D. F. Horne, "Measuring systems and transducers for industrial applications," Bristol: Adam Hilger, 1988.
- [ 61 ] A. J. Caristi, "IEEE-488: general purpose instrumentation bus manual," London: Academic Press, 1989.
- [ 62 ] Littelfuse, "Pulse measuring apparatus (proj. 304)," Internal Report (in Dutch), 1990.
- [ 63 ] I.B. Gertsbakh, "Statistical reliability theory," New York: Marcel Dekker, 1989.
- [ 64 ] W. Gander and J. Hrebicek, "Solving problems in scientific computing using Maple and Matlab," Berlin: Springer, 1993.
- [ 65 ] J.H. Constable, "Electrical resistance as an indicator of fatigue," IEEE Trans. CHMT Vol. 15, No. 6, pp. 1138-1145, Dec. 1992.
- [ 66 ] T. Eversmann and R. Goos, "Bau von rechnergesteuerten Prüfeinrichtungen für die Untersuchung von Halbleiter-Sicherungen," M.Sc. Graduation Report, Germany, Feb. 1993.
- [ 67 ] R. Wilkins, A. Wilkinson and C. Cline, "Endurance of semiconductor fuses under cyclic loading," Proc. ICEFA, Nottingham, pp. 43-48, Sept. 1991.

- [68] J.P. Holman, "*Heat transfer.*" London: McGraw-Hill, 1986.
- [69] F. Kreith and M.S. Bohn, "*Principles of heat transfer.*" St. Paul: West, 1993.
- [70] J.H. Lienhard, "*A heat transfer textbook.*" Englewood Cliffs: Prentice-Hall, 1987.
- [71] W. Elenbaas, "*Dissipation of heat by free convection.*" Philips Research Report No.3, pp. 338-360, pp. 450-465, 1948.
- [72] S. Churchill and H. Chu, "*Correlating equations for laminar and turbulent free convection for a horizontal cylinder,*" International Journal on Heat and Mass Transfer, Vol. 18, pp. 1049-1053, 1975.
- [73] R.H. Perry and C.H. Chilton, "*Chemical engineers' handbook.*" London: McGraw-Hill, 1973.
- [74] T. Tsubouchi and H. Masuda, "*Heat transfer by natural convection from horizontal cylinders at low Rayleigh numbers,*" Tohoku University Report No.190 (Japan), pp. 205-219, 1967/1968.
- [75] J. van Herel, "*Thermal modelling of a miniature fuses in PSPICE.*" (in Dutch). M.Sc. graduation report, Eindhoven University of Technology, 1992
- [76] A. Goldsmith, T.E. Waterman, H.J. Hirschhorn, "*Handbook of thermophysical properties of solid materials.*" Vol. 1, London: Pergamon, 1961.
- [77] M. von Ardenne, "*Tabellen zur angewandten Physik band II,*" Berlin: Deutscher Verlag der Wissenschaften, 1973.
- [ 78 ] X.Z. Meng, A van de Poll, J.G.J. Sloot and H. Rijanto, "*3D thermal modelling of a fuse for the protection of semiconductors,*" Proc. IPEC (International Power Engineering Conference), Singapore, pp. 47-52, 1995.
- [ 79 ] A. van de Poll, "*3D thermal modelling of a low voltage fuse for the protection of semiconductors in EMTP,*" M.Sc. Report EG/94/711.A (in Dutch), Eindhoven University of Technology, 1994.
- [ 80 ] R. Bulbaai, "*EMTP simulation of the temperature distribution of a semiconductor protection fuses for current pulses,*" M.Sc. Report EG/95/760.A (in Dutch), Eindhoven University of Technology, 1995.
- [ 81 ] A. Tslaf, "*Combined properties of conductors.*" Amsterdam: Elsevier, 1981.
- [ 82 ] J.G.J. Sloot and X.Z. Meng, "*Choices for the presentation of fuse melting curves.*" Proc. ICEFA, Nottingham, pp. 206-209, Sept. 1991.
- [ 83 ] P.F. Pei and A.H. Nayfeh, "*Fully nonlinear model of cables.*" AIAA Journal, Vol. 30, No. 12, pp. 2993- 2995, 1992.
- [ 84 ] S.P. Timoshenko and J.M. Gere, "*Theory of elastic stability.*" London: McGraw-Hill, 1961.
- [ 85 ] J. E. Locke and C. Mei, "*Finite element, large deflection random response of thermally buckled beams,*" AIAA Journal, Vol. 28, No. 12, pp. 2125-2131, 1990.

- [ 86 ] J. E. Locke, "*A finite element formulation for the large deflection random response of thermally buckled structures.*" Ph.D. Dissertation, Old Dominion University (USA), 1988.
- [ 87 ] E. Reissner, "*Lateral buckling of beams.*" Computers & Structures, Vol. 33, No. 5, pp. 1289-1306, 1989.
- [ 88 ] H. Ziegler, "*Principles of structural stability.*" London: Blaisdell, 1968.
- [ 89 ] R.D. Cook, "*Concepts and applications of finite element analysis.*" New York: John Wiley, 1981.
- [ 90 ] J.N. Reddy, "*Applied functional analysis and variational methods in engineering.*" London: McGraw-Hill, 1986.
- [ 91 ] P.G. Bergan and R.W. Clough, "*Convergence criteria for iterative processes.*" AIAA Journal, Vol. 10, No. 8, pp. 1107-1108, 1972.
- [ 92 ] G.J. Simitses, "*Dynamic stability of suddenly loaded structures.*" Berlin: Springer, 1990.
- [ 93 ] C.L. Dym, "*Stability theory and its applications to structural mechanics.*" Leyden: Noordhoff, 1974.
- [ 94 ] A. Dasgupta, "*Failure mechanism models for cyclic fatigue.*" IEEE Trans. on Reliability, Vol. 42, No. 4, pp. 548-555, Dec. 1993.
- [ 95 ] H.L. Ewalds and R.J.H. Wanhill, "*Fracture mechanics.*" London: Edward Arnold, 1989.
- [ 96 ] U.R. Evans, "*The corrosion and oxidation of metals, scientific principles and practical applications.*" London: Edward Arnold, 1960.
- [ 97 ] G. Stevenson, "*Cyclic loading of fuses for the protection of semiconductors.*" Proc. ICEFA (int. conf. on electric fuses and their applications), Liverpool, pp. 276-283, April 1976.
- [ 98 ] L.F. Coffin, "*A study of the effects of cyclic thermal stresses on a ductile metal.*" ASME, vol. 76, pp. 931-950, 1954.
- [ 99 ] R.W. Smith, M.H. Hirschberg, and S.S. Manson, "*Fatigue behaviour of materials under strain cycling in low and intermediate life range.*" NASA, technical note D-1574, 1962.
- [ 100 ] Y.H. Pao, "*A fracture mechanics approach to thermal fatigue life prediction of solder joints.*" IEEE Trans. on Components, Hybrids, Manuf. Technol., vol. CHMT-15, No.4, pp. 559-570, Aug. 1992.
- [ 101 ] H.D. Solomon, "*Fatigue of 60/40 solder.*" IEEE Trans. Components, Hybrids, Manuf. Technol., vol. CHMT-9, pp. 423-432, Dec. 1986.
- [ 102 ] W.A. Logsdon, P.K. Liaw and M.A. Burke, "*Fracture behaviour of 63Sn-37Pb solder.*" Eng. Fracture Mech., Vol. 36, No. 2, pp. 183-218, 1990.
- [ 103 ] D.J. White, "*Some contributions to British work on thermal and high strain fatigue.*" Proc. TSTF (int. conf. on thermal stresses and thermal fatigue), Gloucestershire, pp. 1-6, Sept. 1969.



- 
- [ 104 ] A. Sletterink, H. Vlutters and H. v.d. Zwaag, "*The influence of diffusion phenomena on time/current characteristics of fuse links,*" *Holectechniek* Vol. 3, Dec. 1972, pp. 117-123.
- [ 105 ] J.Ossowicki and K. Cwidak, "*Copper fuse elements in h.b.c. fuses for protection of circuits with h.v. motors,*" *Proc. ICSAP*, Sept. 1993, pp. 241-244.

## Summary

This thesis covers the work carried out in Eindhoven University of Technology during the period from October 1991 to September 1995. Professor dr. -ing. H. Rijanto, professor ir. G.C. Damstra and associate professor ir. J.G.J. Sloot are thesis directors.

Among many electrical devices, fuses are well known for their popularity in house apparatus and industrial installations. Because of ageing effects, characteristics of fuses will deteriorate in service. In order to improve the reliability of electrical systems, lifetime estimation of fuses are required by both users and manufacturers. Literature studies show that previous work and existing standards do not provide general valid methods to give lifetime expectancy of fuses. For these reasons, this work was initiated in co-operation with Littelfuse BV Utrecht, the Netherlands and Siba GmbH Lünen, Germany.

This thesis describes efforts to predict lifetimes of miniature fuses and semiconductor protection fuses. Parameters in the models for predicting fuse lifetimes are defined with clear physical meaning; methods for determining these parameters are presented. Related topics, such as electric current distribution, heat transfer, thermal buckling and plastic deformation, are also discussed. In existing manufacturer catalogues, current - time characteristics are normally provided. From the lifetime predictions presented in this thesis, shift of current - time characteristics can be calculated with the number of current pulses as parameter.

### 1. Studies for miniature fuses

Experimental determinations of lifetimes were performed for short and long time current pulses. These tests are comparable to the surge withstand and endurance described in IEC publication 127. Results show that lifetime follows the Weibull distribution; it decreases with current and current conducting time (or on time). During the current pulses, thermal buckling of fuse wire elements has been observed. Resistance of fuses tends to increase during the fuse life in general, although it may have small variations.

To analyse the influence of current pulses, electrical analogue method was used to simulate thermal responses of wire elements. Heat conduction along the wire element, convection and radiation of the element were considered in proposed heat transfer models. For any current pulses, temperature rise could be calculated. Simulations of voltage - current traces and current - time characteristics have been compared with experimental observations for two typical types of miniature fuses.

To explain thermal buckling of wire elements during d.c. current and current pulses, the analytic approach and the finite element formulation were developed. Theoretical results of displacements calculated from both methods have been found in agreement with observations from high speed photography and optical microscope.

In determining the lifetime of miniature fuses for short current pulses, temperature distribution and displacement of wire elements were taken into account. Lifetime relation based on the elastic fracture mechanism has been introduced. Lifetime predictions in theory

and experimental evaluation from high speed photography have been compared with results of lifetime tests.

For long current pulses, the plastic deformation was assumed to be related with power law creep. Material and configuration constants of fuse wire elements were determined by using a few lifetime data with different on times. Afterwards, the number of current pulses that fuses withstand has been calculated based on Manson - Coffin law. Predictions have been compared with various experimental results which are related with current magnitudes below the minimum fusing current and conducting times from several seconds to one hour.

For both short and long current pulses, predictions have been found in reasonable agreement with experimental results. From the lifetime predictions, deterioration of current - time characteristics can be calculated which may provide the information for the fuse replacement.

## **2. Studies for semiconductor protection fuses**

In experiments of lifetimes for short current pulses, typical semiconductor protection fuses with the same current rating (160A) and different element shapes were taken as objects. Results show that lifetime obeys the Weibull distribution; it decreases with the  $I^2t$  value of current pulses. Resistance changes during the fuse life are comparable with the spread of new products.

For the fuse elements with the curved and straight shapes, thermal buckling was confirmed by high speed photography in spite of existence of sand.

After fuses are submitted to current pulses, the surface of the element notch becomes rough. This plastic deformation will increase gradually according to the observation of scanning electron microscope. Considering the local deformation, lifetimes of commercial products have been improved more than ten times for short current pulses.

For analysing the temperature distribution of the notched fuse element, EMTP was used to solve the resulting networks of electrical - thermal problems. In forming networks, non-linear properties of materials can be taken into account by using point by point functions (or look up tables). Simulated results have been compared with melting characteristics and measured voltage time traces. It is concluded that EMTP is a suitable tool for the analysis of three dimensional time dependent modelling of fuses.

In the way similar to that for miniature fuses, the number of short current pulses that semiconductor protection fuses withstand has been predicted. At the moment, the deflection for the straight element was assumed. Predictions have been compared with experimental results of fuses with three different curved element shapes. To improve the accuracy of predictions, further investigations are recommended.

## Samenvatting

Dit proefschrift, levensduur-voorspellingen van smeltveiligheden voor de beveiliging van apparaten en vermogens-halfgeleiders, behandelt het werk dat is uitgevoerd aan de Technische Universiteit Eindhoven gedurende de periode van oktober 1991 tot september 1995 onder leiding van prof. dr. -ing H. Rijanto, prof. ir. G.C. Damstra en ir. J.G.J. Sloot.

Temidden van vele elektrische apparaten zijn smeltveiligheden zeer bekend door hun populariteit voor huishoudelijke apparatuur en industriële installaties. Tijdens het gebruik van smeltveiligheden treedt een veroudering op waardoor de karakteristieken veranderen. Om de betrouwbaarheid van elektrische systemen te verbeteren, zijn schattingen van de levensduur van smeltveiligheden gewenst voor zowel gebruikers als fabrikanten. Uit literatuurstudie volgt dat eerder onderzoek en bestaande normen niet voorzien in algemeen geldige methoden voor de bepaling van de levensduur van smeltveiligheden. Om deze redenen werd dit werk gemiticeerd in samenwerking met Littelfuse te Utrecht en Siba te Lünen (Dld).

Dit proefschrift beschrijft pogingen om de levensduur van miniatuur patronen en smeltveiligheden voor halfgeleiderbeveiliging te voorspellen. Parameters in de modellen voor de voorspelling van de levensduur van smeltveiligheden worden gedefinieerd met een duidelijke fysische betekenis; methoden voor de bepaling van deze parameters worden aangegeven. Hiermee samenhangende onderwerpen zoals de elektrische stroomverdeling, warmte overdracht, thermische buiging en plastische deformatie komen eveneens aan de orde.

### 1. Onderzoek van miniatuursmeltveiligheden

Experimentele levensduurbepalingen werden uitgevoerd voor stroompulsen met een korte en lange tijdsduur. Deze testen zijn vergelijkbaar met de IEC 127 testen voor de bestendigheid tegen piek- en langdurige belasting. Uit de resultaten volgt dat het statistisch gedrag van de levensduur te beschrijven is met Weibull verdelingen; de levensduur neemt af met de stroomsterkte en de duur van de stroombelasting. Tijdens de stroompulsen werd thermische opkruiling van smeltgeleiders waargenomen. De weerstand van smeltgeleiders heeft in het algemeen de neiging om toe te nemen tijdens de levensduur, al kunnen de veranderingen klein zijn.

Om de invloed van stroompulsen te onderzoeken, werden elektrische analoge modellen gebruikt om de thermische respons van draadelementen te simuleren. In de voorgestelde warmteoverdrachtmodellen werd rekening gehouden met warmtegeleiding, convectie en straling. Voor willekeurige stroompulsen bleek het mogelijk om de temperatuurtoename te bepalen. Simulaties van het tijdsverloop van stroom en spanning zijn vergeleken met experimentele observaties voor twee typische miniatuurpatronen.

Om thermische opkruiling van draadelementen tijdens gelijkstroom en stroompulsen te verklaren, werd een analytische benadering met de eindige elementen methode ontwikkeld.

Theoretische resultaten van verplaatsingen, berekend volgens beide methoden bleken in overeenstemming met waarnemingen door middel van hoge snelheidsfotografie en microscoopopnames.

Bij de bepaling van de levensduur voor korte stroompulsen, werd rekening gehouden met de temperatuurverdeling en de uitwijking van draadsegmenten. Voor de levensduur is een uitdrukking voorgesteld, gebaseerd op elastische breuk. Voorspellingen van de levensduur, zowel gebaseerd op een semi empirische relatie als vanuit een zuiver theoretisch model zijn vergeleken met de experimentele resultaten van levensduurbepalingen.

Voor langdurige stroompulsen werd verondersteld dat de plastische deformatie samenhangt met exponentiële kruip. De benodigde materiaal- en configuratieafhankelijke constanten van smeltgeleiders werden afgeleid uit enkele experimentele verbanden van de levensduur bij een beperkt aantal verschillende waarden voor de pulsduur. Vervolgens is een algemeen geldige uitdrukking voor de levensduur afgeleid uit de Manson-Coffin-betrekking. De hiermee gedane voorspellingen zijn vergeleken met een groot aantal experimentele resultaten met een groot bereik van de stroomsterkte en pulstijden van enkele secondes tot een uur.

Voor pulsen met zowel een korte als lange tijdsduur, bleken voorspellingen in overeenstemming met experimentele resultaten.

## 2. Onderzoek van smeltveiligheden voor halfgeleiderbeveiliging

De levensduur werd experimenteel bepaald voor stroompulsen met een korte tijdsduur. Hiervoor werden typische halfgeleiderpatronen met dezelfde nominale stroom (160 A) maar verschillende elementconfiguraties beproefd als testobject. Uit de resultaten volgt dat de levensduur voldoet aan een Weibull verdeling. De levensduur neemt af met de  $I^2t$  waarde horende bij de stroompulsen. De veranderingen van weerstandswaarde gedurende de levensduur waren vergelijkbaar met de spreiding van nieuwe producten.

Voor de smeltgeleider-elementen met gebogen en rechte vorm, werd met snelle fotografie het optreden van thermische opkrulling vastgesteld, ondanks de aanwezigheid van zand. Uit opnames met een scanning microscoop volgde dat het oppervlak van de smeltgeleider ter plaatse van de verbindingen ruw was na afloop van een langdurige pulsbelasting, des te ruwer naarmate de aantal pulsen toenam. Dit duidt op een geleidelijk toenemende plastische vervorming. Door de nadere beschouwing van lokale vervorming kon worden bereikt dat de levensduur van commerciële producten, belast met puls-vormige stromen, een factor tien werd verlengd.

Voor de analyse van de temperatuurverdeling van stripelementen met uitsparingen, werd het programma EMTP gebruikt om de resulterende netwerken horende bij elektrische en thermische problemen op te lossen. Hierbij kan rekening worden gehouden met niet-lineaire materiaal eigenschappen door middel van gedefinieerde functies of opzoektabelen. Simulatiere resultaten zijn vergeleken met smeltkarakteristieken en gemeten spanning-tijd verbanden. Hieruit kan worden geconcludeerd dat EMTP een geschikt instrument is voor de analyse van driedimensionale tijdsafhankelijke modellering van smeltgeleiders.

Op een soortgelijke manier als die bij miniatuursmeltveiligheden werd het aantal stroompulsen berekend, waartegen een smeltveiligheid bestand is. Wel werd hierbij uitgegaan van een veronderstelling voor de optredende uitbuiging. Voorspellingen zijn vergeleken met experimentele resultaten voor smeltveiligheden met drie verschillende gebogen configuraties. Om de betrouwbaarheid van deze laatste voorspellingen te verbeteren wordt verder onderzoek aanbevolen.

## Acknowledgements

In accomplishing this thesis, I have benefited from the advice and help of many people - in Eindhoven University, in industries, and in the student training. I would like to express my thanks to all of you for your expertise, contribution, encouragement, and support.

First of all, I wish to record my thanks to thesis supervisors professor Hendro Rijanto, Geert Damstra and Joop Sloot for their valuable guidance. Especially, Joop, he formulated the proposal for this thesis, stimulated impressive discussion, and provided constant help in my daily life. I wish to thank professor Jimei Wang for introducing me to the field of electrical switching components and installations, and professor Willem van den Heuvel for inviting me to join research activities in the Section of Electrical Energy Systems.

I would like to gratitude Leen Vermij for his practical, concise, valuable advice, and comments. I am indebted to Peter van Rietschoten and Dipl. -ing, H.U. Haas for their contribution in lifetime tests of fuses. I am grateful to Dr. C. M. Menken for his discussion on the buckling concept. Thanks also go to Xining Zhang for his help in scanning electron microscope photography.

To all the other members of group EGI, I owe many thanks for their help of any kind whatsoever I have received. It is a pleasure to mention my former roommate Math Bollen, my colleagues René Smeets and Vlastimil Kalasek for always willing to help. Special thanks go to Hans Vossen for his assistance in high speed photography, Ton Wilmes for his support in electronic circuits and software development, Aric van Staalduinen for his technical work in preparing experimental samples, and Gerard Jacobs for his support in EMTD simulations.

Thanks are given to Jeroen van Herel, Arend van de Poil and Richenel Bulbaai for contributions during their studies, who conducted software programming and network simulations.

I am also grateful to many people who made the introduction of Taiji Quan and Chinese meditation or Qigong into this university possible.

I would like to express my apologies to those whom I may have inadvertently failed to mention. Finally I thank my family, particularly my wife Ying and my daughter Nancy for their support throughout this thesis.

## Curriculum Vitae

The author was born in Ningxia, China, on 06 June 1963.

In July 1979 he finished his high school education. After travelling one thousand kilometres by train, on a heavily rainy day September 1979, he arrived at Xi'an to continue his education. In Xi'an Jiaotong University, he obtained his Bachelor's Degree in July 1983 and Master's Degree in April 1986 in Electrical Engineering with the specialisation of electrical components and installations. Afterwards, he worked in the same university as a teacher until October 1987. Then, he began his study as a research assistant.

In November 1989 he came to work in Eindhoven University of Technology. He involved in a number of activities which cover electric fuses, arcing studies, protection of transformers and motor control centers. During the period from October 1991 to December 1995 he has worked on the reliability of electric fuses in the Section of Electrical Energy Systems. The project was in cooperation with Littelfuse BV, the Netherlands and Siba GmbH, Germany. Some results of the work during this period lead to this thesis. The thesis directors are professor dr. -ing. H. Rijanto, professor ir. G.C. Damstra and ir. J.G.J. Sloot.

# Statements

accompanying the dissertation

## Lifetime Predictions of Miniature Fuses and Semiconductor Protection Fuses

X. Z. Meng

### 1

Large mechanical structures such as oil rigs, bridges, pipelines, chemical plants, nuclear installations and aircraft may in the future be equipped with "fuses", which will give early warnings about stresses in the structure that could lead to catastrophic failures. Different from electric fuses, these "mechanical fuses" do not clear the possible damage however.

- A. Coghlan, '*Fatigue fuses*' blow the whistle on structural stress, New scientist, Vol. 131, pp. 25-25, Sept. 1991.

### 2

Electrical analogue methods can be used to predict electrical and thermal responses of fuses which form the basis of lifetime determination.

- This thesis

### 3

For fuses with and without sand, thermal buckling of the fuse element takes place as the temperature of the element exceeds a certain limit.

- This thesis

### 4

In electric distribution networks, UPS inverters, continuous generators, large motors and electronic relay systems have the shortest ETTF (expected time to failure). Fuses and MV/LV circuit breakers have a relatively long ETTF. In conclusion, performance of inverters, generators, motors and relay systems should be improved to increase the reliability of systems.

- M.H.J. Bollen, "*Literature search for reliability data of components in electric distribution networks.*" EUT Report 93-E-276, Eindhoven: TU Eindhoven, August 1993.



5

In distribution systems, numerical relays capable of communicating with management systems can be designed to enable self-monitoring for better availability and less maintenance. Therefore, they may provide possible advantages in reliability and lifetime costs over traditional electromechanical and electronic protection relays.

6

Power quality is characterised by several indices. Some of these indices are defined by the utility and others by customers. Therefore, agreement between utilities and industries is needed to improve the overall power quality.

7

Because of advanced technology, the average lifetime of people has increased dramatically. However, the maximum lifetime is still more or less the same. So, the need to investigate the mechanism of the maximum lifetime will increase in the future.

8

To pursue a high economy growth rate the natural resources should be considered, such as water, air, food and space. Otherwise, people have to pay back in the long run.

9

Whenever a government stays in power for too long or too short a period, the government will attempt to view the country as its own property. To minimise corruption, the government should be renewed regularly without military interference.

10

The Tao can be expressed (abstract from nature), but words are never sufficient. Names can be given (to describe existence), but descriptions are never complete. What does not exist in thought prepares the beginning of heaven and earth; what does exist in thought is the mother of the world. It is with no mind that miracles are to be observed. It is with mind that changes are to be examined. Both are from the same source and with different descriptions. Continuous repetition of being with mind and with no mind leads to the experience of the Tao.

- Lao Zi, "*Dao De Jing (Tao Te Ching)*," Edition of Lou Guan Tai, Chapter one, about 10 century B.C.